ASSESSMENT OF ONE- AND TWO-EQUATION TURBULENCE MODELS FOR HYPERSONIC TRANSITIONAL FLOWS

Christopher J. Roy‡ and Frederick G. Blottner†

Sandia National Laboratories*

P. O. Box 5800, MS 0835

Albuquerque, NM 87185

Abstract

A number of one- and two-equation turbulence models are examined for hypersonic perfect- and real-gas flows with laminar, transitional, and turbulent flow regions. These models were generally developed for incompressible flows, and the extension to the hypersonic flow regime is discussed. In particular, inconsistencies in the formulation of diffusion terms for one-equation models are examined. For the Spalart-Allmaras model, the standard method for forcing transition at a specified location is found to be inadequate for hypersonic flows. An alternative transition method is proposed and evaluated for a Mach 8 flat plate test case. This test case is also used to evaluate three different two-equation turbulence models: a low Reynolds number $k-\varepsilon$ model, the Menter $k-\omega$ formulation, and the Wilcox (1998) $k-\omega$ model. These one- and two-equation models are then applied to the Mach 20 Reentry F flight vehicle. The Spalart-Allmaras model and both $k-\omega$ formulations are found to provide good agreement with the flight data for heat flux, while the Baldwin-Barth and low Reynolds number $k-\varepsilon$ models overpredict the turbulent heating rates. Careful attention is given to solution verification in the areas of both iterative and grid convergence.

Nomenclature

a	speed of sound, *m/s*
D	turbulence diffusion term
d	distance to the wall, *m*
k	specific turbulent kinetic energy, m^2/s^2
Pr_T	turbulent Prandtl number (= 1.0)
p	pressure, N/m^2
q	heat flux, W/m^2
R_N	vehicle nose radius, *m*
r	radial coordinate, *m*
S_P	turbulence production source term
S_D	turbulence destruction source term
S_{ij}	strain rate tensor, *1/s*
T	temperature, *K*
Tu	freestream turbulence intensity percent
t	time, *s*
U	conserved transport quantity
u_i	velocity, *m/s*
V	velocity magnitude, *m/s*
x	axial coordinate, *m*
y	wall normal direction, *m*
α	angle of attack, *degrees*
γ	ratio of specific heats
δ_{ij}	Kronecker delta function (= 1 when $i=j$)
ε	specific dissipation rate, m^2/s^3
θ_{cone}	cone half-angle, *degrees*
μ	absolute viscosity, $N\cdot s/m^2$
ν	kinematic viscosity, m^2/s
$\tilde{\nu}$	Spalart-Allmaras working variable
ρ	density, kg/m^3
τ_{ij}	turbulent stress tensor, m^2/s^2
φ	non-conserved transport quantity
Ω_{ij}	rotation tensor, *1/s*
ω	specific turbulent frequency, *1/s*

Subscripts

E	exact value
eff	effective value (turbulent + laminar)
RE	Richardson extrapolation
ref	reference value

---

‡ Senior Member of Technical Staff, Member AIAA

† Distinguished Member of Technical Staff, AIAA Fellow

* Sandia is a multiprogram laboratory operated by Sandia Corporation, a Lockheed Martin Company, for the United States Department of Energy under Contract DE-AC04-94AL85000.

T	turbulent quantity
t	transitional quantity
w	wall value
∞	freestream value

Superscripts

+	quantity in wall coordinates
~	denotes Favre (density-weighted) averaging
—	denotes Reynolds (time-based) averaging
′	denotes Favre fluctuating quantity

Introduction

This work is concerned with developing a capability to model high-speed compressible flows with laminar, transitional, and turbulent flow regions. The approach uses one- and two-equation eddy viscosity models to predict the turbulent flow. The same governing equations are presently being used to predict the transitional flow region where the onset to turbulent flow is specified and assumed to be known. The prediction of where onset to turbulent flow occurs is a research area that depends on an analysis of the flow stability, understanding of the flow disturbances outside the boundary layer, and a capability to predict the boundary layer receptivity. The process of entraining disturbances into the boundary layer and producing perturbations that can be amplified is called "receptivity."

The more appropriate books providing information on modeling compressible turbulent flows are Wilcox,[1] Chapter 6 by Gatski,[2] and Smits and Dussauge.[3] The modeling of compressible turbulent flows is still an active area of research. The application of some of the turbulence models to compressible flows is not always clear, as the models were originally developed for incompressible flows. Formulations for incompressible flow are not applicable to compressible flow because some variables (e.g., density, viscosity) have been assumed constant in the development. The turbulent transport equations are often written in substantial differential form, while the equations in conservation form are generally required in compressible Navier-Stokes codes. Problems with the formulation of the governing equations for compressible turbulence models in conservation form are discussed. For example, the form of the diffusion term in the Spalart-Allmaras[4,5] model is rewritten and justification for the new form is given.

The SACCARA (Sandia Advanced Code for Compressible Aerothermodynamics Research and Analysis) code[6-9] is used for the results presented in this paper. For one-equation turbulence models, the SACCARA code has options for both the Baldwin-Barth[10] and Spalart-Allmaras eddy viscosity models. There is evidence that the use of the Baldwin-Barth model does not constitute a well-posed system of governing equations.[11] For boundary layer and shear layer flows, the solutions do not appear to converge to a unique solution as the mesh is refined. Therefore, there is more interest in using the Spalart-Allmaras model, as it has proven to be a numerically robust approach. Part of the present work is concerned with the evaluation of the Spalart-Allmaras model for high-speed flows and the simulation of the transition region with the Spalart-Allmaras model.

The SACCARA code also has options for three popular two-equation eddy viscosity turbulence models: a low Reynolds number $k-\varepsilon$ formulation and two $k-\omega$ models. The $k-\varepsilon$ model[1] employs the low Reynolds number modification of Nagano and Hishida[12] to allow integration to solid walls. The first $k-\omega$ formulation is the hybrid model of Menter[13] which is a blending between a $k-\omega$ formulation (near solid walls) and a $k-\varepsilon$ formulation (in shear layers and freestream flow). Menter proposed this hybrid model to take advantage of the accuracy of the $k-\omega$ model for wall-bounded flows and the $k-\varepsilon$ model for free shear layers. The final model is the Wilcox $k-\omega$ model[1] which was modified in 1998 to improve the predictive accuracy for shear flows. This model is referred to as the Wilcox (1998) model in the current work. The appropriate form of the two-equation eddy viscosity equations are also important because the one-equation formulation can be developed from the two-equation transport relations. This approach may be used to determine the appropriate form of the transport equation for the one-equation models.

Two flow cases have been used to investigate the performance of the one- and two-equation eddy viscosity models. The first case is the flow over a flat plate at Mach 8 and an altitude of 15 *km* where the perfect gas model is appropriate. The skin friction along the flat plate is used to judge the accuracy of the predictions through comparisons with the accurate laminar and turbulent results of Van Driest.[14,15] If the standard turbulence models (without modifications for transition) are employed over the whole domain, the transition location often depends on turbulent intensity in the freestream. This behavior is similar to the bypass transition problem. When a transition plane is specified in which the turbulent eddy viscosity is neglected upstream, the transition locations for the Spalart-Allmaras and low Reynolds number $k-\varepsilon$ models still show sensitivity to the freestream turbulence quantities. The control of the transition location with the Spalart-Allmaras model has been investigated.

The second case investigated is the flow over the Reentry F flight vehicle at Mach 20 and at an altitude of 24.4 *km* (80,000 feet) where real gas effects are significant. The measured heat transfer along the vehicle is used to judge the accuracy of the model predictions. The

transition location is specified to give a reasonable match of the wall heat flux with the flight data. It should be remembered that the prediction of transition location is not included in the modeling. The solutions have been obtained on three meshes with the number of cells in each coordinate direction doubled for each mesh refinement. In addition, the solutions on each mesh are marched in time until the wall heat flux has obtained a steady-state value. The accuracy of the iterative solution relative to the steady-state solution has been estimated for each model. The various uncertainties and assumptions in the flight experiment and prediction are discussed. Real gas effects have been taken into account with the use of an equilibrium air model.

Favre-Averaged Transport Equation for Turbulence Models

The generic form of the turbulent transport equation in substantial derivative form[1] is

$$\bar{\rho}\frac{D\varphi}{Dt} = D + S_P - S_D \qquad (1)$$

where

$$D = D_1 - \bar{D}, \qquad D_1 = \frac{\partial}{\partial x_j}\left(\mu_{eff}\frac{\partial \varphi}{\partial x_j}\right)$$

For example for a one-equation eddy viscosity model, the dependent variable is $\varphi \sim \nu_T$ and the effective diffusion coefficient is μ_{eff}. In some models there are two parts to the diffusion term on the right-hand side of Eq. (1); D_1 is the first part of the diffusion term which can be put in conservation form, and $\bar{D}$ is the remaining part. When $\bar{D}$ is included, it can take on several forms. The source term $S = S_P - S_D$ has a production part S_P and a dissipation part S_D. If the continuity equation is multiplied by φ and added to Eq. (1), the resulting equation is the generic transport equation in conservation form:

$$\frac{\partial U}{\partial t} + \frac{\partial}{\partial x_j}\left\{\bar{\rho}\tilde{u}_j\varphi - \mu_{eff}\frac{\partial \varphi}{\partial x_j}\right\} = \bar{D} + S_P - S_D \qquad (2)$$

The dependent variable is $U = \bar{\rho}\varphi$. This development utilizes Favre (overtilde) and Reynolds (overbar) averaging. See Ref. 1 for notation and for details on the Favre averaging procedure.

One-Equation Turbulence Model

There have been a number of one-equation turbulence models developed which use a transport equation to solve for the eddy viscosity directly. The present work is focused on the Spalart-Allmaras model and a brief description is presented below.

Spalart-Allmaras Model

The transport equation for determining the eddy viscosity with near-wall effects included has been developed by Spalart and Allmaras.[4,5] The governing equation form is slightly different than Eq. (1) and is

$$\bar{\rho}\frac{D\varphi}{Dt} = D + S_P - S_D + S_t, \qquad \tilde{\mu} = \frac{\mu_T}{f_{v1}} = \bar{\rho}\varphi \qquad (3)$$

The dependent variable $\varphi = \tilde{\nu} = \nu_T / f_{v1}$, where f_{v1} is a damping function used in the near-wall region and mainly in the viscous sublayer. This function and the right hand side terms will be defined below. The continuity equation is multiplied by φ and added to Eq. (3) which gives a transport equation in conservation form for the Spalart-Allmaras model in the form of Eq. (2)

Spalart-Allmaras Model

$$\frac{\partial U}{\partial t} + \frac{\partial}{\partial x_j}\left\{\bar{\rho}\tilde{u}_j\varphi - \mu_{eff}\frac{\partial \varphi}{\partial x_j}\right\} = \bar{D} + S_P - S_D + S_t \qquad (4)$$

$$U = \bar{\rho}\tilde{\nu} = \bar{\rho}\varphi, \qquad \mu_{eff} = \frac{\mu + \tilde{\mu}}{\sigma}$$

The right-hand side has contributions from a diffusion term as well as production, destruction, and trip terms. The four terms in the model are written as follows:

Diffusion-Original Form

$$D = \bar{\rho}\frac{\partial}{\partial x_j}\left[\frac{\mu_{eff}}{\bar{\rho}}\frac{\partial \varphi}{\partial x_j}\right] + D_2 = D_1 + \bar{D}$$

$$\mu_{eff} = \frac{\mu + \tilde{\mu}}{\sigma} = \bar{\rho}\left(\frac{\nu + \varphi}{\sigma}\right), \qquad \bar{D} = D_2 - D_3$$

$$D_2 = \frac{c_{b2}\bar{\rho}}{\sigma}\left(\frac{\partial \varphi}{\partial x_j}\right)\left(\frac{\partial \varphi}{\partial x_j}\right), \qquad D_3 = \left(\frac{\mu_{eff}}{\bar{\rho}}\right)\frac{\partial \bar{\rho}}{\partial x_j}\frac{\partial \varphi}{\partial x_j}$$

Diffusion-Modified for Compressible Flow

$$D = D_1 + D_2, \qquad \bar{D} = D_2$$

Production

$$S_P = c_{b1}[1 - f_{t2}]\tilde{S}\bar{\rho}\varphi$$

Destruction

$$S_D = \left\{c_{w1}f_w - \frac{c_{b1}}{\kappa^2}f_{t2}\right\}\bar{\rho}\left(\frac{\varphi}{d}\right)^2$$

Trip Term

$$S_t = f_{t1}\rho(\Delta U)^2$$

In the formal transform of the transport equation into conservation form, the diffusion term D_3 includes a density gradient term. This term is zero when the transport equation (Eq. (4)) is developed from the compressible form of the $k-\varepsilon$ transport equations,[11,16] and is shown above in the term *Diffusion-Modified for Compressible Flow.* This form of the diffusion term is used in the present work. Including this density gradient term has been found to cause stability problems for high-speed flows, while having negligible effect on the predictions. The model controls transition from laminar to turbulent flow with the use of the trip term. With this additional physics, the foregoing governing equation requires some additional terms and definitions for f_{t1} and f_{t2} which involves the coefficients c_{t1} to c_{t4}. Except where noted, the standard values for the model constants are used in the current work.

Boundary Conditions for Spalart-Allmaras Model

At the wall $\mu_T = 0$ or $\tilde{\nu} = 0$. The freestream boundary condition for this model is the specification of the turbulent eddy viscosity μ_T. In the freestream there should be no production of the eddy viscosity, which requires that

$$f_{t2} = c_{t3}e^{-c_{t4}\chi^2} > 1, \qquad (c_{t3} = 1.2, \quad c_{t4} = 0.5)$$

in order to turn off the production term in Eq. (6). The restriction on χ is

$$\chi = \tilde{\nu}/\nu < \sqrt{(\ln c_{t3})/c_{t4}} = 0.604$$

The restriction on the freestream eddy viscosity becomes

$$\frac{\mu_T}{\mu} < \chi f_{v1} = \chi/[1+(c_{v1}/\chi)^3] = 3.713\times10^{-4} \qquad (5)$$
$$c_{v1} = 7.1$$

The freestream eddy viscosity as suggested by Spalart-Allmaras is $\tilde{\nu} < 1/2\nu$, which gives

$$\frac{\mu_t}{\mu} < \tilde{\nu} f_{v1}/\nu = 1.746\times10^{-4}.$$

Control of Laminar and Turbulent Flow with the Spalart-Allmaras Model

The governing equation has three terms that are influenced by the transition model. The complete source term (for the conservative formulation) is

$$S = \frac{c_{b2}\bar{\rho}}{Pr_T}\left(\frac{\partial\tilde{\nu}}{\partial x_j}\right)^2 + c_{b1}[1-\underline{f_{t2}}]\tilde{S}U$$
$$-(c_{w1}f_w - \underline{c_{b1}f_{t2}/\kappa^2})\bar{\rho}\left(\frac{\tilde{\nu}}{d}\right)^2 + \underline{f_{t1}\bar{\rho}(\Delta U)^2} \qquad (6)$$

where the trip terms are underlined in the above equation. The first term is part of the diffusion term and is included in the source term as it is evaluated numerically in an explicit manner. The second term is the production term and it will produce or increase the eddy viscosity if $f_{t2} < 1$. The third term is the destruction term and it will decrease the eddy viscosity if $c_{w1}f_w > c_{b1}f_{t2}/\kappa^2$. The fourth term is the trip term and it will increase the eddy viscosity as $f_{t1} > 0$.

The model generally predicts turbulent flow everywhere when the trip terms are zero

$$f_{t1} = 0 \text{ or } c_{t1} = 0, \qquad f_{t2} = 0 \text{ or } c_{t3} = 0$$

The flow can be made laminar everywhere with the following values of the trip terms:

$$f_{t1} = 0 \text{ and } f_{t2} \geq 1.0 \text{ or } f_{t2} = c_{t3}\Lambda, \quad \Lambda = e^{-c_{t4}\chi^2}$$
$$\text{or} \quad f_{t1} = 0, \qquad f_{t2} = 0, \qquad c_{b1} = 0$$

Several different approaches have been investigated to control transition and to replace the original trip model approach of Spalart-Allmaras.

Method 1 (f_{t2} is modified)

In this approach the value of $f_{t1} = 0$, and $f_{t2} = c_{t3}(1-\lambda)$ where λ varies from the laminar flow region to the turbulent flow region. In the laminar flow region $\lambda = 0$ while in the turbulent flow region $\lambda = 1$. The parameter is increased smoothly and defines the transitional flow region. This method requires specification of the location and length of the transitional region.

Method 2 (c_{b1} is modified)

In this method the trip terms $f_{t1} = 0$ and $f_{t2} = 0$ are set to zero. The coefficient c_{b1} is modified from the laminar flow region to the turbulent flow region as follows:

$$x < x_s: \; c_{b1} = 0, \qquad x > x_e: \; c_{b1} = 0.1355$$

$$x_s \leq x \leq x_e: \; c_{b1} = 0.1355\lambda^p, \quad \lambda = (x-x_s)/(x_e-x_s)$$

In this method, the location of the start of transitional flow x_s and end of transitional flow x_e are specified.

Method 3 ($c_{b1}(1-f_{t2})$ is modified)

In this method the production term coefficient is modified by writing this term as $\alpha c_{b1}(1-f_{t2})$. The parameter α increases from zero to one in the transitional flow region. From the definition of f_{t2}, the following is obtained:

$$\chi = \tilde{\nu}/\nu = \sqrt{-\ln[f_{t2}/c_{t3}]/c_{t4}} \tag{7}$$

The production term switches sign when $f_{t2} = 1$ which gives a critical value of χ which is $\chi^* = 0.604$. When $x < x_t$, set $\alpha = 0$ and there is no production of eddy viscosity upstream of the transition location x_t. When $x > x_t$, α is increased downstream towards one. This increase is controlled by setting

$$\alpha = 1 - f_{t2} = 1 - c_{t3}e^{-c_{t4}\chi^2}$$

When $x > x_t$ and $\chi \le \chi^*$, then $\chi = \chi^*$. When $x > x_t$ and $\chi > \chi^*$, then χ is obtained from Eq. (7). In this method, only the single parameter x_t must be specified.

Two-Equation Turbulence Models

The standard method for specifying transition to turbulence is through analogy with the turbulence intermittency approach. The turbulence transport equations are solved over the entire domain, with a user-defined transition plane specified. Upstream of this plane, the effective viscosity is simply the laminar value, while downstream the effective viscosity is the sum of the laminar and turbulent viscosities.

High Turbulent Reynolds Number $k-\varepsilon$ Model

The high Reynolds number formulation[1] is appropriate for turbulent flows but is not appropriate in the near-wall region. It can be applied in the outer part of boundary layers and combined with an inner boundary layer approach near the wall to obtain a complete formulation. For the standard $k-\varepsilon$ model, the turbulent kinetic energy equation for a compressible fluid takes the same form as Eq. (2) where the variables have the following values:

$$U = \bar{\rho}k = \bar{\rho}\varphi, \qquad \mu_{eff} = \mu_k, \qquad \bar{D} = 0$$
$$S_{Pk} = \bar{\rho}P, \qquad S_{Dk} = \bar{\rho}\varepsilon \tag{8}$$

The production term P takes the standard form for compressible flows (see Ref. 1), and the effective viscosity is defined below in Eq. (10). The transport equation for dissipation of turbulent kinetic energy is the same form as Eq. (2), where the variables have the following values:

$$U = \bar{\rho}\varepsilon = \bar{\rho}\varphi, \qquad \mu_{eff} = \mu_\varepsilon$$
$$\bar{D} = 0, \qquad S_{P\varepsilon} = c_{\varepsilon 1}f_1\bar{\rho}\frac{\varepsilon}{k}P, \qquad S_{D\varepsilon} = c_{\varepsilon 2}f_2\bar{\rho}\frac{\varepsilon}{k} \tag{9}$$

The effective viscosities are obtained from

$$\mu_k = \mu + \mu_T/\sigma_k, \qquad \mu_\varepsilon = \mu + \mu_T/\sigma_\varepsilon$$
$$\text{where} \quad \mu_T = c_\mu f_\mu \bar{\rho}k^2/\varepsilon \tag{10}$$

The constants in the foregoing equations use the standard values.

Low Turbulent Reynolds Number $k-\varepsilon$ Model

The Nagano and Hishida model[12] was developed for incompressible flow and is included in the current formulation. The model uses the following damping function in the eddy viscosity relation given in Eq. (10):

$$f_\mu = [1 - \exp(-y^+/26.5)]^2$$

This damping function is written in terms of the distance from the wall y^+. The source term for the turbulent kinetic energy Eq. (8) is

$$S = \bar{\rho}P - \bar{\rho}\varepsilon + \tilde{D}$$

The production term has been approximated with:

$$\bar{\rho}P \approx \mu_T\left(\frac{\partial \tilde{u}_i}{\partial x_j} + \frac{\partial \tilde{u}_j}{\partial x_i}\right)\frac{\partial \tilde{u}_i}{\partial x_j}$$

The compressible term

$$-\frac{2}{3}(\bar{\rho}k + \mu_T S_{kk})S_{kk}, \quad \text{where} \quad S_{kk} = \frac{\partial \tilde{u}_k}{\partial x_k}$$

has been neglected in the current formulation. The source term for the dissipation rate equation is

$$S = \frac{\varepsilon}{k}(c_{\varepsilon 1}f_1\bar{\rho}P - c_{\varepsilon 2}f_2\bar{\rho}\varepsilon) + \tilde{E}$$

The parameters in these source terms are written as

$$f_1 = 1, \qquad f_2 = 1 - 0.3e^{-R_T^2}, \qquad R_T = k^2/\nu\varepsilon$$
$$\tilde{D} = -2\mu\left(\frac{\partial\sqrt{k}}{\partial y}\right)^2, \qquad \tilde{E} = \mu\nu_T(1-f_\mu)\left(\frac{\partial^2\tilde{u}}{\partial y^2}\right)^2$$

The variables $\tilde{D}$ and $\tilde{E}$ use boundary layer type derivatives normal to the wall and $\tilde{E}$ requires the tangential velocity component.

The Nagano-Hishida and the Launder-Sharma[17] low Reynolds $k-\varepsilon$ turbulence models have been used by Theodoridis, Prinos, and Goulas[18] to predict transitional flow. They have investigated a flat plate flow experiment where the freestream turbulent intensity was ap-

proximately 3 percent and 6 percent. The two turbulence models were used to model the laminar to turbulent bypass transition in which the freestream turbulence determines where the transition to turbulent flow occurs. For this bypass transition case, the Nagano-Hishida model predicts transition to turbulent flow too near the leading edge while the Launder-Sharma model predictions are in reasonable agreement with the experimental data. Of course, neither of these turbulence models were developed to predict where transition will occur in a flow; the performance of the Launder-Sharma model in predicting the location of transition is fortuitous. The failure of the Nagano-Hishida for transitional flow requires caution in the application of this model and a procedure is required to have the model turned on at the appropriate location.

Menter k-ω Model

Two different two-equation turbulence models are described which solve equations for the turbulent kinetic energy, k, and the frequency of turbulent fluctuations, ω. The Menter k-ω model[13] is a hybrid model which uses a blending function to combine the best aspects of both the k-ω and the k-ε turbulence models. Near solid walls, a k-ω formulation is used which allows integration to the wall without any special damping or wall functions. Near the outer edge of the boundary layer and in shear layers, the model blends into a transformed version of the k-ε formulation, thus providing good predictions for free shear flows.

For the Menter k-ω model, the terms in Eq. (2) are as follows:

Turbulent Kinetic Energy Equation

$$U = \bar{\rho}k = \bar{\rho}\varphi, \qquad \mu_{eff} = \mu_k, \qquad \bar{D} = 0$$
$$S_{Pk} = \bar{\rho}P, \qquad S_{Dk} = \beta^*\bar{\rho}k\omega \tag{11}$$

Turbulent Frequency Equation

$$U = \bar{\rho}\omega = \bar{\rho}\varphi, \qquad \mu_{eff} = \mu_\omega$$
$$\bar{D} = 2\bar{\rho}(1-F)\sigma_{\omega 2}\frac{1}{\omega}\frac{\partial k}{\partial x_j}\frac{\partial \omega}{\partial x_j} \tag{12}$$
$$S_{P\omega} = \bar{\rho}\frac{\gamma}{\nu_T}P, \qquad S_{D\omega} = \beta\bar{\rho}\omega^2$$

The cross-diffusion term ($\bar{D}$) in Eq. (12) arises due to the transformation of the ε-equation into an equation for ω. The production term is given by

$$P = \tau_{ij}\frac{\partial u_i}{\partial x_j}, \quad \text{where} \quad \tau_{ij} = -\overline{u_i' u_j'}\,. \tag{13}$$

For 3-D compressible flows, the turbulence stress tensor can be expressed as:

$$\tau_{ij} = 2\nu_t\left(S_{ij} - \frac{1}{3}\frac{\partial \tilde{u}_k}{\partial x_k}\delta_{ij}\right) - \frac{2}{3}k\delta_{ij} \tag{14}$$

The effective viscosities are given by

$$\mu_k = \mu + \sigma_k\mu_T\,, \qquad \mu_\omega = \mu + \sigma_w\mu_T$$
$$\text{where} \quad \mu_T = \bar{\rho}k/\omega \tag{15}$$

and the model constants above are blended values of the k-ω and k-ε parameters. For example, for the constant β,

$$\beta = F\beta_1 + (1-F)\beta_2$$

where F varies from 1 at the wall to zero outside wall boundary layers, and a "1" denotes k-ω constants and "2" denotes k-ε constants. The values for these constants are:

$$\sigma_{k1} = \frac{1}{2}, \quad \sigma_{\omega 1} = \frac{1}{2}, \quad \beta_1 = \frac{3}{40},$$
$$\beta^* = 0.09, \quad \kappa = 0.41, \quad \gamma_1 = \frac{\beta_1}{\beta^*} - \frac{\sigma_{\omega 1}\kappa^2}{\sqrt{\beta^*}}$$

and

$$\sigma_{k2} = 1, \quad \sigma_{\omega 2} = 0.856, \quad \beta_2 = 0.0828,$$
$$\beta^* = 0.09, \quad \kappa = 0.41, \quad \gamma_2 = \frac{\beta_2}{\beta^*} - \frac{\sigma_{\omega 2}\kappa^2}{\sqrt{\beta^*}}\,.$$

Wilcox (1998) k-ω Model

For the Wilcox (1998) k-ω model,[1] the terms in Eq. (2) are as follows:

Turbulent Kinetic Energy Equation

$$U = \bar{\rho}k = \bar{\rho}\varphi, \qquad \mu_{eff} = \mu_k, \qquad \bar{D} = 0$$
$$S_{Pk} = \bar{\rho}P, \qquad S_{Dk} = \beta^*\bar{\rho}k\omega \tag{16}$$

Turbulent Frequency Equation

$$U = \bar{\rho}\omega = \bar{\rho}\varphi, \qquad \mu_{eff} = \mu_\omega, \qquad \bar{D} = 0$$
$$S_{P\omega} = \bar{\rho}\frac{\gamma}{\nu_T}P, \qquad S_{D\omega} = \beta\bar{\rho}\omega^2 \tag{17}$$

where

$$\alpha = \frac{13}{25}, \qquad \beta = \beta_0 f_\beta, \qquad \beta^* = \beta_0^* f_{\beta^*}$$

$$\sigma_k = \sigma_\omega = \frac{1}{2}, \qquad \beta_0^* = \frac{9}{100}$$

$$f_{\beta^*} = \begin{cases} 1, & \chi_k \le 0 \\ \dfrac{1 + 680\chi_k^2}{1 + 400\chi_k^2}, & \chi_k > 0 \end{cases}, \quad \chi_k \equiv \frac{1}{\omega^3}\frac{\partial k}{\partial x_j}\frac{\partial k}{\partial x_j}$$

$$\beta_0 = \frac{9}{125}, \quad f_\beta = \frac{1 + 70\chi_\omega}{1 + 80\chi_\omega}, \quad \chi_\omega \equiv \left| \frac{\Omega_{ij}\Omega_{jk}S_{ki}}{(\beta_0^*\omega)^3} \right|$$

$$\Omega_{ij} = \frac{1}{2}\left(\frac{\partial \tilde{u}_i}{\partial x_j} - \frac{\partial \tilde{u}_j}{\partial x_i}\right), \qquad S_{ij} = \frac{1}{2}\left(\frac{\partial \tilde{u}_i}{\partial x_j} + \frac{\partial \tilde{u}_j}{\partial x_i}\right).$$

The production term, P, and the eddy viscosity definitions are given in Eqs. (13) and (15), respectively. This formulation is a modification to an earlier Wilcox $k-\omega$ model[19] in order to improve model predictions for free shear layers and to reduce the solution sensitivity to freestream ω values.

Flow Predictions for Flat Plate

Flow over a flat plate has been chosen as a high speed test case to illustrate the behavior of the laminar/turbulent flow results obtained with the one- and two-equation turbulence models. The test case is Mach 8 flow over a flat plate with a wall temperature of T_w=1000 K and freestream conditions corresponding to an altitude of 15 km. For this case, the temperature in the flow is sufficiently low that perfect gas assumption with $\gamma = 1.4$ is reasonable.

Freestream Flow Conditions

The freestream conditions[20] for the flat plate case are:

$$p_\infty = 1.21114 \times 10^4 \ kg/m/s^2, \quad T_\infty = 216.65 \ K$$

$$\rho_\infty = 0.19475 \ kg/m^3, \quad a_\infty = \sqrt{\frac{\gamma p_\infty}{\rho_\infty}} = 295.07 \ m/s$$

$$V_\infty = a_\infty M_\infty = 2360.54 \ m/s$$

$$\mu_\infty = \frac{1.458 \times 10^{-6} T_\infty^{3/2}}{(T_\infty + 110.4)} = 1.4216 \times 10^{-5} \ kg/m/s$$

For the Spalart-Allmaras model, the restriction on the freestream eddy viscosity is determined by Eq. (5), which gives

$$\mu_{T_\infty} < 5.27 \times 10^{-9} \ kg/m/s$$

for the Mach 8 flat plate flow case. The freestream eddy viscosity for all models was thus chosen as

$$\mu_{T_\infty} < 1.0 \times 10^{-9} \ kg/m/s$$

unless indicated otherwise. For the two-equation models, the further specification of a freestream turbulence intensity of 0.01% was used to determine the turbulent kinetic energy in the freestream from

$$k = \frac{1.2}{2}\left(\frac{Tu}{100} V_\infty\right)^2 = 6 \times 10^{-9} V_\infty^2.$$

Computational Mesh for the Flat Plate

A parabolic mesh has been used around the flat plate with the (x, y) Cartesian coordinate system fixed at the leading edge. This mesh topology mitigates the effects of the leading edge singularity. The parabolic coordinates ξ, η are related to the Cartesian coordinates as follows:

$$x = \alpha(\xi^2 - \eta^2) \qquad y = 2\alpha\xi\eta \qquad \alpha = 0.05$$

$$0 \le \xi \le \xi_{max} \qquad 0 \le \eta \le 1 \qquad \xi_{max} = \sqrt{1 + 1/\alpha}$$

The value of ξ_{max} has been determined by setting $x = 1$ at $\eta = 1$. This gives a mesh that is slightly longer than one meter along the flat plate. A uniform mesh is used in the ξ coordinate direction while a non-uniform mesh spacing is used in the η coordinate direction. The mesh spacing has been determined with the lower boundary stretching transformation of Roberts[21] (see also Ref. 22). Most of the results have been obtained with 80x160 cells. A coarser mesh of 40x80 and a finer mesh of 160x320 have been used to show that the 80x160 mesh provides results sufficiently accurate for the figures presented. A stretching parameter of $\beta = 1.001$ has been used for the one-equation models. This choice for β gives maximum y^+ values of approximately 2.3 for the coarse 40x80 mesh. As expected, the maximum allowable y^+ values for the two-equation models were found to be much smaller than for the one-equation models, with the larger values resulting in convergence problems. Thus a stretching parameter of $\beta = 1.00007$ was used giving $y^+ \le 0.2$ at the end of the plate for the coarse mesh.

Flat Plate Results with Standard Transition Method

For the freestream conditions and meshes specified above, the laminar/turbulent flow has been calculated with the SACCARA code and compared to the accurate laminar and turbulent results obtained for this case by Van Driest.[14,15] The standard transition method is used

where the laminar viscosity is the sole contributor to the effective viscosity upstream of the transition plane (x_t = 0.1196 m). The L2 norms of the residuals for both the momentum equations and the turbulence equations were reduced at least eight orders of magnitude in each case, suggesting that the results for the flat plate problem are not influenced by iterative convergence error.

Skin friction profiles have been obtained using all five turbulence models for the Mach 8 flat plate case. The Baldwin-Barth and both $k-\omega$ models give transition at the specified transition plane for the given freestream turbulence levels as shown in Fig. 1. In order to move the transition point to the desired location, the freestream eddy viscosity had to be increased to 1×10^{-6} kg/m/s for the Spalart-Allmaras model, and the turbulence intensity had to be increased to 0.1% for the low Reynolds number $k-\varepsilon$ model (see Fig. 2). All of the models which correctly predict turbulent flow downstream of the transition point also predict skin friction in this region in agreement with the theory.

Modified Transition Results for Spalart-Allmaras Model

Solutions have been obtained with the Spalart-Allmaras trip functions f_{t1}, f_{t2} set to zero. The flow is turbulent along the flat plate for this case with the freestream eddy viscosity μ_T varying from 10^{-9} to 10^{-5} *kg/m/s*. Solutions have been obtained with the trip function f_{t2} included and f_{t1} set to zero. For this case the flow transition location is dependent on the freestream eddy viscosity. When the eddy viscosity is 10^{-9} *kg/m/s*, the flow remains laminar over the length of the flat plate. As previously discussed, numerical solutions show that the flow can be maintained laminar by making the production term S_P zero by setting c_{b1} = 0 with the trip functions f_{t1}, f_{t2} set to zero.

The complete Spalart-Allmaras model has trip terms included to control the transition location, but the formulation is not intended to model the transition flow region. The behavior of this model has been investigated with the results for the local skin friction given in Fig. 3 where the trip location x_t is specified. The specified transition location corresponds to $Re_x = 3.84\times10^6$ while the numerical prediction has transition varying as the freestream eddy viscosity is increased above a value of approximately 10^{-9} *kg/m/s*. For these high speed flows, it is difficult to control the transition location with the suggested trip model. In addition, there is no control of the length of the transition region. Because of these experiences with the behavior of the Spalart-Allmaras trip model, different approaches have been investigated.

Three methods have been investigated to control the transition location and the length of transition as previously described. There are two parameters x_t and x_l introduced to control the transition behavior. The parameter x_t is at the middle of the transition region while $x_s = x_t - x_l$ is the location upstream where transition starts and the location downstream $x_e = x_t + x_l$ where the flow becomes fully turbulent. The values of these parameters are:

$$x_t = 0.1196\ m, \quad x_l = 0.1\ m, \quad Re_{x_t} = 3.84\times10^6$$

These locations are also indicated in Fig. 4.

The results for the skin friction with the three proposed approaches for modeling transition have been investigated. All of the methods remain laminar a significant distance after the specified start of transition. With Method 1, where the trip function f_{t2} is modified, transition occurs downstream of the desired location with very rapid transition onset. With Method 2. where the production coefficient c_{b1} is modified, transition occurs near the desired location with a reasonable variation of the skin friction in the transition region. With Method 3, where the production term coefficient $c_{b1}(1-f_{t2})$ is modified, transition occurs downstream of the desired transition location with very rapid transition onset. From this investigation it is concluded that Method 2 provides a reasonable technique to specify the transition location with limited control over the transition region length. The results for method 2 are presented in Fig. 4. When λ varies linearly over the transition region, there is better control. The transition control Method 2 appears to be insensitive to the freestream eddy viscosity. Other approaches need to be considered and evaluated.

Flow Predictions for Reentry F Vehicle

Reentry F Description and Experimental Results

The Reentry F flight experiment[23] was performed in 1968 to provide measurements of wall heat transfer rates at reentry flow conditions that cannot be obtained in ground-based experimental facilities. The data is for the flow over a slender conical vehicle where there is only a small amount of surface ablation localized at the nosetip. The boundary layer flow is laminar, transitional, or turbulent depending on the altitude and location along the body surface. The Reentry F vehicle was a 5 degree sphere-cone with an initial nose radius of 0.1 inch and the vehicle length is 13 feet. A graphite nosetip extended for the first 7.54 inches followed by a conical beryllium frustum. The heat transfer measurements were obtained at altitudes between 120,000 and 60,000 feet. The data at a flight time of 456.0 seconds or an alti-

tude of 80,000 feet (24.383 km) is used to validate the turbulence model predictions. Although this flight experiment provides exceptional data, there are many aspects of the flow conditions, body orientation, body shape, and wall surface temperature that are not completely or precisely known.

In recent years, this experimental data set has been reevaluated with modern computational codes and is documented in Refs. 24-26. Aerothermal predictions have also been presented in these papers. It is important to observe that the freestream conditions for the three predictions are slightly different and the wall temperature in some cases is constant while in others a variation is taken into account. Most of these solutions are for axisymmetric flow with the vehicle at zero degree angle of attack, but full three-dimensional solutions have been obtained with the actual flight angle of attack of 0.14 degrees. There are many details of this flight experiment that are not well defined, but overall the heat transfer predictions are in reasonable agreement with the flight measurements. Of course, none of the modeling includes a capability to predict the transition location. Further information on the flight experiment is given in Wright and Zoby.[23]

The flow conditions at an altitude of 80,000 feet have become the location in the flight trajectory most often analyzed and are also chosen for the present investigation. The present freestream conditions are based on the U. S. Standard Atmosphere, 1976.[20] The assumed turbulent eddy viscosity is given as well as the turbulence intensity for the two-equation models. The freestream flow conditions (in SI units) that have been used in are

$$M_\infty = 19.97, \qquad \alpha = 0^\circ, \qquad \rho_\infty = 0.043523$$

$$T_\infty = 221.034, \qquad T_w = 500, \qquad p_\infty = 2761.41$$

$$V_\infty = 5951.858, \qquad a_\infty = 298.04$$

$$\mu_\infty = 1.445 \times 10^{-5}, \qquad \mu_T = 3.3227 \times 10^{-14}$$

$$Tu = 0.01\%, \qquad x_{body} = 4.0$$

Note that there is some amount of uncertainty in the specification of these properties.

The nosetip of the vehicle is graphite and initially is a sphere-cone with a nose radius $R_N = 0.00254$ *m*. Due to ablation, the nose radius increases to 0.00343 *m* at an altitude of 80,000 feet. This result is an estimated value from an ablation analysis of the nosetip.[26] For the present analysis, it is assumed that the nosetip shape remains a sphere-cone after ablation with the same cone half angle as the conical vehicle, which is $\theta_{cone} = 5^\circ$. The nosetip is illustrated below. The origin in this figure is located at the virtual tip of the conical vehicle. For the approximated sphere-cone configuration for the Reentry

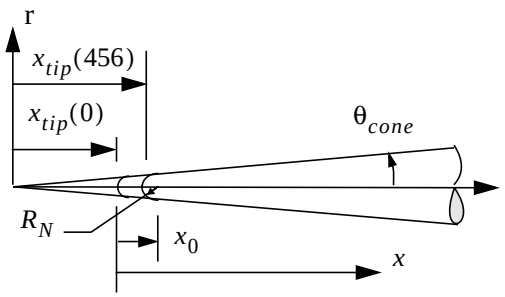

F vehicle simulation, the location of the original nosetip and ablated nosetip is specified as

$$x_0 = 0.012752\ m, \qquad x_{tip}(0) = 0.026603\ m$$

$$x_{tip}(456) = 0.035925\ m$$

In previous analyses of this vehicle, the coordinate x is defined as the axial distance without a clear definition of the origin location given in many cases. Some figures indicate that the origin is located at the ablated nose of the body. The axial location x in this paper is measured from the *nosetip of the un-ablated vehicle*. The uncertainty in the location of the axial heat flux measurements has a negligible impact on the results presented.

Due to the high velocities, the gas temperature is more than 6000 *K* in the nosetip region with dissociation of the oxygen and nitrogen occurring. Downstream of the nose the inviscid flow temperature behind the shock is 420 K, and perfect gas flow occurs. However, in the boundary layer the viscous dissipation increases the gas temperature to around 3000 *K* and dissociation of oxygen occurs. At 80,000 feet, the chemical reactions are sufficiently fast that the air is assumed to be in local thermochemical equilibrium. This is believed to be a reasonable assumption, but a finite rate solution needs to be performed in the future to validate this simplification. There is also some ablation of the nosetip which introduces chemical species from the ablation products into the boundary layer flow. As the amount of ablation is small, this influence has been neglected.

Predictions of Wall Heat Flux for Reentry F Vehicle

Simulation Code and Model Approach

The flow around the Reentry F vehicle has been determined with the SACCARA[6-9] Navier-Stokes code. This investigation is concerned with obtaining accurate numerical solutions of the wall heat flux based upon the input conditions to the code and models used in the simulation. The wall heat flux predictions are then compared with the flight measurements at an altitude of 80,000 feet. The solution is for the flow over the ablated vehicle. The small angle of attack of the vehicle (0.14°) is neglected and the flow is assumed to be axisymmetric. The solutions use a gas model of air in local thermochemical equilibrium and the flow is laminar over the

front part of the body. The flow transitions to turbulent flow at a specified location. The turbulent flow has been modeled with the Baldwin-Barth and Spalart-Allmaras one-equation eddy viscosity approaches and the low Reynolds number $k-\varepsilon$, Menter $k-\omega$, and Wilcox (1998) $k-\omega$ two-equation turbulence models. The solutions have been obtained on three meshes to judge the spatial convergence of the solution. The L2 norms of the momentum and turbulence transport equations exhibited oscillatory behavior after only a two or three order of magnitude drop, thus another method was needed to monitor convergence. The iterative convergence has been initially determined by plotting the wall heat flux at various number of time steps and assuming convergence has been obtained when there is no noticeable change in the results. Further analysis of the steady-state solution error of the wall heat flux has shown that additional time steps are required to obtain adequate steady-state solutions.

Transition Model

As previously discussed, the basic SACCARA code treats the transition process by setting the effective viscosity to the laminar value upstream of a specified transition plane, while downstream of this plane the effective viscosity is the sum of both the laminar and turbulent viscosities. This approach has been used with the Baldwin-Barth one-equation eddy viscosity model and all two-equation models. The transition plane is specified to be perpendicular to the vehicle axis and located at $x = 2.6\ m$. With the Spalart-Allmaras one-equation eddy viscosity model, a different approach has been implemented as described previously, with $x_s = 1.8844\ m$ and $x_e = 2.8844\ m$. From the results of the investigation of the flat plate flow case, it was concluded that Method 2 (coefficient c_{b1} is varied) is the best approach to control the transition process with the Spalart-Allmaras model at this time.

Iterative Convergence of the Numerical Solutions

At an altitude of 80,000 feet, steady-state solutions on three meshes have been obtained by marching the solution in time until there is no further change in the plotted solution. This method is illustrated in Fig. 5 for the coarse Mesh 0-rg (100x40) with the Spalart-Allmaras turbulence model. The laminar flow region takes the longest time to converge as there is a very fine mesh in the wall region. With Mesh 0-rg, the wall heat flux appears to have no significant changes after 4000 time steps. The iterative convergence with Mesh 1-rg (200x80) is shown in Fig. 6, while the behavior of Mesh 2-rg (400x160) is given in Fig. 7. With Mesh 1-rg, the wall heat flux appears to have no significant changes after 7000 time steps while Mesh 2-rg requires approximately 14,000 time steps. However, the results shown in these figures are misleading! A more careful analysis has been performed to estimate the iterative convergence error.

The accuracy of the wall heat flux q^n relative to the steady-state value is determined by expressing the numerical solution at time t^n as

$$q^n = q(t^n) = q_E + \varepsilon^n \tag{18}$$

The exact steady-state value of the wall heat flux is q_E and the convergence error at time t^n is ε^n. The convergence error has been observed to have an exponential decrease in time which gives the following variation as the solution approaches a steady state:

$$\varepsilon^n = \alpha e^{-\beta t^n} \tag{19}$$

Eq. (18) and Eq. (19) are rewritten as

$$\beta t^n = \ln\alpha - \ln(q^n - q_E) \tag{20}$$

Eq. (20) is evaluated at three times, $(n-1)$, n, and $(n+1)$, and the three relations are used to eliminate α and obtain

$$\beta(t^n - t^{n-1}) = \ln[(q^{n-1} - q_E)/(q^n - q_E)]$$
$$\beta(t^{n+1} - t^n) = \ln[(q^n - q_E)/(q^{n+1} - q_E)]$$

If the time increments are equal, then $(t^n - t^{n-1}) = (t^{n+1} - t^n)$ and the above becomes

$$(q^{n-1} - q_E)(q^{n+1} - q_E) = (q^n - q_E)^2$$

The exact steady-state value of the wall heat flux is solved for in the above equation which gives

$$q_E = \frac{q^n - \Lambda^n q^{n-1}}{1 - \Lambda^n}, \qquad \Lambda^n = \frac{(q^{n+1} - q^n)}{(q^n - q^{n-1})} \tag{21}$$

The iterative convergence error becomes

$$\varepsilon^n = -(q^{n+1} - q^n)/(1 - \Lambda^n)$$

and the percent convergence error relative to the exact steady-state value becomes

$$\%\ \text{Error of}\ q^n = -100\left[\frac{q^{n+1} - q^n}{q^n - \Lambda^n q^{n-1}}\right] \tag{22}$$

The foregoing results closely follow the works of Ferziger and Peric[27,28] for determining the convergence error of the numerical iterative solution of difference equations, but their results have been obtained with a different approach. In their work, the parameter Λ^n is the spectral radius (or the magnitude of the largest

eigenvalue) of the iteration matrix. If the eigenvalues are complex, the present approach is not appropriate. The complex eigenvalue case has been considered by Ferziger and Peric.

The above procedure is illustrated for the wall heat flux solution at $x = 2.14892$ m (where the flow is laminar) using the Spalart-Allmaras model. The percent error is shown in Fig. 8 for the three meshes. The percent error obtained from Eq. (22) is indicated by the symbols while the lines are the percent error obtained from the best estimate of the exact solution given by Eq. (21). The initial solution results on the finest mesh (Mesh 2-rg shown in Fig. 7) appeared converged at 10,000 iterations; however, based on the above error analysis, an additional 15,000 iterations were needed to get the error below 0.1%. The flow solution for Reentry F has also been obtained with three meshes (Mesh 0-f, Mesh 1-f and Mesh 2-f) with the same number of cells, but finer spacing near the wall than was used with Mesh rg. Results of iterative convergence similar to Fig. 5, Fig. 6, and Fig. 7 are obtained except the number of time steps is increased significantly for the solutions with finer near-wall spacing. The iterative convergence error for Mesh f is given in Fig. 9. The iterative solution errors are much smaller than the spatial solution errors, as will be demonstrated.

The iterative convergence for the two-equation turbulence models was also examined for Meshes 0-2eq (130x40 cells), 1-2eq (260x80 cells), and 2-2eq (520x160 cells). Results are presented for the low Reynolds number $k-\varepsilon$ model (Fig. 10), the Menter $k-\omega$ model (Fig. 11), and the Wilcox (1998) $k-\omega$ model (Fig. 12). There is some scatter in the symbols due to the fact that the time increments were not always equal. A larger number of iterations were required due to the stricter y^+ requirements for Mesh 2eq verses the one-equation meshes (Mesh rg and Mesh f). The two-equation results were all converged to less than 0.4% error, which is again much smaller than the grid convergence error.

Spatial Convergence of the Numerical Solutions

Spatial convergence has been judged from the steady-state solutions on the three meshes, 0, 1, and 2 (from coarsest to finest). The wall heat flux obtained with the Spalart-Allmaras turbulence model for the three meshes is given in Fig. 13 with the variable spacing given by Mesh rg. The Richardson extrapolation procedure[29] has been used to obtain a more accurate result from the relation

$$q_{RE} = q_{1,2} = q_2 + (q_2 - q_1)/3. \qquad (23)$$

The above relation assumes that the numerical scheme is second-order. The Richardson extrapolation result q_{RE} and the solution on Mesh 2-rg are nearly the same (also shown in Fig. 13). The accuracy of the solutions on the three meshes has been estimated with the exact solution approximated with q_{RE} which gives the solution error as

$$\%\ \text{Error of } q_M = 100(q_M - q_{RE})/q_{RE} \quad M = 1, 2, 3$$

If the mesh has been refined sufficiently where the solution error has second-order behavior, then the errors on the three meshes have the following relationship

$$\%\ \text{Error of } q_2 = \frac{\%\ \text{Error of } q_1}{4} = \frac{\%\ \text{Error of } q_0}{16} \qquad (24)$$

In the above equation, the first equality will always be satisfied when Eq. (23) has been used. The second equality will only be satisfied if the mesh has been sufficiently refined to be in the asymptotic range. The percent error of the wall heat flux along the vehicle is presented in Fig. 14. The laminar flow solution region is in the asymptotic range while the turbulent flow region is not in the asymptotic range. The wall heat flux prediction in the laminar flow region is more accurate than the heat flux prediction in the turbulent flow region.

For Mesh f, spatial convergence has been judged from the steady-state solutions on the three meshes 0, 1, and 2. Richardson extrapolation procedure has been used to obtain a more accurate result. The accuracy of the solutions on the three meshes has been estimated with the exact solution approximated with the Richardson extrapolated result q_{RE} and these results are given in Fig. 15. Again, the laminar flow solution region is in the asymptotic range while the turbulent flow region is not always in the asymptotic range. The wall heat flux prediction in the laminar flow region with Mesh f is less accurate than the results with Mesh rg. The heat flux predictions in the turbulent flow region with Mesh f are more accurate than the results with Mesh rg. Only the solution on Mesh 2-f is considered sufficiently accurate for comparison with the flight measurements and the Richardson extrapolated results provide even a more accurate numerical prediction.

Spatial convergence has also been examined for the three two-equation models. The spatial error of the heat flux is given in Figs. 16-18 for the low Reynolds number $k-\varepsilon$, the Menter $k-\omega$, and the Wilcox (1998) $k-\omega$ models, respectively. The spatial error in the laminar regions is generally below 2%, while in the turbulent regions it varies from approximately 2% for the $k-\varepsilon$ model to 4% for the $k-\omega$ models. The results for the $k-\omega$ models indicate that the heat flux is not fully grid independent in the turbulent region. The spike in the error for the two-equation models is due to movement of the transition location on the different size

meshes and is more apparent for the two-equation models due to the fine axial spacing around the transition point.

Wall Heat Flux

The predictions of the wall heat flux on the Reentry F vehicle at an altitude of 80,000 feet with the one-equation turbulence models are given in Fig. 19 along with the flight data. The Spalart-Allmaras prediction uses the numerical solution with Mesh 2-f and the Richardson extrapolation results for this case. The simulation overpredicts the laminar wall heat flux by roughly 10 percent while the turbulent wall heat flux is overpredicted by roughly 15 percent. At this altitude the vehicle has a 0.14 degree angle of attack and the heat transfer measurements were made on the leeward side of the conical body. A full three-dimensional solution, with the vehicle at angle of attack, would bring the prediction and flight data into closer agreement. The prediction with Mesh 2-f is believed to be a sufficiently accurate steady-state solution that it can be used to validate the turbulence model, but there are small errors in these results due to uncertainty in information used in the simulation as discussed previously.

The Baldwin-Barth turbulence model prediction (also shown in Fig. 19) uses the numerical solution with Mesh 2-rg where the wall temperature is not maintained at 500K. However, these heat transfer results are not expected to be influenced much by this inaccurate wall temperature. The simulation with the Baldwin-Barth turbulence model overpredicts the laminar wall heat flux by roughly 10 percent and is in agreement with the simulation with the Spalart-Allmaras model. Of course, in the laminar flow region the turbulence models should have no impact on the flow solution. The turbulent wall heat flux is overpredicted by roughly 100 percent with the Baldwin-Barth turbulence model. It is recommended that the Spalart-Allmaras model should be used rather than the Baldwin-Barth turbulence model for reentry flows.

Results with the Nagano and Hishida $k-\varepsilon$, the Menter $k-\omega$, and the Wilcox (1998) $k-\omega$ models are presented in Fig. 20. Fine grid results with Mesh 2eq are shown along with the results from Richardson extrapolation. The $k-\varepsilon$ results show an overprediction of the turbulent heating rates by approximately 100%. The two $k-\omega$ models show better agreement with the flight data, with the Menter model within 40% and the Wilcox (1998) model within 30% of the data. All three models display a peak in the turbulent heating just downstream of the specified transition plane, which is possibly due to crude transitional behavior of the standard method.

The present simulations have been performed with a gas model that assumes the air flow is in local thermochemical equilibrium. This study needs to be extended to include solutions obtained with a nonequilibrium thermochemical gas model for air. This type of simulation introduces the modeling of the heterogeneous chemical reactions at the vehicle surface and vibrational nonequilibrium effects.

Conclusions

Many Navier-Stokes codes require that the governing equations be written in conservation form with a source term. The Spalart-Allmaras one-equation model was originally developed in substantial derivative form and when rewritten in conservation form, a density gradient term appears in the source term. This density gradient term causes numerical problems and has a small influence on the numerical predictions. Further work has been performed to understand and to justify the neglect of this term.[11,16] The transition trip term has been included in the one-equation eddy viscosity model of Spalart-Allmaras. Several problems with this model have been discovered when applied to high-speed flows.

For the Mach 8 flat plate boundary layer flow with the standard transition method, the Baldwin-Barth and both $k-\omega$ models gave transition at the specified location. The Spalart-Allmaras and low Reynolds number $k-\varepsilon$ models required an increase in the freestream turbulence levels in order to give transition at the desired location. All models predicted the correct skin friction levels in both the laminar and turbulent flow regions.

For Mach 8 flat plate case, the transition location could not be controlled with the trip terms as given in the Spalart-Allmaras model. Several other approaches have been investigated to allow the specification of the transition location. The approach that appears most appropriate is to vary the coefficient that multiplies the turbulent production term in the governing partial differential equation for the eddy viscosity (Method 2). When this coefficient is zero, the flow remains laminar. The coefficient is increased to its normal value over a specified distance to crudely model the transition region and obtain fully turbulent flow. While this approach provides a reasonable interim solution, a separate effort should be initiated to address the proper transition procedure associated with the turbulent production term. Also, the transition process might be better modeled with the Spalart-Allmaras turbulence model with modification of the damping function f_{v1}. The damping function could be set to zero in the laminar flow region and then turned on through the transition flow region.

Predictions have been obtained for the Reentry F flight vehicle with both one- and two-equation turbulence models where the transition location is specified *a priori*. The axisymmetric turbulent predictions for wall

heat flux with the Spalart-Allmaras, Menter $k-\omega$, and Wilcox (1998) $k-\omega$ models are in reasonable agreement with the flight measurements. The mesh sensitivity has been evaluated by obtaining results on three meshes and more accurate results have been obtained with Richardson extrapolation. The simulation assumes the vehicle is at zero degree angle-of-attack while in fact, the flight vehicle is at 0.14 degree angle-of-attack. For the one-equation models, the Spalart-Allmaras model predictions for this case are much better than the results from the Baldwin-Barth model. For the two-equation models, both $k-\omega$ models give good agreement with the flight data, while the low Reynolds number $k-\varepsilon$ model greatly overpredicts the heating in the fully turbulent region.

Future Work

The Reentry F calculations need to be extended to the finite rate chemistry model. This modification should help to determine if the equilibrium air assumption is appropriate and will help determine if the turbulence model with finite chemistry is reasonable. The present Reentry F calculations have assumed a constant wall temperature and this assumption needs to be improved. As there is only limited flight information on the wall temperature and no data in the nose region, a coupled fluid/heat-conduction analysis is needed to provide the wall temperature variation along the vehicle. Further work could be done to modify the transition mechanism for the two-equation models along the lines of the Spalart-Allmaras modifications presented herein. Finally, including a realizeability limitation has been shown to improve predictions for flows with large normal stresses[30] and may also improve predictions through strong normal shocks.

Acknowledgments

This work was supported by Sandia National Laboratories and the Department of Energy's Accelerated Strategic Computing Initiative.

References

1. D. C. Wilcox, *Turbulence Modeling for CFD, 2nd Ed.*, DCW Industries, Inc. 5354 Palm Drive, La Canada, CA 91011, 1998.

2. R. Peyret (Editor), *Handbook of Computational Fluid Mechanics*, Academic Press, San Diego, CA, 1996.

3. A. J. Smits and J.-P. Dussauge, *Turbulent Shear Layers in Supersonic Flow*, American Institute of Physics, Woodbury, New York, NY, 1996.

4. P. R. Spalart and S. R. Allmaras, "A One-Equation Turbulence Model for Aerodynamic Flows," AIAA Paper 92-0439, 1992.

5. P. R. Spalart and S. R. Allmaras, "A One-Equation Turbulence Model for Aerodynamic Flows," *La Recherche Aerospatiale*, No. 1, pp. 5-21, 1994.

6. C. C. Wong, F. G. Blottner, J. L. Payne, and M. Soetrisno, "Implementation of a Parallel Algorithm for Thermo-Chemical Nonequilibrium Flow Solutions," AIAA Paper 95-0152, Jan. 1995.

7. Wong, C. C., Soetrisno, M., Blottner, F. G., Imlay, S. T., and Payne, J. L., "PINCA: A Scalable Parallel Program for Compressible Gas Dynamics with Nonequilibrium Chemistry," SAND 94-2436, Sandia National Laboratories, Albuquerque, NM, 1995.

8. B. Hassan, D. W. Kuntz, and D. L. Potter, "Coupled Fluid/Thermal Prediction of Ablating Hypersonic Vehicles," AIAA Paper No. 98-0168, Jan. 1998.

9. D. W. Kuntz, B. Hassan, and D. L. Potter, "An Iterative Approach for Coupling Fluid/Thermal Predictions of Ablating Hypersonic Vehicles," AIAA Paper 99-3460, June-July 1999.

10. B. S. Baldwin and T. J. Barth, "A One-Equation Transport Model for High Reynolds Number Wall-Bounded Flows," NASA TM-102847, Aug. 1990.

11. F. R. Menter, "Eddy Viscosity Transport Equations and Their Relation to the $k-\varepsilon$ Model," *Journal of Fluids Engineering*, Vol. 119, Dec. 1997, pp. 876-884.

12. Y. Nagano and M. Hishida, "Improved Form of the $k-\varepsilon$ Model for Wall Turbulent Shear Flows." *Journal of Fluids Engineering*, Vol. 109, pp 156-160, June 1987.

13. F. R. Menter, "Two-Equation Eddy-Viscosity Turbulence Models for Engineering Applications," *AIAA Journal*, Vol. 32, No. 8, Aug. 1994, pp. 1598-1605.

14. E. R. Van Driest. "Investigation of Laminar Boundary Layer in Compressible Fluids Using the Crocco Method," National Advisory Committee for Aeronautics, NACA TN-2597, January 1952.

15. E. R. Van Driest, "Problem of Aerodynamic Heating," *Aeronautical Engineering Review*, Vol. 15, No. 10, pp. 26-41, Oct. 1956.

16. F. R. Menter, H. Grotjans, and F. Unger, "Numerical Aspects of Turbulence Modeling for the Reynolds Averaged Navier-Stokes Equations," *Computational Fluid Dynamics Lecture Series* 1997-02, von Karman Institute for Fluid Dynamics, March 3-7, 1997.

17. B. E. Launder and B. E. Sharma, "Application of the Energy Dissipation Model of Turbulence to the Calculation of Flow Near a Spinning Disc," *Letters in Heat and Mass Transfer*, Vol. 1, No. 2, pp. 131-138.

18. G. Theodoridis, P. Prinos and A. Goulas, "Test Case T3 - Free Stream Turbulence," in *Numerical Simulation of Unsteady Flows and Transition to Turbulence*, Edited by O. Pironneau, W. Rodi, I. L. Ryhming, A. M. Savill, and T. V. Truong, Cambridge University press, 1992.

19. D. C. Wilcox, "Reassessment of the Scale Determining Equation for Advanced Turbulence Models," *AIAA Journal*, Vol. 26, No. 11, 1988, pp. 1299-1310.

20. *US Standard Atmosphere*, National Oceanic and Atmospheric Administration, NASA, and the U. S. Air Force, Washington, D. C., October 1976.

21. G. O. Roberts, "Computational Meshes for Boundary Layer Problems," Proceedings of the Second International Conference on Numerical Methods in Fluid Dynamics, *Lecture Notes in Physics*, Vol. 8, Springer-Verlag, New York, pp. 171-177.

22. J. C. Tannehill, D. A. Anderson, and R. H. Pletcher, *Computational Fluid Mechanics and Heat Transfer*, Taylor & Francis, Bristol, PA, 1997, p. 335.

23. R. L. Wright and E. V. Zoby, "Flight Boundary-Layer Transition Measurements on Slender Cone at Mach 20," AIAA Paper 77-719, June 27-29, 1977.

24. K. Sutton, E. V. Zoby and H. H. Hamilton, "Overview of CFD Methods and Comparison with Flight Aerothermal Data," *AGARD Symposium on Validation of Computational Fluid Dynamics*, Lisbon, Portugal May 2-5, 1988.

25. R. A Thompson, E. V. Zoby, K. E. Wurster, P. A. Gnoffo, "Aerothermodynamic Study of Slender Conical Vehicles," *Journal of Thermophysics and Heat Transfer*, Vol. 3, pp. 361-367, October 1989.

26. K. E. Wurster, E. V. Zoby, and R. A. Thompson, "Flow and Vehicle Parameter Influence on results of Engineering Aerothermal Methods," *AIAA Journal of Spacecraft and Rockets*, Vol. 28, Jan.-Feb. 1991, pp. 16-22.

27. J. H. Ferziger and M. Peric, *Computational Methods for Fluid Dynamics*, Springer-Verlag, Berlin, Heidelberg, and New York, 1996.

28. J. H. Ferziger and M. Peric, "Further Discussion of Numerical Errors in CFD," *International Journal for Numerical Methods in Fluids*, Vol. 23, pp. 1263-1274, 1996.

29. P. Roache, "Ch. 3: A Methodology for Accuracy Verification of Codes: the Method of Manufactured Solutions," *Verification and Validation in Computational Science and Engineering*, Hermosa Publishers, New Mexico, 1998.

30. J. G. Moore and J. Moore, "Realizeability in Two-Equation Turbulence Models," AIAA Paper 99-3779, June-July 1999.

Figures

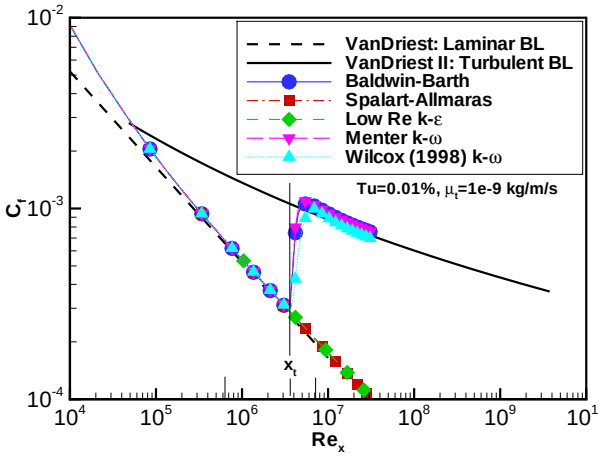

Fig. 1: Transition location with one- and two-equation turbulence models for Mach 8 flat plate flow with the standard transition model.

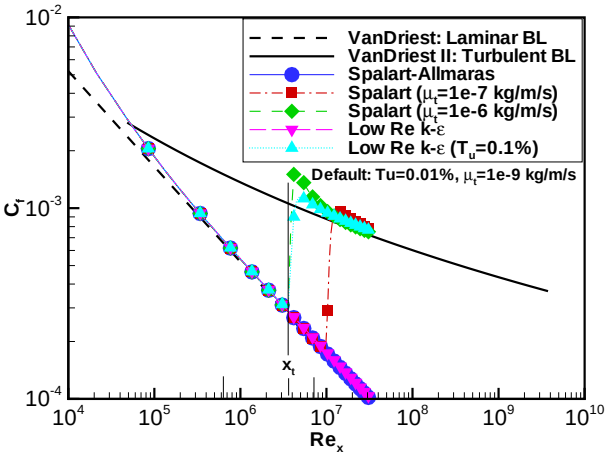

Fig. 2: Transition location for various freestream turb. levels with the Spalart-Allmaras and $k-\varepsilon$ turb. models for Mach 8 flat plate flow.

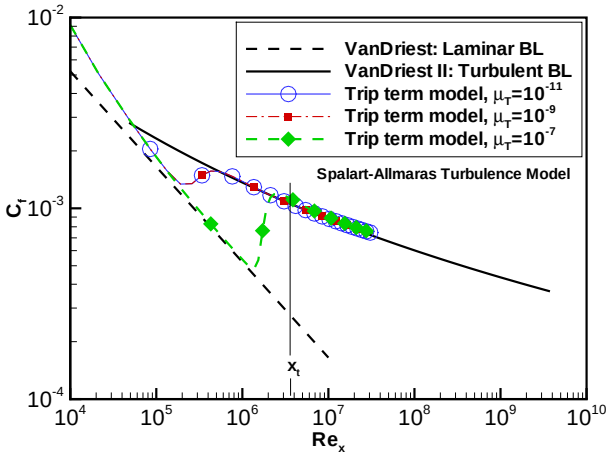

Fig. 3: Transition location for different freestream eddy viscosities with the Spalart-Allmaras turbulence model for Mach 8 flat plate flow.

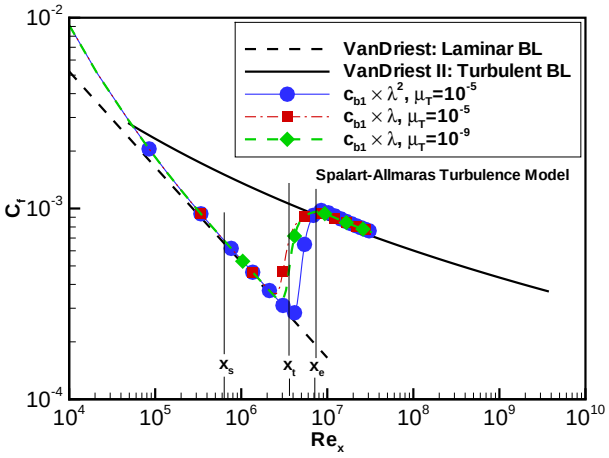

Fig. 4: Transitional flow behavior for Spalart-Allmaras (Meth. 2) with various freestream eddy viscosities for Mach 8 flat plate flow.

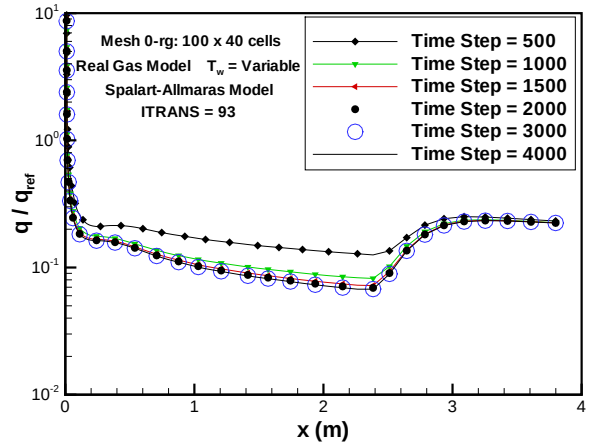

Fig. 5: Iterative convergence of heat flux on *Mesh 0-rg* with the Spalart-Allmaras turbulence model.

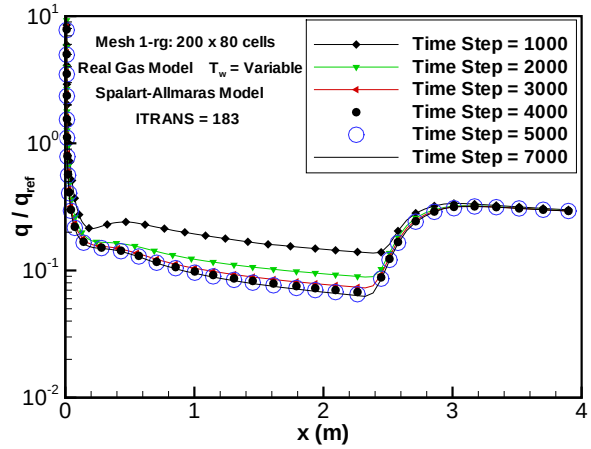

Fig. 6: Iterative convergence of heat flux on Mesh 1-rg with the Spalart-Allmaras turbulence model.

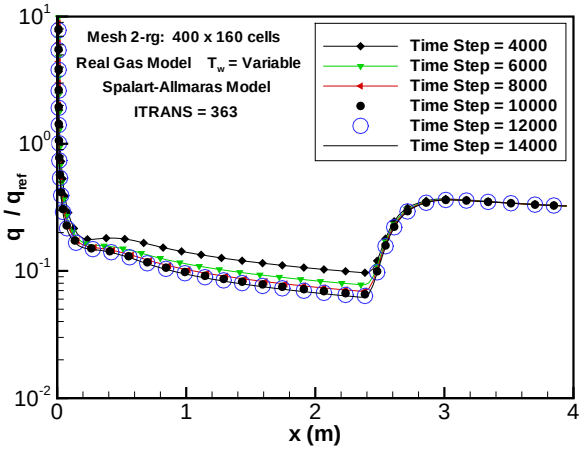

Fig. 7: Iterative convergence of heat flux on Mesh 2-rg with the Spalart-Allmaras turbulence model.

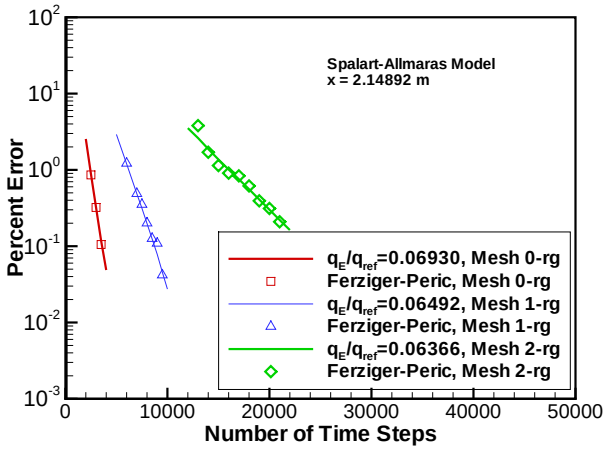

Fig. 8: Iterative convergence error of wall heat flux for the Spalart-Allmaras model at x = 2.14892 m with Mesh rg.

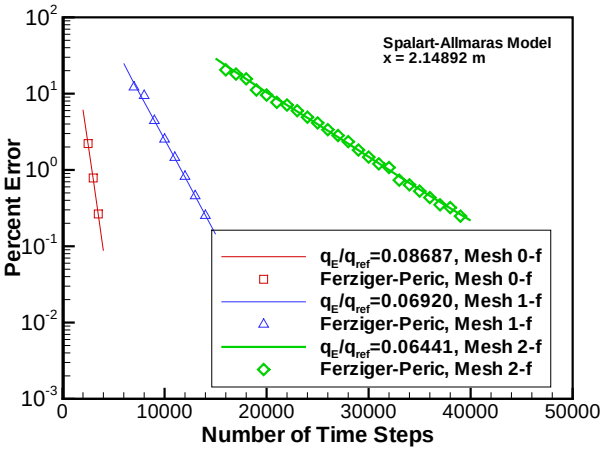

Fig. 9: Iterative convergence error of wall heat flux for the Spalart-Allmaras model at x = 2.14892 m with Mesh f.

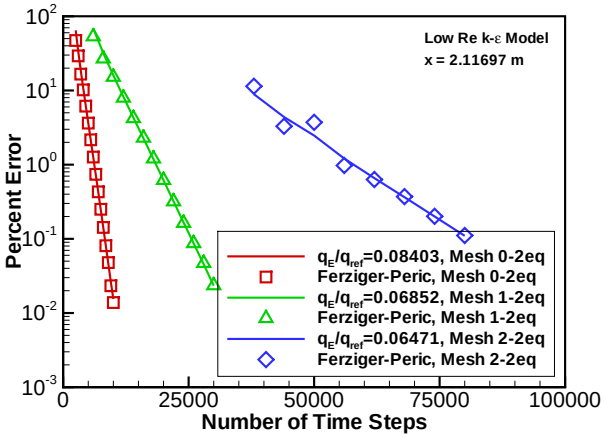

Fig. 10: Iterative convergence error of wall heat flux for the $k-\varepsilon$ model at x = 2.11697 m with Mesh 2eq.

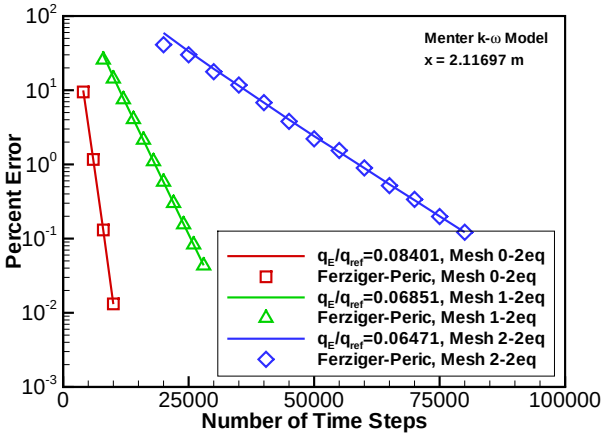

Fig. 11: Iterative convergence error of wall heat flux for the Menter $k-\omega$ model at x = 2.11697 m with Mesh 2eq.

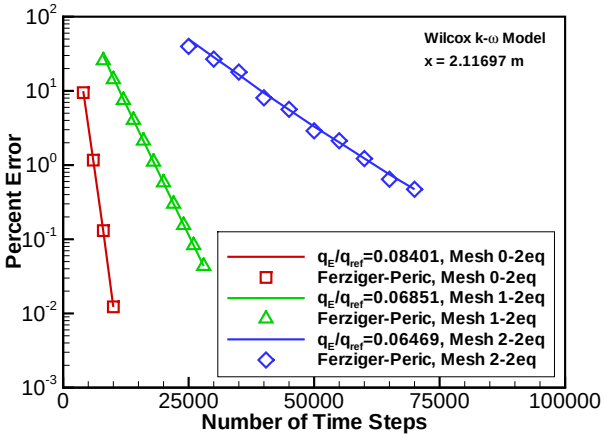

Fig. 12: Iterative convergence error of wall heat flux for the Wilcox (1998) $k-\omega$ model at x = 2.11697 m with Mesh 2eq.

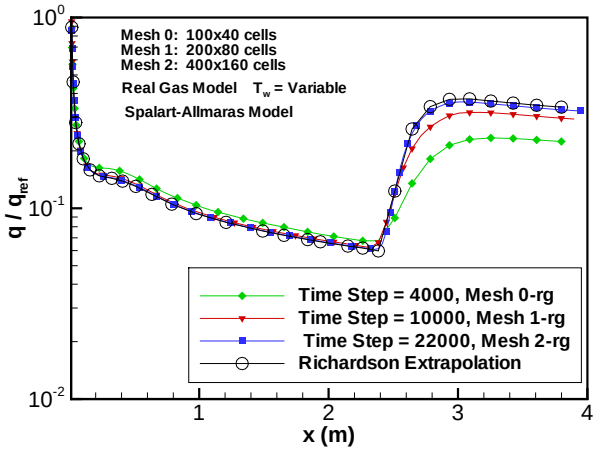

Fig. 13: Spatial convergence of heat flux as the Mesh rg is refined with the Spalart-Allmaras turbulence model.

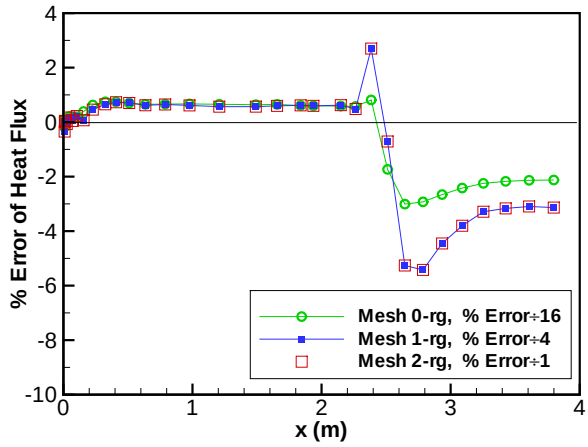

Fig. 14: Error in heat flux along the vehicle with Mesh rg refinement using the Spalart-Allmaras model.

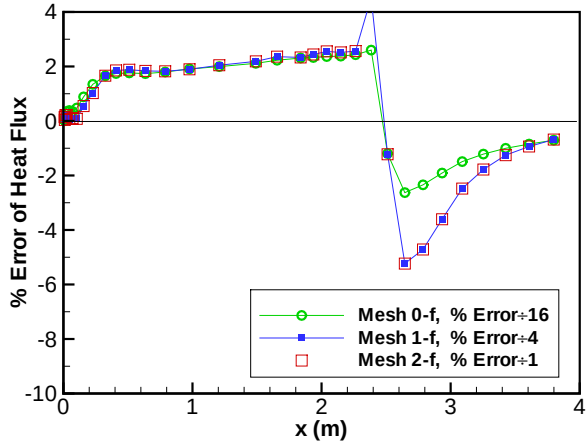

Fig. 15: Error in heat flux along the vehicle with Mesh f refinement using the Spalart-Allmaras model.

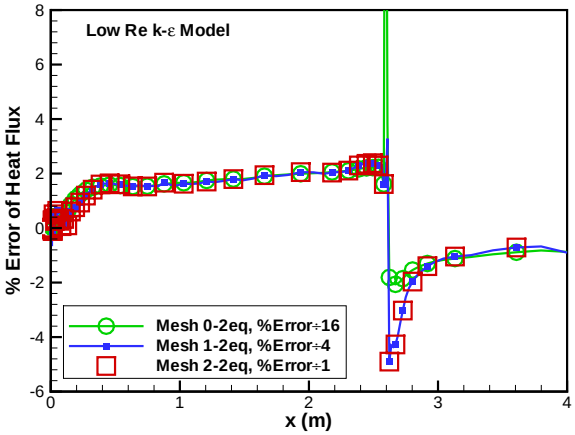

Fig. 16: Error in heat flux along the vehicle with Mesh 2eq refinement using the low Reynolds number $k-\varepsilon$ model.

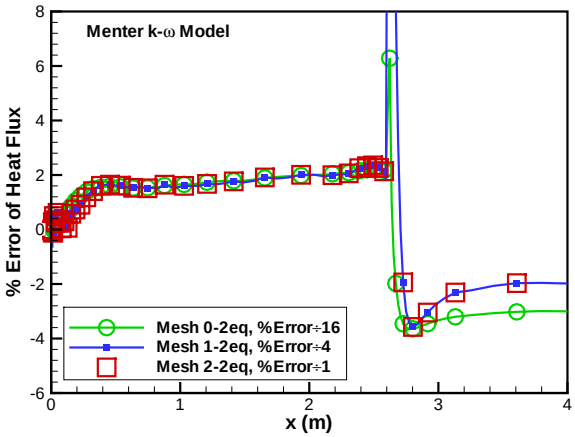

Fig. 17: Error in heat flux along the vehicle with Mesh 2eq refinement using the Menter $k-\omega$ model.

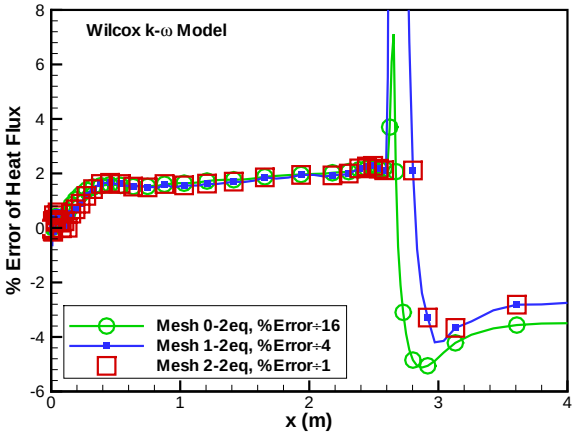

Fig. 18: Error in heat flux along the vehicle with Mesh 2eq refinement using the Wilcox (1998) $k-\omega$ model.

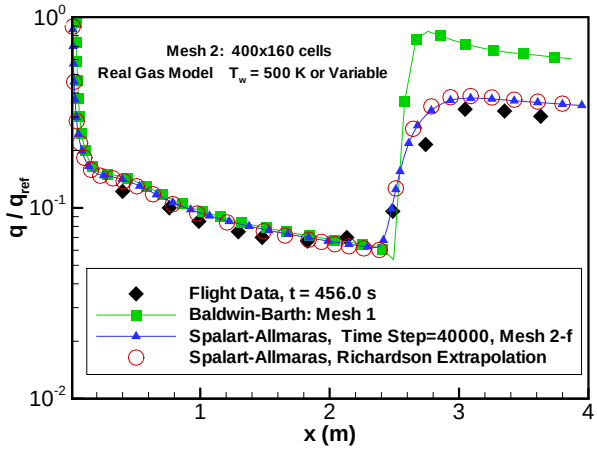

Fig. 19: Comparison of flight data for wall heat flux along Reentry F vehicle at an altitude of 80,000 feet with predictions of the one-equation turbulence models.

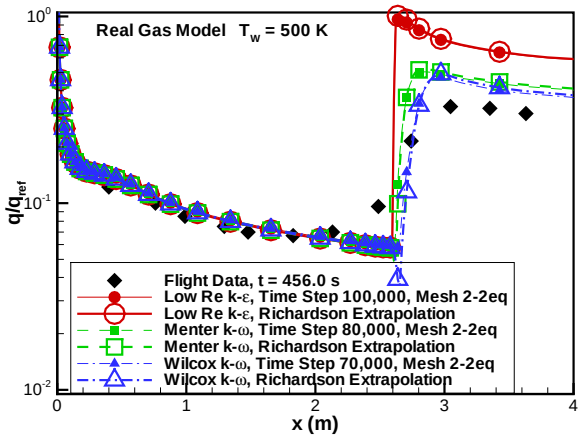

Fig. 20: Comparison of flight data for wall heat flux along Reentry F vehicle at an altitude of 80,000 feet with predictions of the two-equation turbulence models.

ASSESSMENT OF ONE- AND TWO-EQUATION TURBULENCE MODELS FOR HYPERSONIC TRANSITIONAL FLOWS

Christopher J. Roy‡ and Frederick G. Blottner†

Sandia National Laboratories*

P. O. Box 5800, MS 0835

Albuquerque, NM 87185

Abstract

A number of one- and two-equation turbulence models are examined for hypersonic perfect- and real-gas flows with laminar, transitional, and turbulent flow regions. These models were generally developed for incompressible flows, and the extension to the hypersonic flow regime is discussed. In particular, inconsistencies in the formulation of diffusion terms for one-equation models are examined. For the Spalart-Allmaras model, the standard method for forcing transition at a specified location is found to be inadequate for hypersonic flows. An alternative transition method is proposed and evaluated for a Mach 8 flat plate test case. This test case is also used to evaluate three different two-equation turbulence models: a low Reynolds number $k-\varepsilon$ model, the Menter $k-\omega$ formulation, and the Wilcox (1998) $k-\omega$ model. These one- and two-equation models are then applied to the Mach 20 Reentry F flight vehicle. The Spalart-Allmaras model and both $k-\omega$ formulations are found to provide good agreement with the flight data for heat flux, while the Baldwin-Barth and low Reynolds number $k-\varepsilon$ models overpredict the turbulent heating rates. Careful attention is given to solution verification in the areas of both iterative and grid convergence.

Nomenclature

a	speed of sound, *m/s*
D	turbulence diffusion term
d	distance to the wall, *m*
k	specific turbulent kinetic energy, m^2/s^2
Pr_T	turbulent Prandtl number (= 1.0)
p	pressure, N/m^2
q	heat flux, W/m^2
R_N	vehicle nose radius, *m*
r	radial coordinate, *m*
S_P	turbulence production source term
S_D	turbulence destruction source term
S_{ij}	strain rate tensor, *1/s*
T	temperature, *K*
Tu	freestream turbulence intensity percent
t	time, *s*
U	conserved transport quantity
u_i	velocity, *m/s*
V	velocity magnitude, *m/s*
x	axial coordinate, *m*
y	wall normal direction, *m*
α	angle of attack, *degrees*
γ	ratio of specific heats
δ_{ij}	Kronecker delta function (= 1 when $i=j$)
ε	specific dissipation rate, m^2/s^3
θ_{cone}	cone half-angle, *degrees*
μ	absolute viscosity, $N\cdot s/m^2$
ν	kinematic viscosity, m^2/s
$\tilde{\nu}$	Spalart-Allmaras working variable
ρ	density, kg/m^3
τ_{ij}	turbulent stress tensor, m^2/s^2
φ	non-conserved transport quantity
Ω_{ij}	rotation tensor, *1/s*
ω	specific turbulent frequency, *1/s*

Subscripts

E	exact value
eff	effective value (turbulent + laminar)
RE	Richardson extrapolation
ref	reference value

---

‡ Senior Member of Technical Staff, Member AIAA

† Distinguished Member of Technical Staff, AIAA Fellow

* Sandia is a multiprogram laboratory operated by Sandia Corporation, a Lockheed Martin Company, for the United States Department of Energy under Contract DE-AC04-94AL85000.

T	turbulent quantity
t	transitional quantity
w	wall value
∞	freestream value

Superscripts

+	quantity in wall coordinates
~	denotes Favre (density-weighted) averaging
—	denotes Reynolds (time-based) averaging
′	denotes Favre fluctuating quantity

Introduction

This work is concerned with developing a capability to model high-speed compressible flows with laminar, transitional, and turbulent flow regions. The approach uses one- and two-equation eddy viscosity models to predict the turbulent flow. The same governing equations are presently being used to predict the transitional flow region where the onset to turbulent flow is specified and assumed to be known. The prediction of where onset to turbulent flow occurs is a research area that depends on an analysis of the flow stability, understanding of the flow disturbances outside the boundary layer, and a capability to predict the boundary layer receptivity. The process of entraining disturbances into the boundary layer and producing perturbations that can be amplified is called "receptivity."

The more appropriate books providing information on modeling compressible turbulent flows are Wilcox,[1] Chapter 6 by Gatski,[2] and Smits and Dussauge.[3] The modeling of compressible turbulent flows is still an active area of research. The application of some of the turbulence models to compressible flows is not always clear, as the models were originally developed for incompressible flows. Formulations for incompressible flow are not applicable to compressible flow because some variables (e.g., density, viscosity) have been assumed constant in the development. The turbulent transport equations are often written in substantial differential form, while the equations in conservation form are generally required in compressible Navier-Stokes codes. Problems with the formulation of the governing equations for compressible turbulence models in conservation form are discussed. For example, the form of the diffusion term in the Spalart-Allmaras[4,5] model is rewritten and justification for the new form is given.

The SACCARA (Sandia Advanced Code for Compressible Aerothermodynamics Research and Analysis) code[6-9] is used for the results presented in this paper. For one-equation turbulence models, the SACCARA code has options for both the Baldwin-Barth[10] and Spalart-Allmaras eddy viscosity models. There is evidence that the use of the Baldwin-Barth model does not constitute a well-posed system of governing equations.[11] For boundary layer and shear layer flows, the solutions do not appear to converge to a unique solution as the mesh is refined. Therefore, there is more interest in using the Spalart-Allmaras model, as it has proven to be a numerically robust approach. Part of the present work is concerned with the evaluation of the Spalart-Allmaras model for high-speed flows and the simulation of the transition region with the Spalart-Allmaras model.

The SACCARA code also has options for three popular two-equation eddy viscosity turbulence models: a low Reynolds number $k-\varepsilon$ formulation and two $k-\omega$ models. The $k-\varepsilon$ model[1] employs the low Reynolds number modification of Nagano and Hishida[12] to allow integration to solid walls. The first $k-\omega$ formulation is the hybrid model of Menter[13] which is a blending between a $k-\omega$ formulation (near solid walls) and a $k-\varepsilon$ formulation (in shear layers and freestream flow). Menter proposed this hybrid model to take advantage of the accuracy of the $k-\omega$ model for wall-bounded flows and the $k-\varepsilon$ model for free shear layers. The final model is the Wilcox $k-\omega$ model[1] which was modified in 1998 to improve the predictive accuracy for shear flows. This model is referred to as the Wilcox (1998) model in the current work. The appropriate form of the two-equation eddy viscosity equations are also important because the one-equation formulation can be developed from the two-equation transport relations. This approach may be used to determine the appropriate form of the transport equation for the one-equation models.

Two flow cases have been used to investigate the performance of the one- and two-equation eddy viscosity models. The first case is the flow over a flat plate at Mach 8 and an altitude of 15 *km* where the perfect gas model is appropriate. The skin friction along the flat plate is used to judge the accuracy of the predictions through comparisons with the accurate laminar and turbulent results of Van Driest.[14,15] If the standard turbulence models (without modifications for transition) are employed over the whole domain, the transition location often depends on turbulent intensity in the freestream. This behavior is similar to the bypass transition problem. When a transition plane is specified in which the turbulent eddy viscosity is neglected upstream, the transition locations for the Spalart-Allmaras and low Reynolds number $k-\varepsilon$ models still show sensitivity to the freestream turbulence quantities. The control of the transition location with the Spalart-Allmaras model has been investigated.

The second case investigated is the flow over the Reentry F flight vehicle at Mach 20 and at an altitude of 24.4 *km* (80,000 feet) where real gas effects are significant. The measured heat transfer along the vehicle is used to judge the accuracy of the model predictions. The

transition location is specified to give a reasonable match of the wall heat flux with the flight data. It should be remembered that the prediction of transition location is not included in the modeling. The solutions have been obtained on three meshes with the number of cells in each coordinate direction doubled for each mesh refinement. In addition, the solutions on each mesh are marched in time until the wall heat flux has obtained a steady-state value. The accuracy of the iterative solution relative to the steady-state solution has been estimated for each model. The various uncertainties and assumptions in the flight experiment and prediction are discussed. Real gas effects have been taken into account with the use of an equilibrium air model.

Favre-Averaged Transport Equation for Turbulence Models

The generic form of the turbulent transport equation in substantial derivative form[1] is

$$\bar{\rho}\frac{D\varphi}{Dt} = D + S_P - S_D \qquad (1)$$

where

$$D = D_1 - \bar{D}, \qquad D_1 = \frac{\partial}{\partial x_j}\left(\mu_{eff}\frac{\partial \varphi}{\partial x_j}\right)$$

For example for a one-equation eddy viscosity model, the dependent variable is $\varphi \sim \nu_T$ and the effective diffusion coefficient is μ_{eff}. In some models there are two parts to the diffusion term on the right-hand side of Eq. (1); D_1 is the first part of the diffusion term which can be put in conservation form, and $\bar{D}$ is the remaining part. When $\bar{D}$ is included, it can take on several forms. The source term $S = S_P - S_D$ has a production part S_P and a dissipation part S_D. If the continuity equation is multiplied by φ and added to Eq. (1), the resulting equation is the generic transport equation in conservation form:

$$\frac{\partial U}{\partial t} + \frac{\partial}{\partial x_j}\left\{\bar{\rho}\tilde{u}_j\varphi - \mu_{eff}\frac{\partial \varphi}{\partial x_j}\right\} = \bar{D} + S_P - S_D \qquad (2)$$

The dependent variable is $U = \bar{\rho}\varphi$. This development utilizes Favre (overtilde) and Reynolds (overbar) averaging. See Ref. 1 for notation and for details on the Favre averaging procedure.

One-Equation Turbulence Model

There have been a number of one-equation turbulence models developed which use a transport equation to solve for the eddy viscosity directly. The present work is focused on the Spalart-Allmaras model and a brief description is presented below.

Spalart-Allmaras Model

The transport equation for determining the eddy viscosity with near-wall effects included has been developed by Spalart and Allmaras.[4,5] The governing equation form is slightly different than Eq. (1) and is

$$\bar{\rho}\frac{D\varphi}{Dt} = D + S_P - S_D + S_t, \qquad \tilde{\mu} = \frac{\mu_T}{f_{v1}} = \bar{\rho}\varphi \qquad (3)$$

The dependent variable $\varphi = \tilde{\nu} = \nu_T / f_{v1}$, where f_{v1} is a damping function used in the near-wall region and mainly in the viscous sublayer. This function and the right hand side terms will be defined below. The continuity equation is multiplied by φ and added to Eq. (3) which gives a transport equation in conservation form for the Spalart-Allmaras model in the form of Eq. (2)

Spalart-Allmaras Model

$$\frac{\partial U}{\partial t} + \frac{\partial}{\partial x_j}\left\{\bar{\rho}\tilde{u}_j\varphi - \mu_{eff}\frac{\partial \varphi}{\partial x_j}\right\} = \bar{D} + S_P - S_D + S_t \qquad (4)$$

$$U = \bar{\rho}\tilde{\nu} = \bar{\rho}\varphi, \qquad \mu_{eff} = \frac{\mu + \tilde{\mu}}{\sigma}$$

The right-hand side has contributions from a diffusion term as well as production, destruction, and trip terms. The four terms in the model are written as follows:

Diffusion-Original Form

$$D = \bar{\rho}\frac{\partial}{\partial x_j}\left[\frac{\mu_{eff}}{\bar{\rho}}\frac{\partial \varphi}{\partial x_j}\right] + D_2 = D_1 + \bar{D}$$

$$\mu_{eff} = \frac{\mu + \tilde{\mu}}{\sigma} = \bar{\rho}\left(\frac{\nu + \varphi}{\sigma}\right), \qquad \bar{D} = D_2 - D_3$$

$$D_2 = \frac{c_{b2}\bar{\rho}}{\sigma}\left(\frac{\partial \varphi}{\partial x_j}\right)\left(\frac{\partial \varphi}{\partial x_j}\right), \qquad D_3 = \left(\frac{\mu_{eff}}{\bar{\rho}}\right)\frac{\partial \bar{\rho}}{\partial x_j}\frac{\partial \varphi}{\partial x_j}$$

Diffusion-Modified for Compressible Flow

$$D = D_1 + D_2, \qquad \bar{D} = D_2$$

Production

$$S_P = c_{b1}[1 - f_{t2}]\tilde{S}\bar{\rho}\varphi$$

Destruction

$$S_D = \left\{c_{w1}f_w - \frac{c_{b1}}{\kappa^2}f_{t2}\right\}\bar{\rho}\left(\frac{\varphi}{d}\right)^2$$

Trip Term

$$S_t = f_{t1}\rho(\Delta U)^2$$

In the formal transform of the transport equation into conservation form, the diffusion term D_3 includes a density gradient term. This term is zero when the transport equation (Eq. (4)) is developed from the compressible form of the $k-\varepsilon$ transport equations,[11,16] and is shown above in the term *Diffusion-Modified for Compressible Flow.* This form of the diffusion term is used in the present work. Including this density gradient term has been found to cause stability problems for high-speed flows, while having negligible effect on the predictions. The model controls transition from laminar to turbulent flow with the use of the trip term. With this additional physics, the foregoing governing equation requires some additional terms and definitions for f_{t1} and f_{t2} which involves the coefficients c_{t1} to c_{t4}. Except where noted, the standard values for the model constants are used in the current work.

Boundary Conditions for Spalart-Allmaras Model

At the wall $\mu_T = 0$ or $\tilde{\nu} = 0$. The freestream boundary condition for this model is the specification of the turbulent eddy viscosity μ_T. In the freestream there should be no production of the eddy viscosity, which requires that

$$f_{t2} = c_{t3}e^{-c_{t4}\chi^2} > 1, \qquad (c_{t3} = 1.2, \quad c_{t4} = 0.5)$$

in order to turn off the production term in Eq. (6). The restriction on χ is

$$\chi = \tilde{\nu}/\nu < \sqrt{(\ln c_{t3})/c_{t4}} = 0.604$$

The restriction on the freestream eddy viscosity becomes

$$\frac{\mu_T}{\mu} < \chi f_{v1} = \chi/[1+(c_{v1}/\chi)^3] = 3.713\times10^{-4} \qquad (5)$$
$$c_{v1} = 7.1$$

The freestream eddy viscosity as suggested by Spalart-Allmaras is $\tilde{\nu} < 1/2\nu$, which gives

$$\frac{\mu_t}{\mu} < \tilde{\nu} f_{v1}/\nu = 1.746\times10^{-4}.$$

Control of Laminar and Turbulent Flow with the Spalart-Allmaras Model

The governing equation has three terms that are influenced by the transition model. The complete source term (for the conservative formulation) is

$$S = \frac{c_{b2}\bar{\rho}}{Pr_T}\left(\frac{\partial\tilde{\nu}}{\partial x_j}\right)^2 + c_{b1}[1-\underline{f_{t2}}]\tilde{S}U$$
$$-(c_{w1}f_w - \underline{c_{b1}f_{t2}/\kappa^2})\bar{\rho}\left(\frac{\tilde{\nu}}{d}\right)^2 + \underline{f_{t1}\bar{\rho}(\Delta U)^2} \qquad (6)$$

where the trip terms are underlined in the above equation. The first term is part of the diffusion term and is included in the source term as it is evaluated numerically in an explicit manner. The second term is the production term and it will produce or increase the eddy viscosity if $f_{t2} < 1$. The third term is the destruction term and it will decrease the eddy viscosity if $c_{w1}f_w > c_{b1}f_{t2}/\kappa^2$. The fourth term is the trip term and it will increase the eddy viscosity as $f_{t1} > 0$.

The model generally predicts turbulent flow everywhere when the trip terms are zero

$$f_{t1} = 0 \text{ or } c_{t1} = 0, \qquad f_{t2} = 0 \text{ or } c_{t3} = 0$$

The flow can be made laminar everywhere with the following values of the trip terms:

$$f_{t1} = 0 \text{ and } f_{t2} \geq 1.0 \text{ or } f_{t2} = c_{t3}\Lambda, \quad \Lambda = e^{-c_{t4}\chi^2}$$
$$\text{or} \quad f_{t1} = 0, \qquad f_{t2} = 0, \qquad c_{b1} = 0$$

Several different approaches have been investigated to control transition and to replace the original trip model approach of Spalart-Allmaras.

Method 1 (f_{t2} is modified)

In this approach the value of $f_{t1} = 0$, and $f_{t2} = c_{t3}(1-\lambda)$ where λ varies from the laminar flow region to the turbulent flow region. In the laminar flow region $\lambda = 0$ while in the turbulent flow region $\lambda = 1$. The parameter is increased smoothly and defines the transitional flow region. This method requires specification of the location and length of the transitional region.

Method 2 (c_{b1} is modified)

In this method the trip terms $f_{t1} = 0$ and $f_{t2} = 0$ are set to zero. The coefficient c_{b1} is modified from the laminar flow region to the turbulent flow region as follows:

$$x < x_s: \; c_{b1} = 0, \qquad x > x_e: \; c_{b1} = 0.1355$$

$$x_s \leq x \leq x_e: \; c_{b1} = 0.1355\lambda^p, \quad \lambda = (x-x_s)/(x_e-x_s)$$

In this method, the location of the start of transitional flow x_s and end of transitional flow x_e are specified.

Method 3 ($c_{b1}(1-f_{t2})$ is modified)

In this method the production term coefficient is modified by writing this term as $\alpha c_{b1}(1-f_{t2})$. The parameter α increases from zero to one in the transitional flow region. From the definition of f_{t2}, the following is obtained:

$$\chi = \tilde{\nu}/\nu = \sqrt{-\ln[f_{t2}/c_{t3}]/c_{t4}} \tag{7}$$

The production term switches sign when $f_{t2} = 1$ which gives a critical value of χ which is $\chi^* = 0.604$. When $x < x_t$, set $\alpha = 0$ and there is no production of eddy viscosity upstream of the transition location x_t. When $x > x_t$, α is increased downstream towards one. This increase is controlled by setting

$$\alpha = 1 - f_{t2} = 1 - c_{t3}e^{-c_{t4}\chi^2}$$

When $x > x_t$ and $\chi \le \chi^*$, then $\chi = \chi^*$. When $x > x_t$ and $\chi > \chi^*$, then χ is obtained from Eq. (7). In this method, only the single parameter x_t must be specified.

Two-Equation Turbulence Models

The standard method for specifying transition to turbulence is through analogy with the turbulence intermittency approach. The turbulence transport equations are solved over the entire domain, with a user-defined transition plane specified. Upstream of this plane, the effective viscosity is simply the laminar value, while downstream the effective viscosity is the sum of the laminar and turbulent viscosities.

High Turbulent Reynolds Number $k-\varepsilon$ Model

The high Reynolds number formulation[1] is appropriate for turbulent flows but is not appropriate in the near-wall region. It can be applied in the outer part of boundary layers and combined with an inner boundary layer approach near the wall to obtain a complete formulation. For the standard $k-\varepsilon$ model, the turbulent kinetic energy equation for a compressible fluid takes the same form as Eq. (2) where the variables have the following values:

$$U = \bar{\rho}k = \bar{\rho}\varphi, \qquad \mu_{eff} = \mu_k, \qquad \bar{D} = 0$$
$$S_{Pk} = \bar{\rho}P, \qquad S_{Dk} = \bar{\rho}\varepsilon \tag{8}$$

The production term P takes the standard form for compressible flows (see Ref. 1), and the effective viscosity is defined below in Eq. (10). The transport equation for dissipation of turbulent kinetic energy is the same form as Eq. (2), where the variables have the following values:

$$U = \bar{\rho}\varepsilon = \bar{\rho}\varphi, \qquad \mu_{eff} = \mu_\varepsilon$$
$$\bar{D} = 0, \qquad S_{P\varepsilon} = c_{\varepsilon 1}f_1\bar{\rho}\frac{\varepsilon}{k}P, \qquad S_{D\varepsilon} = c_{\varepsilon 2}f_2\bar{\rho}\frac{\varepsilon}{k} \tag{9}$$

The effective viscosities are obtained from

$$\mu_k = \mu + \mu_T/\sigma_k, \qquad \mu_\varepsilon = \mu + \mu_T/\sigma_\varepsilon$$
$$\text{where} \quad \mu_T = c_\mu f_\mu \bar{\rho}k^2/\varepsilon \tag{10}$$

The constants in the foregoing equations use the standard values.

Low Turbulent Reynolds Number $k-\varepsilon$ Model

The Nagano and Hishida model[12] was developed for incompressible flow and is included in the current formulation. The model uses the following damping function in the eddy viscosity relation given in Eq. (10):

$$f_\mu = [1 - \exp(-y^+/26.5)]^2$$

This damping function is written in terms of the distance from the wall y^+. The source term for the turbulent kinetic energy Eq. (8) is

$$S = \bar{\rho}P - \bar{\rho}\varepsilon + \tilde{D}$$

The production term has been approximated with:

$$\bar{\rho}P \approx \mu_T\left(\frac{\partial \tilde{u}_i}{\partial x_j} + \frac{\partial \tilde{u}_j}{\partial x_i}\right)\frac{\partial \tilde{u}_i}{\partial x_j}$$

The compressible term

$$-\frac{2}{3}(\bar{\rho}k + \mu_T S_{kk})S_{kk}, \quad \text{where} \quad S_{kk} = \frac{\partial \tilde{u}_k}{\partial x_k}$$

has been neglected in the current formulation. The source term for the dissipation rate equation is

$$S = \frac{\varepsilon}{k}(c_{\varepsilon 1}f_1\bar{\rho}P - c_{\varepsilon 2}f_2\bar{\rho}\varepsilon) + \tilde{E}$$

The parameters in these source terms are written as

$$f_1 = 1, \qquad f_2 = 1 - 0.3e^{-R_T^2}, \qquad R_T = k^2/\nu\varepsilon$$
$$\tilde{D} = -2\mu\left(\frac{\partial\sqrt{k}}{\partial y}\right)^2, \qquad \tilde{E} = \mu\nu_T(1-f_\mu)\left(\frac{\partial^2\tilde{u}}{\partial y^2}\right)^2$$

The variables $\tilde{D}$ and $\tilde{E}$ use boundary layer type derivatives normal to the wall and $\tilde{E}$ requires the tangential velocity component.

The Nagano-Hishida and the Launder-Sharma[17] low Reynolds $k-\varepsilon$ turbulence models have been used by Theodoridis, Prinos, and Goulas[18] to predict transitional flow. They have investigated a flat plate flow experiment where the freestream turbulent intensity was ap-

proximately 3 percent and 6 percent. The two turbulence models were used to model the laminar to turbulent bypass transition in which the freestream turbulence determines where the transition to turbulent flow occurs. For this bypass transition case, the Nagano-Hishida model predicts transition to turbulent flow too near the leading edge while the Launder-Sharma model predictions are in reasonable agreement with the experimental data. Of course, neither of these turbulence models were developed to predict where transition will occur in a flow; the performance of the Launder-Sharma model in predicting the location of transition is fortuitous. The failure of the Nagano-Hishida for transitional flow requires caution in the application of this model and a procedure is required to have the model turned on at the appropriate location.

Menter k-ω Model

Two different two-equation turbulence models are described which solve equations for the turbulent kinetic energy, k, and the frequency of turbulent fluctuations, ω. The Menter k-ω model[13] is a hybrid model which uses a blending function to combine the best aspects of both the k-ω and the k-ε turbulence models. Near solid walls, a k-ω formulation is used which allows integration to the wall without any special damping or wall functions. Near the outer edge of the boundary layer and in shear layers, the model blends into a transformed version of the k-ε formulation, thus providing good predictions for free shear flows.

For the Menter k-ω model, the terms in Eq. (2) are as follows:

Turbulent Kinetic Energy Equation

$$U = \bar{\rho}k = \bar{\rho}\varphi, \qquad \mu_{eff} = \mu_k, \qquad \bar{D} = 0$$
$$S_{Pk} = \bar{\rho}P, \qquad S_{Dk} = \beta^*\bar{\rho}k\omega \tag{11}$$

Turbulent Frequency Equation

$$U = \bar{\rho}\omega = \bar{\rho}\varphi, \qquad \mu_{eff} = \mu_\omega$$
$$\bar{D} = 2\bar{\rho}(1-F)\sigma_{\omega 2}\frac{1}{\omega}\frac{\partial k}{\partial x_j}\frac{\partial \omega}{\partial x_j} \tag{12}$$
$$S_{P\omega} = \bar{\rho}\frac{\gamma}{\nu_T}P, \qquad S_{D\omega} = \beta\bar{\rho}\omega^2$$

The cross-diffusion term ($\bar{D}$) in Eq. (12) arises due to the transformation of the ε-equation into an equation for ω. The production term is given by

$$P = \tau_{ij}\frac{\partial u_i}{\partial x_j}, \quad \text{where} \quad \tau_{ij} = -\overline{u_i' u_j'}\,. \tag{13}$$

For 3-D compressible flows, the turbulence stress tensor can be expressed as:

$$\tau_{ij} = 2\nu_t\left(S_{ij} - \frac{1}{3}\frac{\partial \tilde{u}_k}{\partial x_k}\delta_{ij}\right) - \frac{2}{3}k\delta_{ij} \tag{14}$$

The effective viscosities are given by

$$\mu_k = \mu + \sigma_k\mu_T\,, \qquad \mu_\omega = \mu + \sigma_w\mu_T$$
$$\text{where} \quad \mu_T = \bar{\rho}k/\omega \tag{15}$$

and the model constants above are blended values of the k-ω and k-ε parameters. For example, for the constant β,

$$\beta = F\beta_1 + (1-F)\beta_2$$

where F varies from 1 at the wall to zero outside wall boundary layers, and a "1" denotes k-ω constants and "2" denotes k-ε constants. The values for these constants are:

$$\sigma_{k1} = \frac{1}{2}, \quad \sigma_{\omega 1} = \frac{1}{2}, \quad \beta_1 = \frac{3}{40},$$
$$\beta^* = 0.09, \quad \kappa = 0.41, \quad \gamma_1 = \frac{\beta_1}{\beta^*} - \frac{\sigma_{\omega 1}\kappa^2}{\sqrt{\beta^*}}$$

and

$$\sigma_{k2} = 1, \quad \sigma_{\omega 2} = 0.856, \quad \beta_2 = 0.0828,$$
$$\beta^* = 0.09, \quad \kappa = 0.41, \quad \gamma_2 = \frac{\beta_2}{\beta^*} - \frac{\sigma_{\omega 2}\kappa^2}{\sqrt{\beta^*}}\,.$$

Wilcox (1998) k-ω Model

For the Wilcox (1998) k-ω model,[1] the terms in Eq. (2) are as follows:

Turbulent Kinetic Energy Equation

$$U = \bar{\rho}k = \bar{\rho}\varphi, \qquad \mu_{eff} = \mu_k, \qquad \bar{D} = 0$$
$$S_{Pk} = \bar{\rho}P, \qquad S_{Dk} = \beta^*\bar{\rho}k\omega \tag{16}$$

Turbulent Frequency Equation

$$U = \bar{\rho}\omega = \bar{\rho}\varphi, \qquad \mu_{eff} = \mu_\omega, \qquad \bar{D} = 0$$
$$S_{P\omega} = \bar{\rho}\frac{\gamma}{\nu_T}P, \qquad S_{D\omega} = \beta\bar{\rho}\omega^2 \tag{17}$$

where

$$\alpha = \frac{13}{25}, \qquad \beta = \beta_0 f_\beta, \qquad \beta^* = \beta_0^* f_{\beta^*}$$

$$\sigma_k = \sigma_\omega = \frac{1}{2}, \qquad \beta_0^* = \frac{9}{100}$$

$$f_{\beta^*} = \begin{cases} 1, & \chi_k \le 0 \\ \dfrac{1 + 680\chi_k^2}{1 + 400\chi_k^2}, & \chi_k > 0 \end{cases}, \quad \chi_k \equiv \frac{1}{\omega^3}\frac{\partial k}{\partial x_j}\frac{\partial k}{\partial x_j}$$

$$\beta_0 = \frac{9}{125}, \quad f_\beta = \frac{1 + 70\chi_\omega}{1 + 80\chi_\omega}, \quad \chi_\omega \equiv \left| \frac{\Omega_{ij}\Omega_{jk}S_{ki}}{(\beta_0^*\omega)^3} \right|$$

$$\Omega_{ij} = \frac{1}{2}\left(\frac{\partial \tilde{u}_i}{\partial x_j} - \frac{\partial \tilde{u}_j}{\partial x_i}\right), \qquad S_{ij} = \frac{1}{2}\left(\frac{\partial \tilde{u}_i}{\partial x_j} + \frac{\partial \tilde{u}_j}{\partial x_i}\right).$$

The production term, P, and the eddy viscosity definitions are given in Eqs. (13) and (15), respectively. This formulation is a modification to an earlier Wilcox $k-\omega$ model[19] in order to improve model predictions for free shear layers and to reduce the solution sensitivity to freestream ω values.

Flow Predictions for Flat Plate

Flow over a flat plate has been chosen as a high speed test case to illustrate the behavior of the laminar/turbulent flow results obtained with the one- and two-equation turbulence models. The test case is Mach 8 flow over a flat plate with a wall temperature of T_w=1000 K and freestream conditions corresponding to an altitude of 15 km. For this case, the temperature in the flow is sufficiently low that perfect gas assumption with $\gamma = 1.4$ is reasonable.

Freestream Flow Conditions

The freestream conditions[20] for the flat plate case are:

$$p_\infty = 1.21114 \times 10^4 \ kg/m/s^2, \quad T_\infty = 216.65 \ K$$

$$\rho_\infty = 0.19475 \ kg/m^3, \quad a_\infty = \sqrt{\frac{\gamma p_\infty}{\rho_\infty}} = 295.07 \ m/s$$

$$V_\infty = a_\infty M_\infty = 2360.54 \ m/s$$

$$\mu_\infty = \frac{1.458 \times 10^{-6} T_\infty^{3/2}}{(T_\infty + 110.4)} = 1.4216 \times 10^{-5} \ kg/m/s$$

For the Spalart-Allmaras model, the restriction on the freestream eddy viscosity is determined by Eq. (5), which gives

$$\mu_{T_\infty} < 5.27 \times 10^{-9} \ kg/m/s$$

for the Mach 8 flat plate flow case. The freestream eddy viscosity for all models was thus chosen as

$$\mu_{T_\infty} < 1.0 \times 10^{-9} \ kg/m/s$$

unless indicated otherwise. For the two-equation models, the further specification of a freestream turbulence intensity of 0.01% was used to determine the turbulent kinetic energy in the freestream from

$$k = \frac{1.2}{2}\left(\frac{Tu}{100} V_\infty\right)^2 = 6 \times 10^{-9} V_\infty^2.$$

Computational Mesh for the Flat Plate

A parabolic mesh has been used around the flat plate with the (x, y) Cartesian coordinate system fixed at the leading edge. This mesh topology mitigates the effects of the leading edge singularity. The parabolic coordinates ξ, η are related to the Cartesian coordinates as follows:

$$x = \alpha(\xi^2 - \eta^2) \qquad y = 2\alpha\xi\eta \qquad \alpha = 0.05$$

$$0 \le \xi \le \xi_{max} \qquad 0 \le \eta \le 1 \qquad \xi_{max} = \sqrt{1 + 1/\alpha}$$

The value of ξ_{max} has been determined by setting $x = 1$ at $\eta = 1$. This gives a mesh that is slightly longer than one meter along the flat plate. A uniform mesh is used in the ξ coordinate direction while a non-uniform mesh spacing is used in the η coordinate direction. The mesh spacing has been determined with the lower boundary stretching transformation of Roberts[21] (see also Ref. 22). Most of the results have been obtained with 80x160 cells. A coarser mesh of 40x80 and a finer mesh of 160x320 have been used to show that the 80x160 mesh provides results sufficiently accurate for the figures presented. A stretching parameter of $\beta = 1.001$ has been used for the one-equation models. This choice for β gives maximum y^+ values of approximately 2.3 for the coarse 40x80 mesh. As expected, the maximum allowable y^+ values for the two-equation models were found to be much smaller than for the one-equation models, with the larger values resulting in convergence problems. Thus a stretching parameter of $\beta = 1.00007$ was used giving $y^+ \le 0.2$ at the end of the plate for the coarse mesh.

Flat Plate Results with Standard Transition Method

For the freestream conditions and meshes specified above, the laminar/turbulent flow has been calculated with the SACCARA code and compared to the accurate laminar and turbulent results obtained for this case by Van Driest.[14,15] The standard transition method is used

where the laminar viscosity is the sole contributor to the effective viscosity upstream of the transition plane (x_t = 0.1196 m). The L2 norms of the residuals for both the momentum equations and the turbulence equations were reduced at least eight orders of magnitude in each case, suggesting that the results for the flat plate problem are not influenced by iterative convergence error.

Skin friction profiles have been obtained using all five turbulence models for the Mach 8 flat plate case. The Baldwin-Barth and both $k-\omega$ models give transition at the specified transition plane for the given freestream turbulence levels as shown in Fig. 1. In order to move the transition point to the desired location, the freestream eddy viscosity had to be increased to 1×10^{-6} kg/m/s for the Spalart-Allmaras model, and the turbulence intensity had to be increased to 0.1% for the low Reynolds number $k-\varepsilon$ model (see Fig. 2). All of the models which correctly predict turbulent flow downstream of the transition point also predict skin friction in this region in agreement with the theory.

Modified Transition Results for Spalart-Allmaras Model

Solutions have been obtained with the Spalart-Allmaras trip functions f_{t1}, f_{t2} set to zero. The flow is turbulent along the flat plate for this case with the freestream eddy viscosity μ_T varying from 10^{-9} to 10^{-5} *kg/m/s*. Solutions have been obtained with the trip function f_{t2} included and f_{t1} set to zero. For this case the flow transition location is dependent on the freestream eddy viscosity. When the eddy viscosity is 10^{-9} *kg/m/s*, the flow remains laminar over the length of the flat plate. As previously discussed, numerical solutions show that the flow can be maintained laminar by making the production term S_P zero by setting c_{b1} = 0 with the trip functions f_{t1}, f_{t2} set to zero.

The complete Spalart-Allmaras model has trip terms included to control the transition location, but the formulation is not intended to model the transition flow region. The behavior of this model has been investigated with the results for the local skin friction given in Fig. 3 where the trip location x_t is specified. The specified transition location corresponds to $Re_x = 3.84\times10^6$ while the numerical prediction has transition varying as the freestream eddy viscosity is increased above a value of approximately 10^{-9} *kg/m/s*. For these high speed flows, it is difficult to control the transition location with the suggested trip model. In addition, there is no control of the length of the transition region. Because of these experiences with the behavior of the Spalart-Allmaras trip model, different approaches have been investigated.

Three methods have been investigated to control the transition location and the length of transition as previously described. There are two parameters x_t and x_l introduced to control the transition behavior. The parameter x_t is at the middle of the transition region while $x_s = x_t - x_l$ is the location upstream where transition starts and the location downstream $x_e = x_t + x_l$ where the flow becomes fully turbulent. The values of these parameters are:

$$x_t = 0.1196\ m, \quad x_l = 0.1\ m, \quad Re_{x_t} = 3.84\times10^6$$

These locations are also indicated in Fig. 4.

The results for the skin friction with the three proposed approaches for modeling transition have been investigated. All of the methods remain laminar a significant distance after the specified start of transition. With Method 1, where the trip function f_{t2} is modified, transition occurs downstream of the desired location with very rapid transition onset. With Method 2. where the production coefficient c_{b1} is modified, transition occurs near the desired location with a reasonable variation of the skin friction in the transition region. With Method 3, where the production term coefficient $c_{b1}(1-f_{t2})$ is modified, transition occurs downstream of the desired transition location with very rapid transition onset. From this investigation it is concluded that Method 2 provides a reasonable technique to specify the transition location with limited control over the transition region length. The results for method 2 are presented in Fig. 4. When λ varies linearly over the transition region, there is better control. The transition control Method 2 appears to be insensitive to the freestream eddy viscosity. Other approaches need to be considered and evaluated.

Flow Predictions for Reentry F Vehicle

Reentry F Description and Experimental Results

The Reentry F flight experiment[23] was performed in 1968 to provide measurements of wall heat transfer rates at reentry flow conditions that cannot be obtained in ground-based experimental facilities. The data is for the flow over a slender conical vehicle where there is only a small amount of surface ablation localized at the nosetip. The boundary layer flow is laminar, transitional, or turbulent depending on the altitude and location along the body surface. The Reentry F vehicle was a 5 degree sphere-cone with an initial nose radius of 0.1 inch and the vehicle length is 13 feet. A graphite nosetip extended for the first 7.54 inches followed by a conical beryllium frustum. The heat transfer measurements were obtained at altitudes between 120,000 and 60,000 feet. The data at a flight time of 456.0 seconds or an alti-

tude of 80,000 feet (24.383 km) is used to validate the turbulence model predictions. Although this flight experiment provides exceptional data, there are many aspects of the flow conditions, body orientation, body shape, and wall surface temperature that are not completely or precisely known.

In recent years, this experimental data set has been reevaluated with modern computational codes and is documented in Refs. 24-26. Aerothermal predictions have also been presented in these papers. It is important to observe that the freestream conditions for the three predictions are slightly different and the wall temperature in some cases is constant while in others a variation is taken into account. Most of these solutions are for axisymmetric flow with the vehicle at zero degree angle of attack, but full three-dimensional solutions have been obtained with the actual flight angle of attack of 0.14 degrees. There are many details of this flight experiment that are not well defined, but overall the heat transfer predictions are in reasonable agreement with the flight measurements. Of course, none of the modeling includes a capability to predict the transition location. Further information on the flight experiment is given in Wright and Zoby.[23]

The flow conditions at an altitude of 80,000 feet have become the location in the flight trajectory most often analyzed and are also chosen for the present investigation. The present freestream conditions are based on the U. S. Standard Atmosphere, 1976.[20] The assumed turbulent eddy viscosity is given as well as the turbulence intensity for the two-equation models. The freestream flow conditions (in SI units) that have been used in are

$$M_\infty = 19.97, \qquad \alpha = 0^\circ, \qquad \rho_\infty = 0.043523$$

$$T_\infty = 221.034, \qquad T_w = 500, \qquad p_\infty = 2761.41$$

$$V_\infty = 5951.858, \qquad a_\infty = 298.04$$

$$\mu_\infty = 1.445 \times 10^{-5}, \qquad \mu_T = 3.3227 \times 10^{-14}$$

$$Tu = 0.01\%, \qquad x_{body} = 4.0$$

Note that there is some amount of uncertainty in the specification of these properties.

The nosetip of the vehicle is graphite and initially is a sphere-cone with a nose radius $R_N = 0.00254$ *m*. Due to ablation, the nose radius increases to 0.00343 *m* at an altitude of 80,000 feet. This result is an estimated value from an ablation analysis of the nosetip.[26] For the present analysis, it is assumed that the nosetip shape remains a sphere-cone after ablation with the same cone half angle as the conical vehicle, which is $\theta_{cone} = 5^\circ$. The nosetip is illustrated below. The origin in this figure is located at the virtual tip of the conical vehicle. For the approximated sphere-cone configuration for the Reentry

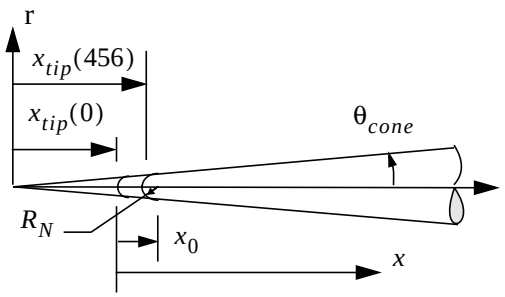

F vehicle simulation, the location of the original nosetip and ablated nosetip is specified as

$$x_0 = 0.012752\ m, \qquad x_{tip}(0) = 0.026603\ m$$

$$x_{tip}(456) = 0.035925\ m$$

In previous analyses of this vehicle, the coordinate x is defined as the axial distance without a clear definition of the origin location given in many cases. Some figures indicate that the origin is located at the ablated nose of the body. The axial location x in this paper is measured from the *nosetip of the un-ablated vehicle*. The uncertainty in the location of the axial heat flux measurements has a negligible impact on the results presented.

Due to the high velocities, the gas temperature is more than 6000 *K* in the nosetip region with dissociation of the oxygen and nitrogen occurring. Downstream of the nose the inviscid flow temperature behind the shock is 420 K, and perfect gas flow occurs. However, in the boundary layer the viscous dissipation increases the gas temperature to around 3000 *K* and dissociation of oxygen occurs. At 80,000 feet, the chemical reactions are sufficiently fast that the air is assumed to be in local thermochemical equilibrium. This is believed to be a reasonable assumption, but a finite rate solution needs to be performed in the future to validate this simplification. There is also some ablation of the nosetip which introduces chemical species from the ablation products into the boundary layer flow. As the amount of ablation is small, this influence has been neglected.

Predictions of Wall Heat Flux for Reentry F Vehicle

Simulation Code and Model Approach

The flow around the Reentry F vehicle has been determined with the SACCARA[6-9] Navier-Stokes code. This investigation is concerned with obtaining accurate numerical solutions of the wall heat flux based upon the input conditions to the code and models used in the simulation. The wall heat flux predictions are then compared with the flight measurements at an altitude of 80,000 feet. The solution is for the flow over the ablated vehicle. The small angle of attack of the vehicle (0.14°) is neglected and the flow is assumed to be axisymmetric. The solutions use a gas model of air in local thermochemical equilibrium and the flow is laminar over the

front part of the body. The flow transitions to turbulent flow at a specified location. The turbulent flow has been modeled with the Baldwin-Barth and Spalart-Allmaras one-equation eddy viscosity approaches and the low Reynolds number $k-\varepsilon$, Menter $k-\omega$, and Wilcox (1998) $k-\omega$ two-equation turbulence models. The solutions have been obtained on three meshes to judge the spatial convergence of the solution. The L2 norms of the momentum and turbulence transport equations exhibited oscillatory behavior after only a two or three order of magnitude drop, thus another method was needed to monitor convergence. The iterative convergence has been initially determined by plotting the wall heat flux at various number of time steps and assuming convergence has been obtained when there is no noticeable change in the results. Further analysis of the steady-state solution error of the wall heat flux has shown that additional time steps are required to obtain adequate steady-state solutions.

Transition Model

As previously discussed, the basic SACCARA code treats the transition process by setting the effective viscosity to the laminar value upstream of a specified transition plane, while downstream of this plane the effective viscosity is the sum of both the laminar and turbulent viscosities. This approach has been used with the Baldwin-Barth one-equation eddy viscosity model and all two-equation models. The transition plane is specified to be perpendicular to the vehicle axis and located at $x = 2.6\ m$. With the Spalart-Allmaras one-equation eddy viscosity model, a different approach has been implemented as described previously, with $x_s = 1.8844\ m$ and $x_e = 2.8844\ m$. From the results of the investigation of the flat plate flow case, it was concluded that Method 2 (coefficient c_{b1} is varied) is the best approach to control the transition process with the Spalart-Allmaras model at this time.

Iterative Convergence of the Numerical Solutions

At an altitude of 80,000 feet, steady-state solutions on three meshes have been obtained by marching the solution in time until there is no further change in the plotted solution. This method is illustrated in Fig. 5 for the coarse Mesh 0-rg (100x40) with the Spalart-Allmaras turbulence model. The laminar flow region takes the longest time to converge as there is a very fine mesh in the wall region. With Mesh 0-rg, the wall heat flux appears to have no significant changes after 4000 time steps. The iterative convergence with Mesh 1-rg (200x80) is shown in Fig. 6, while the behavior of Mesh 2-rg (400x160) is given in Fig. 7. With Mesh 1-rg, the wall heat flux appears to have no significant changes after 7000 time steps while Mesh 2-rg requires approximately 14,000 time steps. However, the results shown in these figures are misleading! A more careful analysis has been performed to estimate the iterative convergence error.

The accuracy of the wall heat flux q^n relative to the steady-state value is determined by expressing the numerical solution at time t^n as

$$q^n = q(t^n) = q_E + \varepsilon^n \tag{18}$$

The exact steady-state value of the wall heat flux is q_E and the convergence error at time t^n is ε^n. The convergence error has been observed to have an exponential decrease in time which gives the following variation as the solution approaches a steady state:

$$\varepsilon^n = \alpha e^{-\beta t^n} \tag{19}$$

Eq. (18) and Eq. (19) are rewritten as

$$\beta t^n = \ln\alpha - \ln(q^n - q_E) \tag{20}$$

Eq. (20) is evaluated at three times, $(n-1)$, n, and $(n+1)$, and the three relations are used to eliminate α and obtain

$$\beta(t^n - t^{n-1}) = \ln[(q^{n-1} - q_E)/(q^n - q_E)]$$
$$\beta(t^{n+1} - t^n) = \ln[(q^n - q_E)/(q^{n+1} - q_E)]$$

If the time increments are equal, then $(t^n - t^{n-1}) = (t^{n+1} - t^n)$ and the above becomes

$$(q^{n-1} - q_E)(q^{n+1} - q_E) = (q^n - q_E)^2$$

The exact steady-state value of the wall heat flux is solved for in the above equation which gives

$$q_E = \frac{q^n - \Lambda^n q^{n-1}}{1 - \Lambda^n}, \qquad \Lambda^n = \frac{(q^{n+1} - q^n)}{(q^n - q^{n-1})} \tag{21}$$

The iterative convergence error becomes

$$\varepsilon^n = -(q^{n+1} - q^n)/(1 - \Lambda^n)$$

and the percent convergence error relative to the exact steady-state value becomes

$$\%\ \text{Error of}\ q^n = -100\left[\frac{q^{n+1} - q^n}{q^n - \Lambda^n q^{n-1}}\right] \tag{22}$$

The foregoing results closely follow the works of Ferziger and Peric[27,28] for determining the convergence error of the numerical iterative solution of difference equations, but their results have been obtained with a different approach. In their work, the parameter Λ^n is the spectral radius (or the magnitude of the largest

eigenvalue) of the iteration matrix. If the eigenvalues are complex, the present approach is not appropriate. The complex eigenvalue case has been considered by Ferziger and Peric.

The above procedure is illustrated for the wall heat flux solution at $x = 2.14892$ m (where the flow is laminar) using the Spalart-Allmaras model. The percent error is shown in Fig. 8 for the three meshes. The percent error obtained from Eq. (22) is indicated by the symbols while the lines are the percent error obtained from the best estimate of the exact solution given by Eq. (21). The initial solution results on the finest mesh (Mesh 2-rg shown in Fig. 7) appeared converged at 10,000 iterations; however, based on the above error analysis, an additional 15,000 iterations were needed to get the error below 0.1%. The flow solution for Reentry F has also been obtained with three meshes (Mesh 0-f, Mesh 1-f and Mesh 2-f) with the same number of cells, but finer spacing near the wall than was used with Mesh rg. Results of iterative convergence similar to Fig. 5, Fig. 6, and Fig. 7 are obtained except the number of time steps is increased significantly for the solutions with finer near-wall spacing. The iterative convergence error for Mesh f is given in Fig. 9. The iterative solution errors are much smaller than the spatial solution errors, as will be demonstrated.

The iterative convergence for the two-equation turbulence models was also examined for Meshes 0-2eq (130x40 cells), 1-2eq (260x80 cells), and 2-2eq (520x160 cells). Results are presented for the low Reynolds number $k-\varepsilon$ model (Fig. 10), the Menter $k-\omega$ model (Fig. 11), and the Wilcox (1998) $k-\omega$ model (Fig. 12). There is some scatter in the symbols due to the fact that the time increments were not always equal. A larger number of iterations were required due to the stricter y^+ requirements for Mesh 2eq verses the one-equation meshes (Mesh rg and Mesh f). The two-equation results were all converged to less than 0.4% error, which is again much smaller than the grid convergence error.

Spatial Convergence of the Numerical Solutions

Spatial convergence has been judged from the steady-state solutions on the three meshes, 0, 1, and 2 (from coarsest to finest). The wall heat flux obtained with the Spalart-Allmaras turbulence model for the three meshes is given in Fig. 13 with the variable spacing given by Mesh rg. The Richardson extrapolation procedure[29] has been used to obtain a more accurate result from the relation

$$q_{RE} = q_{1,2} = q_2 + (q_2 - q_1)/3. \qquad (23)$$

The above relation assumes that the numerical scheme is second-order. The Richardson extrapolation result q_{RE} and the solution on Mesh 2-rg are nearly the same (also shown in Fig. 13). The accuracy of the solutions on the three meshes has been estimated with the exact solution approximated with q_{RE} which gives the solution error as

$$\%\ \text{Error of } q_M = 100(q_M - q_{RE})/q_{RE} \quad M = 1, 2, 3$$

If the mesh has been refined sufficiently where the solution error has second-order behavior, then the errors on the three meshes have the following relationship

$$\%\ \text{Error of } q_2 = \frac{\%\ \text{Error of } q_1}{4} = \frac{\%\ \text{Error of } q_0}{16} \qquad (24)$$

In the above equation, the first equality will always be satisfied when Eq. (23) has been used. The second equality will only be satisfied if the mesh has been sufficiently refined to be in the asymptotic range. The percent error of the wall heat flux along the vehicle is presented in Fig. 14. The laminar flow solution region is in the asymptotic range while the turbulent flow region is not in the asymptotic range. The wall heat flux prediction in the laminar flow region is more accurate than the heat flux prediction in the turbulent flow region.

For Mesh f, spatial convergence has been judged from the steady-state solutions on the three meshes 0, 1, and 2. Richardson extrapolation procedure has been used to obtain a more accurate result. The accuracy of the solutions on the three meshes has been estimated with the exact solution approximated with the Richardson extrapolated result q_{RE} and these results are given in Fig. 15. Again, the laminar flow solution region is in the asymptotic range while the turbulent flow region is not always in the asymptotic range. The wall heat flux prediction in the laminar flow region with Mesh f is less accurate than the results with Mesh rg. The heat flux predictions in the turbulent flow region with Mesh f are more accurate than the results with Mesh rg. Only the solution on Mesh 2-f is considered sufficiently accurate for comparison with the flight measurements and the Richardson extrapolated results provide even a more accurate numerical prediction.

Spatial convergence has also been examined for the three two-equation models. The spatial error of the heat flux is given in Figs. 16-18 for the low Reynolds number $k-\varepsilon$, the Menter $k-\omega$, and the Wilcox (1998) $k-\omega$ models, respectively. The spatial error in the laminar regions is generally below 2%, while in the turbulent regions it varies from approximately 2% for the $k-\varepsilon$ model to 4% for the $k-\omega$ models. The results for the $k-\omega$ models indicate that the heat flux is not fully grid independent in the turbulent region. The spike in the error for the two-equation models is due to movement of the transition location on the different size

meshes and is more apparent for the two-equation models due to the fine axial spacing around the transition point.

Wall Heat Flux

The predictions of the wall heat flux on the Reentry F vehicle at an altitude of 80,000 feet with the one-equation turbulence models are given in Fig. 19 along with the flight data. The Spalart-Allmaras prediction uses the numerical solution with Mesh 2-f and the Richardson extrapolation results for this case. The simulation overpredicts the laminar wall heat flux by roughly 10 percent while the turbulent wall heat flux is overpredicted by roughly 15 percent. At this altitude the vehicle has a 0.14 degree angle of attack and the heat transfer measurements were made on the leeward side of the conical body. A full three-dimensional solution, with the vehicle at angle of attack, would bring the prediction and flight data into closer agreement. The prediction with Mesh 2-f is believed to be a sufficiently accurate steady-state solution that it can be used to validate the turbulence model, but there are small errors in these results due to uncertainty in information used in the simulation as discussed previously.

The Baldwin-Barth turbulence model prediction (also shown in Fig. 19) uses the numerical solution with Mesh 2-rg where the wall temperature is not maintained at 500K. However, these heat transfer results are not expected to be influenced much by this inaccurate wall temperature. The simulation with the Baldwin-Barth turbulence model overpredicts the laminar wall heat flux by roughly 10 percent and is in agreement with the simulation with the Spalart-Allmaras model. Of course, in the laminar flow region the turbulence models should have no impact on the flow solution. The turbulent wall heat flux is overpredicted by roughly 100 percent with the Baldwin-Barth turbulence model. It is recommended that the Spalart-Allmaras model should be used rather than the Baldwin-Barth turbulence model for reentry flows.

Results with the Nagano and Hishida $k-\varepsilon$, the Menter $k-\omega$, and the Wilcox (1998) $k-\omega$ models are presented in Fig. 20. Fine grid results with Mesh 2eq are shown along with the results from Richardson extrapolation. The $k-\varepsilon$ results show an overprediction of the turbulent heating rates by approximately 100%. The two $k-\omega$ models show better agreement with the flight data, with the Menter model within 40% and the Wilcox (1998) model within 30% of the data. All three models display a peak in the turbulent heating just downstream of the specified transition plane, which is possibly due to crude transitional behavior of the standard method.

The present simulations have been performed with a gas model that assumes the air flow is in local thermochemical equilibrium. This study needs to be extended to include solutions obtained with a nonequilibrium thermochemical gas model for air. This type of simulation introduces the modeling of the heterogeneous chemical reactions at the vehicle surface and vibrational nonequilibrium effects.

Conclusions

Many Navier-Stokes codes require that the governing equations be written in conservation form with a source term. The Spalart-Allmaras one-equation model was originally developed in substantial derivative form and when rewritten in conservation form, a density gradient term appears in the source term. This density gradient term causes numerical problems and has a small influence on the numerical predictions. Further work has been performed to understand and to justify the neglect of this term.[11,16] The transition trip term has been included in the one-equation eddy viscosity model of Spalart-Allmaras. Several problems with this model have been discovered when applied to high-speed flows.

For the Mach 8 flat plate boundary layer flow with the standard transition method, the Baldwin-Barth and both $k-\omega$ models gave transition at the specified location. The Spalart-Allmaras and low Reynolds number $k-\varepsilon$ models required an increase in the freestream turbulence levels in order to give transition at the desired location. All models predicted the correct skin friction levels in both the laminar and turbulent flow regions.

For Mach 8 flat plate case, the transition location could not be controlled with the trip terms as given in the Spalart-Allmaras model. Several other approaches have been investigated to allow the specification of the transition location. The approach that appears most appropriate is to vary the coefficient that multiplies the turbulent production term in the governing partial differential equation for the eddy viscosity (Method 2). When this coefficient is zero, the flow remains laminar. The coefficient is increased to its normal value over a specified distance to crudely model the transition region and obtain fully turbulent flow. While this approach provides a reasonable interim solution, a separate effort should be initiated to address the proper transition procedure associated with the turbulent production term. Also, the transition process might be better modeled with the Spalart-Allmaras turbulence model with modification of the damping function f_{v1}. The damping function could be set to zero in the laminar flow region and then turned on through the transition flow region.

Predictions have been obtained for the Reentry F flight vehicle with both one- and two-equation turbulence models where the transition location is specified *a priori*. The axisymmetric turbulent predictions for wall

heat flux with the Spalart-Allmaras, Menter $k-\omega$, and Wilcox (1998) $k-\omega$ models are in reasonable agreement with the flight measurements. The mesh sensitivity has been evaluated by obtaining results on three meshes and more accurate results have been obtained with Richardson extrapolation. The simulation assumes the vehicle is at zero degree angle-of-attack while in fact, the flight vehicle is at 0.14 degree angle-of-attack. For the one-equation models, the Spalart-Allmaras model predictions for this case are much better than the results from the Baldwin-Barth model. For the two-equation models, both $k-\omega$ models give good agreement with the flight data, while the low Reynolds number $k-\varepsilon$ model greatly overpredicts the heating in the fully turbulent region.

Future Work

The Reentry F calculations need to be extended to the finite rate chemistry model. This modification should help to determine if the equilibrium air assumption is appropriate and will help determine if the turbulence model with finite chemistry is reasonable. The present Reentry F calculations have assumed a constant wall temperature and this assumption needs to be improved. As there is only limited flight information on the wall temperature and no data in the nose region, a coupled fluid/heat-conduction analysis is needed to provide the wall temperature variation along the vehicle. Further work could be done to modify the transition mechanism for the two-equation models along the lines of the Spalart-Allmaras modifications presented herein. Finally, including a realizeability limitation has been shown to improve predictions for flows with large normal stresses[30] and may also improve predictions through strong normal shocks.

Acknowledgments

This work was supported by Sandia National Laboratories and the Department of Energy's Accelerated Strategic Computing Initiative.

References

1. D. C. Wilcox, *Turbulence Modeling for CFD, 2nd Ed.*, DCW Industries, Inc. 5354 Palm Drive, La Canada, CA 91011, 1998.

2. R. Peyret (Editor), *Handbook of Computational Fluid Mechanics*, Academic Press, San Diego, CA, 1996.

3. A. J. Smits and J.-P. Dussauge, *Turbulent Shear Layers in Supersonic Flow*, American Institute of Physics, Woodbury, New York, NY, 1996.

4. P. R. Spalart and S. R. Allmaras, "A One-Equation Turbulence Model for Aerodynamic Flows," AIAA Paper 92-0439, 1992.

5. P. R. Spalart and S. R. Allmaras, "A One-Equation Turbulence Model for Aerodynamic Flows," *La Recherche Aerospatiale*, No. 1, pp. 5-21, 1994.

6. C. C. Wong, F. G. Blottner, J. L. Payne, and M. Soetrisno, "Implementation of a Parallel Algorithm for Thermo-Chemical Nonequilibrium Flow Solutions," AIAA Paper 95-0152, Jan. 1995.

7. Wong, C. C., Soetrisno, M., Blottner, F. G., Imlay, S. T., and Payne, J. L., "PINCA: A Scalable Parallel Program for Compressible Gas Dynamics with Nonequilibrium Chemistry," SAND 94-2436, Sandia National Laboratories, Albuquerque, NM, 1995.

8. B. Hassan, D. W. Kuntz, and D. L. Potter, "Coupled Fluid/Thermal Prediction of Ablating Hypersonic Vehicles," AIAA Paper No. 98-0168, Jan. 1998.

9. D. W. Kuntz, B. Hassan, and D. L. Potter, "An Iterative Approach for Coupling Fluid/Thermal Predictions of Ablating Hypersonic Vehicles," AIAA Paper 99-3460, June-July 1999.

10. B. S. Baldwin and T. J. Barth, "A One-Equation Transport Model for High Reynolds Number Wall-Bounded Flows," NASA TM-102847, Aug. 1990.

11. F. R. Menter, "Eddy Viscosity Transport Equations and Their Relation to the $k-\varepsilon$ Model," *Journal of Fluids Engineering*, Vol. 119, Dec. 1997, pp. 876-884.

12. Y. Nagano and M. Hishida, "Improved Form of the $k-\varepsilon$ Model for Wall Turbulent Shear Flows." *Journal of Fluids Engineering*, Vol. 109, pp 156-160, June 1987.

13. F. R. Menter, "Two-Equation Eddy-Viscosity Turbulence Models for Engineering Applications," *AIAA Journal*, Vol. 32, No. 8, Aug. 1994, pp. 1598-1605.

14. E. R. Van Driest. "Investigation of Laminar Boundary Layer in Compressible Fluids Using the Crocco Method," National Advisory Committee for Aeronautics, NACA TN-2597, January 1952.

15. E. R. Van Driest, "Problem of Aerodynamic Heating," *Aeronautical Engineering Review*, Vol. 15, No. 10, pp. 26-41, Oct. 1956.

16. F. R. Menter, H. Grotjans, and F. Unger, "Numerical Aspects of Turbulence Modeling for the Reynolds Averaged Navier-Stokes Equations," *Computational Fluid Dynamics Lecture Series* 1997-02, von Karman Institute for Fluid Dynamics, March 3-7, 1997.

17. B. E. Launder and B. E. Sharma, "Application of the Energy Dissipation Model of Turbulence to the Calculation of Flow Near a Spinning Disc," *Letters in Heat and Mass Transfer*, Vol. 1, No. 2, pp. 131-138.

18. G. Theodoridis, P. Prinos and A. Goulas, "Test Case T3 - Free Stream Turbulence," in *Numerical Simulation of Unsteady Flows and Transition to Turbulence*, Edited by O. Pironneau, W. Rodi, I. L. Ryhming, A. M. Savill, and T. V. Truong, Cambridge University press, 1992.

19. D. C. Wilcox, "Reassessment of the Scale Determining Equation for Advanced Turbulence Models," *AIAA Journal*, Vol. 26, No. 11, 1988, pp. 1299-1310.

20. *US Standard Atmosphere*, National Oceanic and Atmospheric Administration, NASA, and the U. S. Air Force, Washington, D. C., October 1976.

21. G. O. Roberts, "Computational Meshes for Boundary Layer Problems," Proceedings of the Second International Conference on Numerical Methods in Fluid Dynamics, *Lecture Notes in Physics*, Vol. 8, Springer-Verlag, New York, pp. 171-177.

22. J. C. Tannehill, D. A. Anderson, and R. H. Pletcher, *Computational Fluid Mechanics and Heat Transfer*, Taylor & Francis, Bristol, PA, 1997, p. 335.

23. R. L. Wright and E. V. Zoby, "Flight Boundary-Layer Transition Measurements on Slender Cone at Mach 20," AIAA Paper 77-719, June 27-29, 1977.

24. K. Sutton, E. V. Zoby and H. H. Hamilton, "Overview of CFD Methods and Comparison with Flight Aerothermal Data," *AGARD Symposium on Validation of Computational Fluid Dynamics*, Lisbon, Portugal May 2-5, 1988.

25. R. A Thompson, E. V. Zoby, K. E. Wurster, P. A. Gnoffo, "Aerothermodynamic Study of Slender Conical Vehicles," *Journal of Thermophysics and Heat Transfer*, Vol. 3, pp. 361-367, October 1989.

26. K. E. Wurster, E. V. Zoby, and R. A. Thompson, "Flow and Vehicle Parameter Influence on results of Engineering Aerothermal Methods," *AIAA Journal of Spacecraft and Rockets*, Vol. 28, Jan.-Feb. 1991, pp. 16-22.

27. J. H. Ferziger and M. Peric, *Computational Methods for Fluid Dynamics*, Springer-Verlag, Berlin, Heidelberg, and New York, 1996.

28. J. H. Ferziger and M. Peric, "Further Discussion of Numerical Errors in CFD," *International Journal for Numerical Methods in Fluids*, Vol. 23, pp. 1263-1274, 1996.

29. P. Roache, "Ch. 3: A Methodology for Accuracy Verification of Codes: the Method of Manufactured Solutions," *Verification and Validation in Computational Science and Engineering*, Hermosa Publishers, New Mexico, 1998.

30. J. G. Moore and J. Moore, "Realizeability in Two-Equation Turbulence Models," AIAA Paper 99-3779, June-July 1999.

Figures

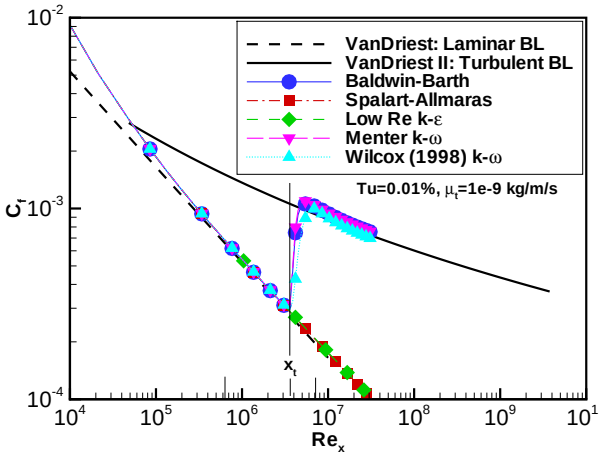

Fig. 1: Transition location with one- and two-equation turbulence models for Mach 8 flat plate flow with the standard transition model.

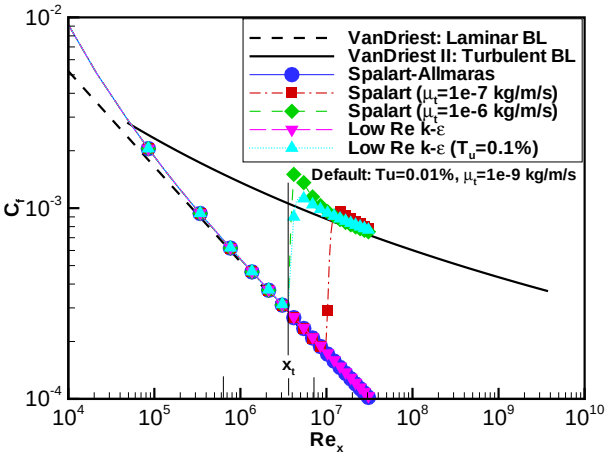

Fig. 2: Transition location for various freestream turb. levels with the Spalart-Allmaras and $k-\varepsilon$ turb. models for Mach 8 flat plate flow.

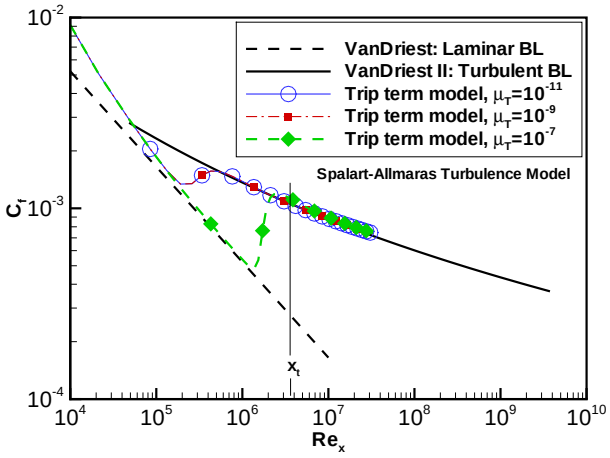

Fig. 3: Transition location for different freestream eddy viscosities with the Spalart-Allmaras turbulence model for Mach 8 flat plate flow.

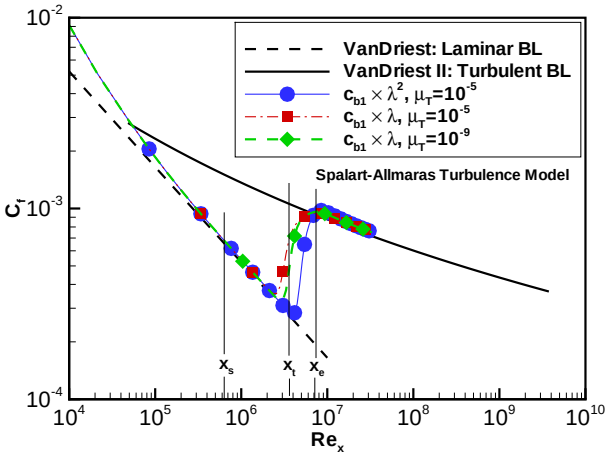

Fig. 4: Transitional flow behavior for Spalart-Allmaras (Meth. 2) with various freestream eddy viscosities for Mach 8 flat plate flow.

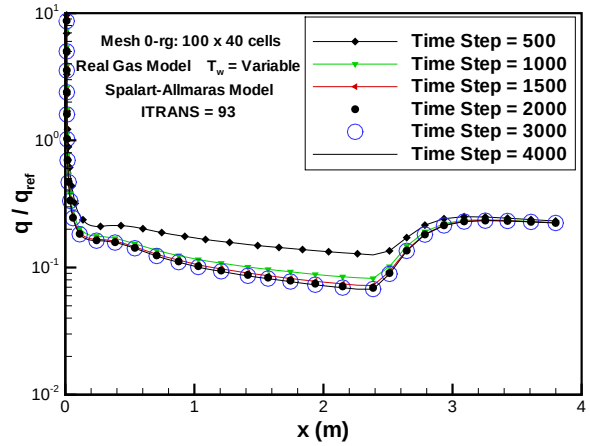

Fig. 5: Iterative convergence of heat flux on *Mesh 0-rg* with the Spalart-Allmaras turbulence model.

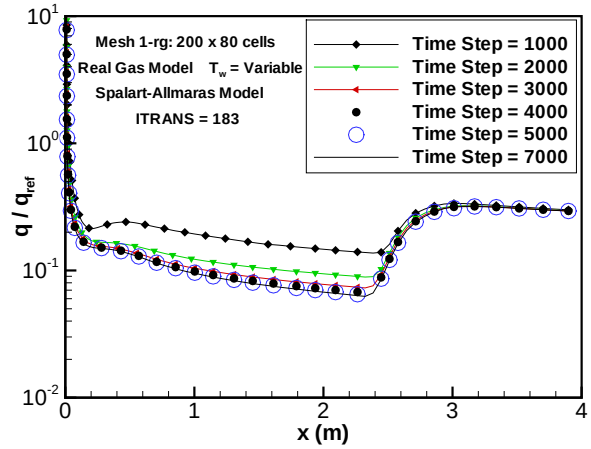

Fig. 6: Iterative convergence of heat flux on Mesh 1-rg with the Spalart-Allmaras turbulence model.

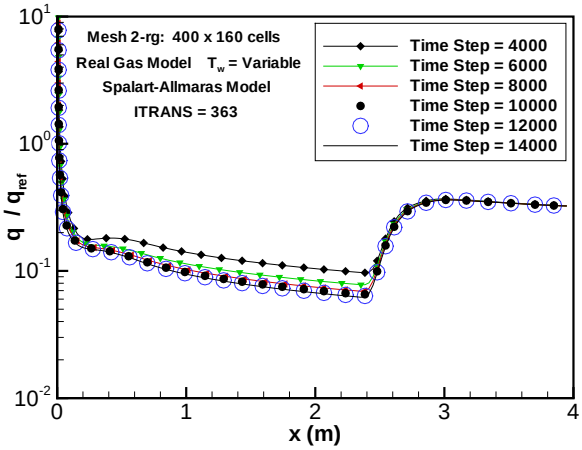

Fig. 7: Iterative convergence of heat flux on Mesh 2-rg with the Spalart-Allmaras turbulence model.

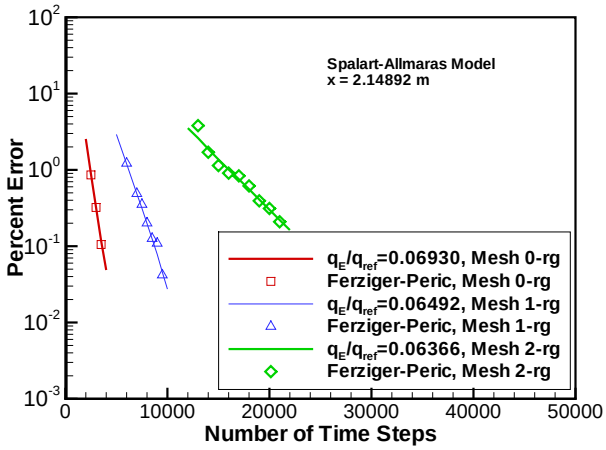

Fig. 8: Iterative convergence error of wall heat flux for the Spalart-Allmaras model at x = 2.14892 m with Mesh rg.

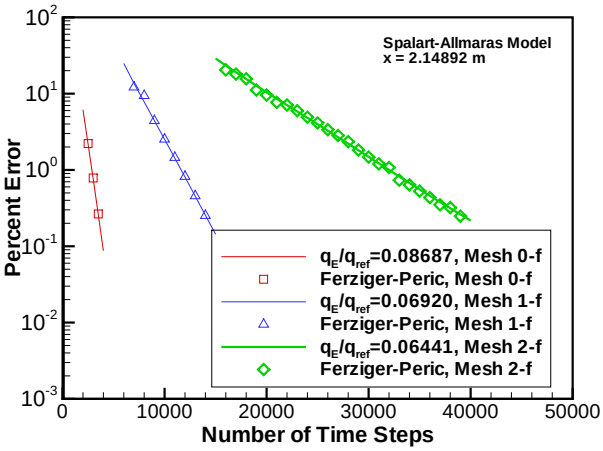

Fig. 9: Iterative convergence error of wall heat flux for the Spalart-Allmaras model at x = 2.14892 m with Mesh f.

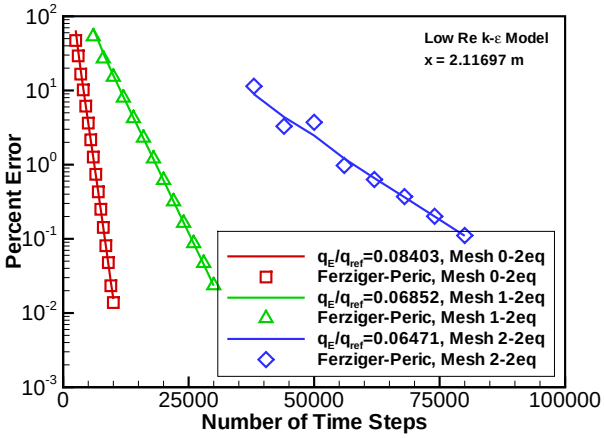

Fig. 10: Iterative convergence error of wall heat flux for the $k-\varepsilon$ model at x = 2.11697 m with Mesh 2eq.

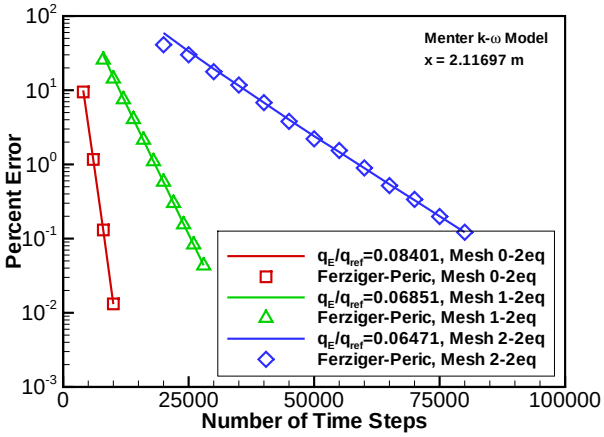

Fig. 11: Iterative convergence error of wall heat flux for the Menter $k-\omega$ model at x = 2.11697 m with Mesh 2eq.

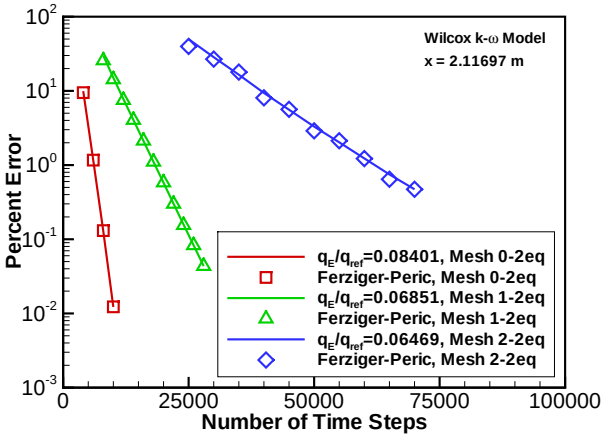

Fig. 12: Iterative convergence error of wall heat flux for the Wilcox (1998) $k-\omega$ model at x = 2.11697 m with Mesh 2eq.

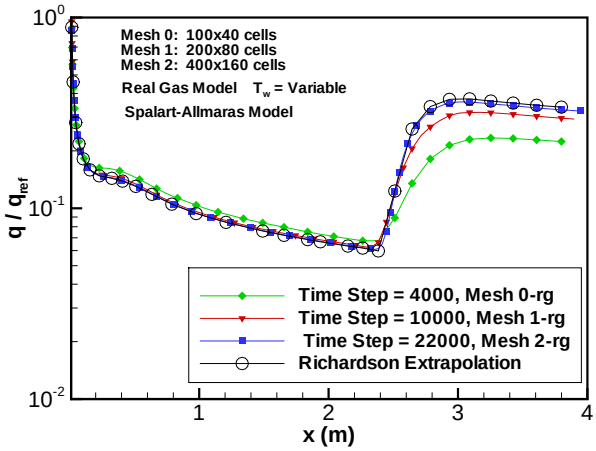

Fig. 13: Spatial convergence of heat flux as the Mesh rg is refined with the Spalart-Allmaras turbulence model.

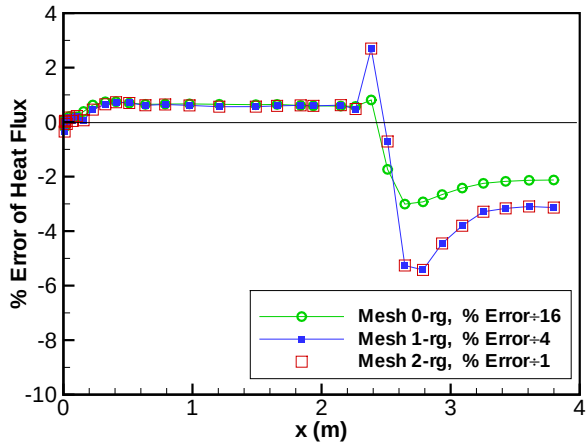

Fig. 14: Error in heat flux along the vehicle with Mesh rg refinement using the Spalart-Allmaras model.

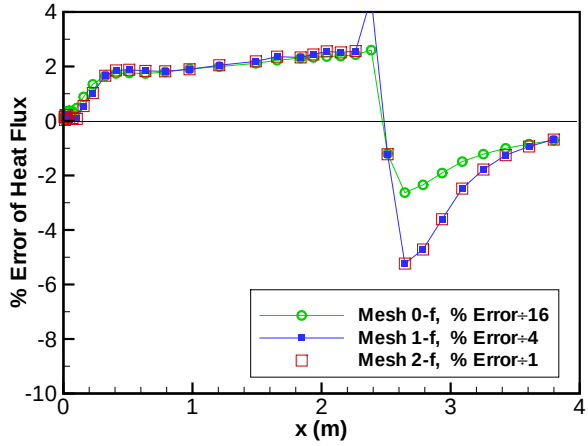

Fig. 15: Error in heat flux along the vehicle with Mesh f refinement using the Spalart-Allmaras model.

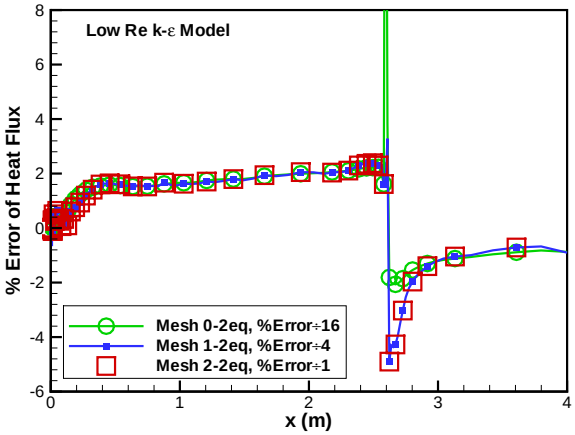

Fig. 16: Error in heat flux along the vehicle with Mesh 2eq refinement using the low Reynolds number $k-\varepsilon$ model.

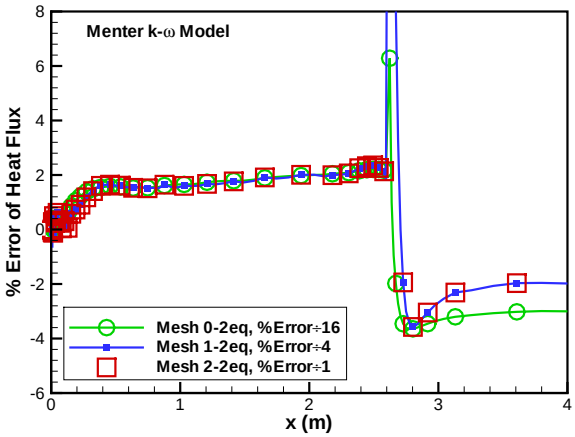

Fig. 17: Error in heat flux along the vehicle with Mesh 2eq refinement using the Menter $k-\omega$ model.

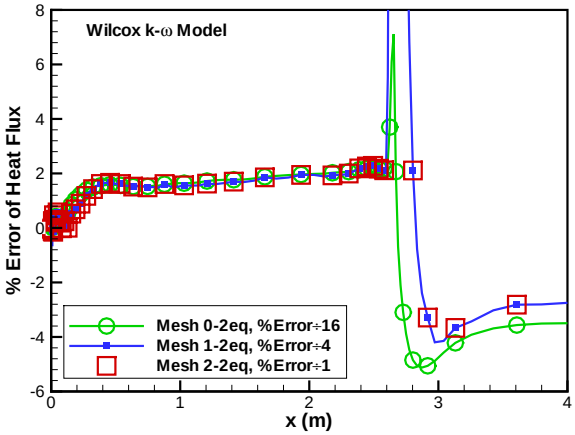

Fig. 18: Error in heat flux along the vehicle with Mesh 2eq refinement using the Wilcox (1998) $k-\omega$ model.

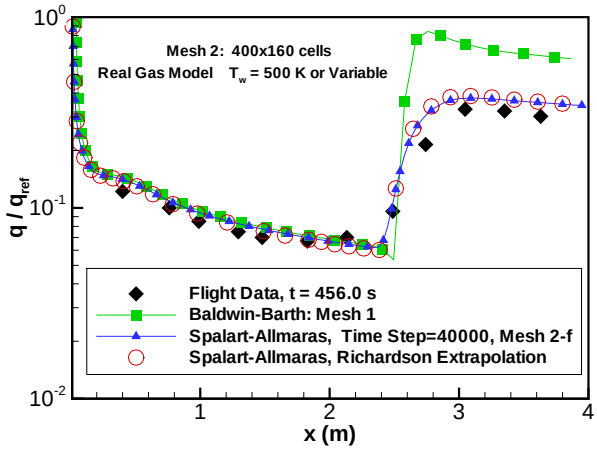

Fig. 19: Comparison of flight data for wall heat flux along Reentry F vehicle at an altitude of 80,000 feet with predictions of the one-equation turbulence models.

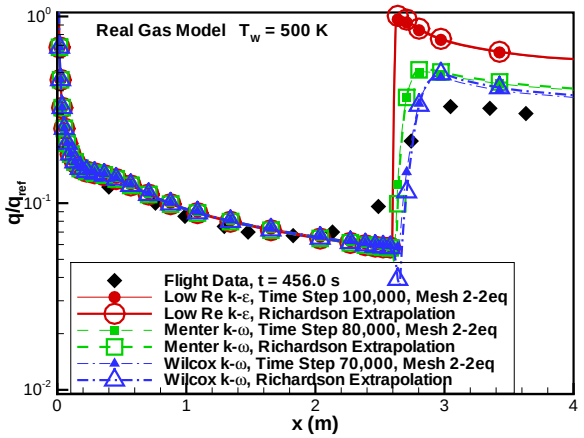

Fig. 20: Comparison of flight data for wall heat flux along Reentry F vehicle at an altitude of 80,000 feet with predictions of the two-equation turbulence models.

ASSESSMENT OF ONE- AND TWO-EQUATION TURBULENCE MODELS FOR HYPERSONIC TRANSITIONAL FLOWS

Christopher J. Roy‡ and Frederick G. Blottner†

Sandia National Laboratories*

P. O. Box 5800, MS 0835

Albuquerque, NM 87185

Abstract

A number of one- and two-equation turbulence models are examined for hypersonic perfect- and real-gas flows with laminar, transitional, and turbulent flow regions. These models were generally developed for incompressible flows, and the extension to the hypersonic flow regime is discussed. In particular, inconsistencies in the formulation of diffusion terms for one-equation models are examined. For the Spalart-Allmaras model, the standard method for forcing transition at a specified location is found to be inadequate for hypersonic flows. An alternative transition method is proposed and evaluated for a Mach 8 flat plate test case. This test case is also used to evaluate three different two-equation turbulence models: a low Reynolds number $k-\varepsilon$ model, the Menter $k-\omega$ formulation, and the Wilcox (1998) $k-\omega$ model. These one- and two-equation models are then applied to the Mach 20 Reentry F flight vehicle. The Spalart-Allmaras model and both $k-\omega$ formulations are found to provide good agreement with the flight data for heat flux, while the Baldwin-Barth and low Reynolds number $k-\varepsilon$ models overpredict the turbulent heating rates. Careful attention is given to solution verification in the areas of both iterative and grid convergence.

Nomenclature

a	speed of sound, *m/s*
D	turbulence diffusion term
d	distance to the wall, *m*
k	specific turbulent kinetic energy, m^2/s^2
Pr_T	turbulent Prandtl number (= 1.0)
p	pressure, N/m^2
q	heat flux, W/m^2
R_N	vehicle nose radius, *m*
r	radial coordinate, *m*
S_P	turbulence production source term
S_D	turbulence destruction source term
S_{ij}	strain rate tensor, *1/s*
T	temperature, *K*
Tu	freestream turbulence intensity percent
t	time, *s*
U	conserved transport quantity
u_i	velocity, *m/s*
V	velocity magnitude, *m/s*
x	axial coordinate, *m*
y	wall normal direction, *m*
α	angle of attack, *degrees*
γ	ratio of specific heats
δ_{ij}	Kronecker delta function (= 1 when $i=j$)
ε	specific dissipation rate, m^2/s^3
θ_{cone}	cone half-angle, *degrees*
μ	absolute viscosity, $N\cdot s/m^2$
ν	kinematic viscosity, m^2/s
$\tilde{\nu}$	Spalart-Allmaras working variable
ρ	density, kg/m^3
τ_{ij}	turbulent stress tensor, m^2/s^2
φ	non-conserved transport quantity
Ω_{ij}	rotation tensor, *1/s*
ω	specific turbulent frequency, *1/s*

Subscripts

E	exact value
eff	effective value (turbulent + laminar)
RE	Richardson extrapolation
ref	reference value

---

‡ Senior Member of Technical Staff, Member AIAA

† Distinguished Member of Technical Staff, AIAA Fellow

* Sandia is a multiprogram laboratory operated by Sandia Corporation, a Lockheed Martin Company, for the United States Department of Energy under Contract DE-AC04-94AL85000.

T	turbulent quantity
t	transitional quantity
w	wall value
∞	freestream value

Superscripts

+	quantity in wall coordinates
~	denotes Favre (density-weighted) averaging
—	denotes Reynolds (time-based) averaging
′	denotes Favre fluctuating quantity

Introduction

This work is concerned with developing a capability to model high-speed compressible flows with laminar, transitional, and turbulent flow regions. The approach uses one- and two-equation eddy viscosity models to predict the turbulent flow. The same governing equations are presently being used to predict the transitional flow region where the onset to turbulent flow is specified and assumed to be known. The prediction of where onset to turbulent flow occurs is a research area that depends on an analysis of the flow stability, understanding of the flow disturbances outside the boundary layer, and a capability to predict the boundary layer receptivity. The process of entraining disturbances into the boundary layer and producing perturbations that can be amplified is called "receptivity."

The more appropriate books providing information on modeling compressible turbulent flows are Wilcox,[1] Chapter 6 by Gatski,[2] and Smits and Dussauge.[3] The modeling of compressible turbulent flows is still an active area of research. The application of some of the turbulence models to compressible flows is not always clear, as the models were originally developed for incompressible flows. Formulations for incompressible flow are not applicable to compressible flow because some variables (e.g., density, viscosity) have been assumed constant in the development. The turbulent transport equations are often written in substantial differential form, while the equations in conservation form are generally required in compressible Navier-Stokes codes. Problems with the formulation of the governing equations for compressible turbulence models in conservation form are discussed. For example, the form of the diffusion term in the Spalart-Allmaras[4,5] model is rewritten and justification for the new form is given.

The SACCARA (Sandia Advanced Code for Compressible Aerothermodynamics Research and Analysis) code[6-9] is used for the results presented in this paper. For one-equation turbulence models, the SACCARA code has options for both the Baldwin-Barth[10] and Spalart-Allmaras eddy viscosity models. There is evidence that the use of the Baldwin-Barth model does not constitute a well-posed system of governing equations.[11] For boundary layer and shear layer flows, the solutions do not appear to converge to a unique solution as the mesh is refined. Therefore, there is more interest in using the Spalart-Allmaras model, as it has proven to be a numerically robust approach. Part of the present work is concerned with the evaluation of the Spalart-Allmaras model for high-speed flows and the simulation of the transition region with the Spalart-Allmaras model.

The SACCARA code also has options for three popular two-equation eddy viscosity turbulence models: a low Reynolds number $k-\varepsilon$ formulation and two $k-\omega$ models. The $k-\varepsilon$ model[1] employs the low Reynolds number modification of Nagano and Hishida[12] to allow integration to solid walls. The first $k-\omega$ formulation is the hybrid model of Menter[13] which is a blending between a $k-\omega$ formulation (near solid walls) and a $k-\varepsilon$ formulation (in shear layers and freestream flow). Menter proposed this hybrid model to take advantage of the accuracy of the $k-\omega$ model for wall-bounded flows and the $k-\varepsilon$ model for free shear layers. The final model is the Wilcox $k-\omega$ model[1] which was modified in 1998 to improve the predictive accuracy for shear flows. This model is referred to as the Wilcox (1998) model in the current work. The appropriate form of the two-equation eddy viscosity equations are also important because the one-equation formulation can be developed from the two-equation transport relations. This approach may be used to determine the appropriate form of the transport equation for the one-equation models.

Two flow cases have been used to investigate the performance of the one- and two-equation eddy viscosity models. The first case is the flow over a flat plate at Mach 8 and an altitude of 15 *km* where the perfect gas model is appropriate. The skin friction along the flat plate is used to judge the accuracy of the predictions through comparisons with the accurate laminar and turbulent results of Van Driest.[14,15] If the standard turbulence models (without modifications for transition) are employed over the whole domain, the transition location often depends on turbulent intensity in the freestream. This behavior is similar to the bypass transition problem. When a transition plane is specified in which the turbulent eddy viscosity is neglected upstream, the transition locations for the Spalart-Allmaras and low Reynolds number $k-\varepsilon$ models still show sensitivity to the freestream turbulence quantities. The control of the transition location with the Spalart-Allmaras model has been investigated.

The second case investigated is the flow over the Reentry F flight vehicle at Mach 20 and at an altitude of 24.4 *km* (80,000 feet) where real gas effects are significant. The measured heat transfer along the vehicle is used to judge the accuracy of the model predictions. The

transition location is specified to give a reasonable match of the wall heat flux with the flight data. It should be remembered that the prediction of transition location is not included in the modeling. The solutions have been obtained on three meshes with the number of cells in each coordinate direction doubled for each mesh refinement. In addition, the solutions on each mesh are marched in time until the wall heat flux has obtained a steady-state value. The accuracy of the iterative solution relative to the steady-state solution has been estimated for each model. The various uncertainties and assumptions in the flight experiment and prediction are discussed. Real gas effects have been taken into account with the use of an equilibrium air model.

Favre-Averaged Transport Equation for Turbulence Models

The generic form of the turbulent transport equation in substantial derivative form[1] is

$$\bar{\rho}\frac{D\varphi}{Dt} = D + S_P - S_D \qquad (1)$$

where

$$D = D_1 - \bar{D}, \qquad D_1 = \frac{\partial}{\partial x_j}\left(\mu_{eff}\frac{\partial \varphi}{\partial x_j}\right)$$

For example for a one-equation eddy viscosity model, the dependent variable is $\varphi \sim \nu_T$ and the effective diffusion coefficient is μ_{eff}. In some models there are two parts to the diffusion term on the right-hand side of Eq. (1); D_1 is the first part of the diffusion term which can be put in conservation form, and $\bar{D}$ is the remaining part. When $\bar{D}$ is included, it can take on several forms. The source term $S = S_P - S_D$ has a production part S_P and a dissipation part S_D. If the continuity equation is multiplied by φ and added to Eq. (1), the resulting equation is the generic transport equation in conservation form:

$$\frac{\partial U}{\partial t} + \frac{\partial}{\partial x_j}\left\{\bar{\rho}\tilde{u}_j\varphi - \mu_{eff}\frac{\partial \varphi}{\partial x_j}\right\} = \bar{D} + S_P - S_D \qquad (2)$$

The dependent variable is $U = \bar{\rho}\varphi$. This development utilizes Favre (overtilde) and Reynolds (overbar) averaging. See Ref. 1 for notation and for details on the Favre averaging procedure.

One-Equation Turbulence Model

There have been a number of one-equation turbulence models developed which use a transport equation to solve for the eddy viscosity directly. The present work is focused on the Spalart-Allmaras model and a brief description is presented below.

Spalart-Allmaras Model

The transport equation for determining the eddy viscosity with near-wall effects included has been developed by Spalart and Allmaras.[4,5] The governing equation form is slightly different than Eq. (1) and is

$$\bar{\rho}\frac{D\varphi}{Dt} = D + S_P - S_D + S_t, \qquad \tilde{\mu} = \frac{\mu_T}{f_{v1}} = \bar{\rho}\varphi \qquad (3)$$

The dependent variable $\varphi = \tilde{\nu} = \nu_T / f_{v1}$, where f_{v1} is a damping function used in the near-wall region and mainly in the viscous sublayer. This function and the right hand side terms will be defined below. The continuity equation is multiplied by φ and added to Eq. (3) which gives a transport equation in conservation form for the Spalart-Allmaras model in the form of Eq. (2)

Spalart-Allmaras Model

$$\frac{\partial U}{\partial t} + \frac{\partial}{\partial x_j}\left\{\bar{\rho}\tilde{u}_j\varphi - \mu_{eff}\frac{\partial \varphi}{\partial x_j}\right\} = \bar{D} + S_P - S_D + S_t \qquad (4)$$

$$U = \bar{\rho}\tilde{\nu} = \bar{\rho}\varphi, \qquad \mu_{eff} = \frac{\mu + \tilde{\mu}}{\sigma}$$

The right-hand side has contributions from a diffusion term as well as production, destruction, and trip terms. The four terms in the model are written as follows:

Diffusion-Original Form

$$D = \bar{\rho}\frac{\partial}{\partial x_j}\left[\frac{\mu_{eff}}{\bar{\rho}}\frac{\partial \varphi}{\partial x_j}\right] + D_2 = D_1 + \bar{D}$$

$$\mu_{eff} = \frac{\mu + \tilde{\mu}}{\sigma} = \bar{\rho}\left(\frac{\nu + \varphi}{\sigma}\right), \qquad \bar{D} = D_2 - D_3$$

$$D_2 = \frac{c_{b2}\bar{\rho}}{\sigma}\left(\frac{\partial \varphi}{\partial x_j}\right)\left(\frac{\partial \varphi}{\partial x_j}\right), \qquad D_3 = \left(\frac{\mu_{eff}}{\bar{\rho}}\right)\frac{\partial \bar{\rho}}{\partial x_j}\frac{\partial \varphi}{\partial x_j}$$

Diffusion-Modified for Compressible Flow

$$D = D_1 + D_2, \qquad \bar{D} = D_2$$

Production

$$S_P = c_{b1}[1 - f_{t2}]\tilde{S}\bar{\rho}\varphi$$

Destruction

$$S_D = \left\{c_{w1}f_w - \frac{c_{b1}}{\kappa^2}f_{t2}\right\}\bar{\rho}\left(\frac{\varphi}{d}\right)^2$$

Trip Term

$$S_t = f_{t1}\rho(\Delta U)^2$$

In the formal transform of the transport equation into conservation form, the diffusion term D_3 includes a density gradient term. This term is zero when the transport equation (Eq. (4)) is developed from the compressible form of the $k-\varepsilon$ transport equations,[11,16] and is shown above in the term *Diffusion-Modified for Compressible Flow.* This form of the diffusion term is used in the present work. Including this density gradient term has been found to cause stability problems for high-speed flows, while having negligible effect on the predictions. The model controls transition from laminar to turbulent flow with the use of the trip term. With this additional physics, the foregoing governing equation requires some additional terms and definitions for f_{t1} and f_{t2} which involves the coefficients c_{t1} to c_{t4}. Except where noted, the standard values for the model constants are used in the current work.

Boundary Conditions for Spalart-Allmaras Model

At the wall $\mu_T = 0$ or $\tilde{\nu} = 0$. The freestream boundary condition for this model is the specification of the turbulent eddy viscosity μ_T. In the freestream there should be no production of the eddy viscosity, which requires that

$$f_{t2} = c_{t3}e^{-c_{t4}\chi^2} > 1, \qquad (c_{t3} = 1.2, \quad c_{t4} = 0.5)$$

in order to turn off the production term in Eq. (6). The restriction on χ is

$$\chi = \tilde{\nu}/\nu < \sqrt{(\ln c_{t3})/c_{t4}} = 0.604$$

The restriction on the freestream eddy viscosity becomes

$$\frac{\mu_T}{\mu} < \chi f_{v1} = \chi/[1+(c_{v1}/\chi)^3] = 3.713\times10^{-4} \qquad (5)$$
$$c_{v1} = 7.1$$

The freestream eddy viscosity as suggested by Spalart-Allmaras is $\tilde{\nu} < 1/2\nu$, which gives

$$\frac{\mu_t}{\mu} < \tilde{\nu} f_{v1}/\nu = 1.746\times10^{-4}.$$

Control of Laminar and Turbulent Flow with the Spalart-Allmaras Model

The governing equation has three terms that are influenced by the transition model. The complete source term (for the conservative formulation) is

$$S = \frac{c_{b2}\bar{\rho}}{Pr_T}\left(\frac{\partial\tilde{\nu}}{\partial x_j}\right)^2 + c_{b1}[1-\underline{f_{t2}}]\tilde{S}U$$
$$-(c_{w1}f_w - \underline{c_{b1}f_{t2}/\kappa^2})\bar{\rho}\left(\frac{\tilde{\nu}}{d}\right)^2 + \underline{f_{t1}\bar{\rho}(\Delta U)^2} \qquad (6)$$

where the trip terms are underlined in the above equation. The first term is part of the diffusion term and is included in the source term as it is evaluated numerically in an explicit manner. The second term is the production term and it will produce or increase the eddy viscosity if $f_{t2} < 1$. The third term is the destruction term and it will decrease the eddy viscosity if $c_{w1}f_w > c_{b1}f_{t2}/\kappa^2$. The fourth term is the trip term and it will increase the eddy viscosity as $f_{t1} > 0$.

The model generally predicts turbulent flow everywhere when the trip terms are zero

$$f_{t1} = 0 \text{ or } c_{t1} = 0, \qquad f_{t2} = 0 \text{ or } c_{t3} = 0$$

The flow can be made laminar everywhere with the following values of the trip terms:

$$f_{t1} = 0 \text{ and } f_{t2} \geq 1.0 \text{ or } f_{t2} = c_{t3}\Lambda, \quad \Lambda = e^{-c_{t4}\chi^2}$$
$$\text{or} \quad f_{t1} = 0, \qquad f_{t2} = 0, \qquad c_{b1} = 0$$

Several different approaches have been investigated to control transition and to replace the original trip model approach of Spalart-Allmaras.

Method 1 (f_{t2} is modified)

In this approach the value of $f_{t1} = 0$, and $f_{t2} = c_{t3}(1-\lambda)$ where λ varies from the laminar flow region to the turbulent flow region. In the laminar flow region $\lambda = 0$ while in the turbulent flow region $\lambda = 1$. The parameter is increased smoothly and defines the transitional flow region. This method requires specification of the location and length of the transitional region.

Method 2 (c_{b1} is modified)

In this method the trip terms $f_{t1} = 0$ and $f_{t2} = 0$ are set to zero. The coefficient c_{b1} is modified from the laminar flow region to the turbulent flow region as follows:

$$x < x_s: \; c_{b1} = 0, \qquad x > x_e: \; c_{b1} = 0.1355$$

$$x_s \leq x \leq x_e: \; c_{b1} = 0.1355\lambda^p, \quad \lambda = (x-x_s)/(x_e-x_s)$$

In this method, the location of the start of transitional flow x_s and end of transitional flow x_e are specified.

Method 3 ($c_{b1}(1-f_{t2})$ is modified)

In this method the production term coefficient is modified by writing this term as $\alpha c_{b1}(1-f_{t2})$. The parameter α increases from zero to one in the transitional flow region. From the definition of f_{t2}, the following is obtained:

$$\chi = \tilde{\nu}/\nu = \sqrt{-\ln[f_{t2}/c_{t3}]/c_{t4}} \tag{7}$$

The production term switches sign when $f_{t2} = 1$ which gives a critical value of χ which is $\chi^* = 0.604$. When $x < x_t$, set $\alpha = 0$ and there is no production of eddy viscosity upstream of the transition location x_t. When $x > x_t$, α is increased downstream towards one. This increase is controlled by setting

$$\alpha = 1 - f_{t2} = 1 - c_{t3}e^{-c_{t4}\chi^2}$$

When $x > x_t$ and $\chi \le \chi^*$, then $\chi = \chi^*$. When $x > x_t$ and $\chi > \chi^*$, then χ is obtained from Eq. (7). In this method, only the single parameter x_t must be specified.

Two-Equation Turbulence Models

The standard method for specifying transition to turbulence is through analogy with the turbulence intermittency approach. The turbulence transport equations are solved over the entire domain, with a user-defined transition plane specified. Upstream of this plane, the effective viscosity is simply the laminar value, while downstream the effective viscosity is the sum of the laminar and turbulent viscosities.

High Turbulent Reynolds Number $k-\varepsilon$ Model

The high Reynolds number formulation[1] is appropriate for turbulent flows but is not appropriate in the near-wall region. It can be applied in the outer part of boundary layers and combined with an inner boundary layer approach near the wall to obtain a complete formulation. For the standard $k-\varepsilon$ model, the turbulent kinetic energy equation for a compressible fluid takes the same form as Eq. (2) where the variables have the following values:

$$U = \bar{\rho}k = \bar{\rho}\varphi, \qquad \mu_{eff} = \mu_k, \qquad \bar{D} = 0$$
$$S_{Pk} = \bar{\rho}P, \qquad S_{Dk} = \bar{\rho}\varepsilon \tag{8}$$

The production term P takes the standard form for compressible flows (see Ref. 1), and the effective viscosity is defined below in Eq. (10). The transport equation for dissipation of turbulent kinetic energy is the same form as Eq. (2), where the variables have the following values:

$$U = \bar{\rho}\varepsilon = \bar{\rho}\varphi, \qquad \mu_{eff} = \mu_\varepsilon$$
$$\bar{D} = 0, \qquad S_{P\varepsilon} = c_{\varepsilon 1}f_1\bar{\rho}\frac{\varepsilon}{k}P, \qquad S_{D\varepsilon} = c_{\varepsilon 2}f_2\bar{\rho}\frac{\varepsilon}{k} \tag{9}$$

The effective viscosities are obtained from

$$\mu_k = \mu + \mu_T/\sigma_k, \qquad \mu_\varepsilon = \mu + \mu_T/\sigma_\varepsilon$$
$$\text{where} \quad \mu_T = c_\mu f_\mu \bar{\rho}k^2/\varepsilon \tag{10}$$

The constants in the foregoing equations use the standard values.

Low Turbulent Reynolds Number $k-\varepsilon$ Model

The Nagano and Hishida model[12] was developed for incompressible flow and is included in the current formulation. The model uses the following damping function in the eddy viscosity relation given in Eq. (10):

$$f_\mu = [1 - \exp(-y^+/26.5)]^2$$

This damping function is written in terms of the distance from the wall y^+. The source term for the turbulent kinetic energy Eq. (8) is

$$S = \bar{\rho}P - \bar{\rho}\varepsilon + \tilde{D}$$

The production term has been approximated with:

$$\bar{\rho}P \approx \mu_T\left(\frac{\partial \tilde{u}_i}{\partial x_j} + \frac{\partial \tilde{u}_j}{\partial x_i}\right)\frac{\partial \tilde{u}_i}{\partial x_j}$$

The compressible term

$$-\frac{2}{3}(\bar{\rho}k + \mu_T S_{kk})S_{kk}, \quad \text{where} \quad S_{kk} = \frac{\partial \tilde{u}_k}{\partial x_k}$$

has been neglected in the current formulation. The source term for the dissipation rate equation is

$$S = \frac{\varepsilon}{k}(c_{\varepsilon 1}f_1\bar{\rho}P - c_{\varepsilon 2}f_2\bar{\rho}\varepsilon) + \tilde{E}$$

The parameters in these source terms are written as

$$f_1 = 1, \qquad f_2 = 1 - 0.3e^{-R_T^2}, \qquad R_T = k^2/\nu\varepsilon$$
$$\tilde{D} = -2\mu\left(\frac{\partial\sqrt{k}}{\partial y}\right)^2, \qquad \tilde{E} = \mu\nu_T(1-f_\mu)\left(\frac{\partial^2\tilde{u}}{\partial y^2}\right)^2$$

The variables $\tilde{D}$ and $\tilde{E}$ use boundary layer type derivatives normal to the wall and $\tilde{E}$ requires the tangential velocity component.

The Nagano-Hishida and the Launder-Sharma[17] low Reynolds $k-\varepsilon$ turbulence models have been used by Theodoridis, Prinos, and Goulas[18] to predict transitional flow. They have investigated a flat plate flow experiment where the freestream turbulent intensity was ap-

proximately 3 percent and 6 percent. The two turbulence models were used to model the laminar to turbulent bypass transition in which the freestream turbulence determines where the transition to turbulent flow occurs. For this bypass transition case, the Nagano-Hishida model predicts transition to turbulent flow too near the leading edge while the Launder-Sharma model predictions are in reasonable agreement with the experimental data. Of course, neither of these turbulence models were developed to predict where transition will occur in a flow; the performance of the Launder-Sharma model in predicting the location of transition is fortuitous. The failure of the Nagano-Hishida for transitional flow requires caution in the application of this model and a procedure is required to have the model turned on at the appropriate location.

Menter k-ω Model

Two different two-equation turbulence models are described which solve equations for the turbulent kinetic energy, k, and the frequency of turbulent fluctuations, ω. The Menter k-ω model[13] is a hybrid model which uses a blending function to combine the best aspects of both the k-ω and the k-ε turbulence models. Near solid walls, a k-ω formulation is used which allows integration to the wall without any special damping or wall functions. Near the outer edge of the boundary layer and in shear layers, the model blends into a transformed version of the k-ε formulation, thus providing good predictions for free shear flows.

For the Menter k-ω model, the terms in Eq. (2) are as follows:

Turbulent Kinetic Energy Equation

$$U = \bar{\rho}k = \bar{\rho}\varphi, \qquad \mu_{eff} = \mu_k, \qquad \bar{D} = 0$$
$$S_{Pk} = \bar{\rho}P, \qquad S_{Dk} = \beta^*\bar{\rho}k\omega \tag{11}$$

Turbulent Frequency Equation

$$U = \bar{\rho}\omega = \bar{\rho}\varphi, \qquad \mu_{eff} = \mu_\omega$$
$$\bar{D} = 2\bar{\rho}(1-F)\sigma_{\omega 2}\frac{1}{\omega}\frac{\partial k}{\partial x_j}\frac{\partial \omega}{\partial x_j} \tag{12}$$
$$S_{P\omega} = \bar{\rho}\frac{\gamma}{\nu_T}P, \qquad S_{D\omega} = \beta\bar{\rho}\omega^2$$

The cross-diffusion term ($\bar{D}$) in Eq. (12) arises due to the transformation of the ε-equation into an equation for ω. The production term is given by

$$P = \tau_{ij}\frac{\partial u_i}{\partial x_j}, \quad \text{where} \quad \tau_{ij} = -\overline{u_i' u_j'}\,. \tag{13}$$

For 3-D compressible flows, the turbulence stress tensor can be expressed as:

$$\tau_{ij} = 2\nu_t\left(S_{ij} - \frac{1}{3}\frac{\partial \tilde{u}_k}{\partial x_k}\delta_{ij}\right) - \frac{2}{3}k\delta_{ij} \tag{14}$$

The effective viscosities are given by

$$\mu_k = \mu + \sigma_k\mu_T\,, \qquad \mu_\omega = \mu + \sigma_w\mu_T$$
$$\text{where} \quad \mu_T = \bar{\rho}k/\omega \tag{15}$$

and the model constants above are blended values of the k-ω and k-ε parameters. For example, for the constant β,

$$\beta = F\beta_1 + (1-F)\beta_2$$

where F varies from 1 at the wall to zero outside wall boundary layers, and a "1" denotes k-ω constants and "2" denotes k-ε constants. The values for these constants are:

$$\sigma_{k1} = \frac{1}{2}, \quad \sigma_{\omega 1} = \frac{1}{2}, \quad \beta_1 = \frac{3}{40},$$
$$\beta^* = 0.09, \quad \kappa = 0.41, \quad \gamma_1 = \frac{\beta_1}{\beta^*} - \frac{\sigma_{\omega 1}\kappa^2}{\sqrt{\beta^*}}$$

and

$$\sigma_{k2} = 1, \quad \sigma_{\omega 2} = 0.856, \quad \beta_2 = 0.0828,$$
$$\beta^* = 0.09, \quad \kappa = 0.41, \quad \gamma_2 = \frac{\beta_2}{\beta^*} - \frac{\sigma_{\omega 2}\kappa^2}{\sqrt{\beta^*}}\,.$$

Wilcox (1998) k-ω Model

For the Wilcox (1998) k-ω model,[1] the terms in Eq. (2) are as follows:

Turbulent Kinetic Energy Equation

$$U = \bar{\rho}k = \bar{\rho}\varphi, \qquad \mu_{eff} = \mu_k, \qquad \bar{D} = 0$$
$$S_{Pk} = \bar{\rho}P, \qquad S_{Dk} = \beta^*\bar{\rho}k\omega \tag{16}$$

Turbulent Frequency Equation

$$U = \bar{\rho}\omega = \bar{\rho}\varphi, \qquad \mu_{eff} = \mu_\omega, \qquad \bar{D} = 0$$
$$S_{P\omega} = \bar{\rho}\frac{\gamma}{\nu_T}P, \qquad S_{D\omega} = \beta\bar{\rho}\omega^2 \tag{17}$$

where

$$\alpha = \frac{13}{25}, \qquad \beta = \beta_0 f_\beta, \qquad \beta^* = \beta_0^* f_{\beta^*}$$

$$\sigma_k = \sigma_\omega = \frac{1}{2}, \qquad \beta_0^* = \frac{9}{100}$$

$$f_{\beta^*} = \begin{cases} 1, & \chi_k \le 0 \\ \dfrac{1 + 680\chi_k^2}{1 + 400\chi_k^2}, & \chi_k > 0 \end{cases}, \quad \chi_k \equiv \frac{1}{\omega^3}\frac{\partial k}{\partial x_j}\frac{\partial k}{\partial x_j}$$

$$\beta_0 = \frac{9}{125}, \quad f_\beta = \frac{1 + 70\chi_\omega}{1 + 80\chi_\omega}, \quad \chi_\omega \equiv \left| \frac{\Omega_{ij}\Omega_{jk}S_{ki}}{(\beta_0^*\omega)^3} \right|$$

$$\Omega_{ij} = \frac{1}{2}\left(\frac{\partial \tilde{u}_i}{\partial x_j} - \frac{\partial \tilde{u}_j}{\partial x_i}\right), \qquad S_{ij} = \frac{1}{2}\left(\frac{\partial \tilde{u}_i}{\partial x_j} + \frac{\partial \tilde{u}_j}{\partial x_i}\right).$$

The production term, P, and the eddy viscosity definitions are given in Eqs. (13) and (15), respectively. This formulation is a modification to an earlier Wilcox $k-\omega$ model[19] in order to improve model predictions for free shear layers and to reduce the solution sensitivity to freestream ω values.

Flow Predictions for Flat Plate

Flow over a flat plate has been chosen as a high speed test case to illustrate the behavior of the laminar/turbulent flow results obtained with the one- and two-equation turbulence models. The test case is Mach 8 flow over a flat plate with a wall temperature of T_w=1000 K and freestream conditions corresponding to an altitude of 15 km. For this case, the temperature in the flow is sufficiently low that perfect gas assumption with $\gamma = 1.4$ is reasonable.

Freestream Flow Conditions

The freestream conditions[20] for the flat plate case are:

$$p_\infty = 1.21114 \times 10^4 \ kg/m/s^2, \quad T_\infty = 216.65 \ K$$

$$\rho_\infty = 0.19475 \ kg/m^3, \quad a_\infty = \sqrt{\frac{\gamma p_\infty}{\rho_\infty}} = 295.07 \ m/s$$

$$V_\infty = a_\infty M_\infty = 2360.54 \ m/s$$

$$\mu_\infty = \frac{1.458 \times 10^{-6} T_\infty^{3/2}}{(T_\infty + 110.4)} = 1.4216 \times 10^{-5} \ kg/m/s$$

For the Spalart-Allmaras model, the restriction on the freestream eddy viscosity is determined by Eq. (5), which gives

$$\mu_{T_\infty} < 5.27 \times 10^{-9} \ kg/m/s$$

for the Mach 8 flat plate flow case. The freestream eddy viscosity for all models was thus chosen as

$$\mu_{T_\infty} < 1.0 \times 10^{-9} \ kg/m/s$$

unless indicated otherwise. For the two-equation models, the further specification of a freestream turbulence intensity of 0.01% was used to determine the turbulent kinetic energy in the freestream from

$$k = \frac{1.2}{2}\left(\frac{Tu}{100} V_\infty\right)^2 = 6 \times 10^{-9} V_\infty^2.$$

Computational Mesh for the Flat Plate

A parabolic mesh has been used around the flat plate with the (x, y) Cartesian coordinate system fixed at the leading edge. This mesh topology mitigates the effects of the leading edge singularity. The parabolic coordinates ξ, η are related to the Cartesian coordinates as follows:

$$x = \alpha(\xi^2 - \eta^2) \qquad y = 2\alpha\xi\eta \qquad \alpha = 0.05$$

$$0 \le \xi \le \xi_{max} \qquad 0 \le \eta \le 1 \qquad \xi_{max} = \sqrt{1 + 1/\alpha}$$

The value of ξ_{max} has been determined by setting $x = 1$ at $\eta = 1$. This gives a mesh that is slightly longer than one meter along the flat plate. A uniform mesh is used in the ξ coordinate direction while a non-uniform mesh spacing is used in the η coordinate direction. The mesh spacing has been determined with the lower boundary stretching transformation of Roberts[21] (see also Ref. 22). Most of the results have been obtained with 80x160 cells. A coarser mesh of 40x80 and a finer mesh of 160x320 have been used to show that the 80x160 mesh provides results sufficiently accurate for the figures presented. A stretching parameter of $\beta = 1.001$ has been used for the one-equation models. This choice for β gives maximum y^+ values of approximately 2.3 for the coarse 40x80 mesh. As expected, the maximum allowable y^+ values for the two-equation models were found to be much smaller than for the one-equation models, with the larger values resulting in convergence problems. Thus a stretching parameter of $\beta = 1.00007$ was used giving $y^+ \le 0.2$ at the end of the plate for the coarse mesh.

Flat Plate Results with Standard Transition Method

For the freestream conditions and meshes specified above, the laminar/turbulent flow has been calculated with the SACCARA code and compared to the accurate laminar and turbulent results obtained for this case by Van Driest.[14,15] The standard transition method is used

where the laminar viscosity is the sole contributor to the effective viscosity upstream of the transition plane (x_t = 0.1196 m). The L2 norms of the residuals for both the momentum equations and the turbulence equations were reduced at least eight orders of magnitude in each case, suggesting that the results for the flat plate problem are not influenced by iterative convergence error.

Skin friction profiles have been obtained using all five turbulence models for the Mach 8 flat plate case. The Baldwin-Barth and both $k-\omega$ models give transition at the specified transition plane for the given freestream turbulence levels as shown in Fig. 1. In order to move the transition point to the desired location, the freestream eddy viscosity had to be increased to 1×10^{-6} kg/m/s for the Spalart-Allmaras model, and the turbulence intensity had to be increased to 0.1% for the low Reynolds number $k-\varepsilon$ model (see Fig. 2). All of the models which correctly predict turbulent flow downstream of the transition point also predict skin friction in this region in agreement with the theory.

Modified Transition Results for Spalart-Allmaras Model

Solutions have been obtained with the Spalart-Allmaras trip functions f_{t1}, f_{t2} set to zero. The flow is turbulent along the flat plate for this case with the freestream eddy viscosity μ_T varying from 10^{-9} to 10^{-5} *kg/m/s*. Solutions have been obtained with the trip function f_{t2} included and f_{t1} set to zero. For this case the flow transition location is dependent on the freestream eddy viscosity. When the eddy viscosity is 10^{-9} *kg/m/s*, the flow remains laminar over the length of the flat plate. As previously discussed, numerical solutions show that the flow can be maintained laminar by making the production term S_P zero by setting c_{b1} = 0 with the trip functions f_{t1}, f_{t2} set to zero.

The complete Spalart-Allmaras model has trip terms included to control the transition location, but the formulation is not intended to model the transition flow region. The behavior of this model has been investigated with the results for the local skin friction given in Fig. 3 where the trip location x_t is specified. The specified transition location corresponds to $Re_x = 3.84\times10^6$ while the numerical prediction has transition varying as the freestream eddy viscosity is increased above a value of approximately 10^{-9} *kg/m/s*. For these high speed flows, it is difficult to control the transition location with the suggested trip model. In addition, there is no control of the length of the transition region. Because of these experiences with the behavior of the Spalart-Allmaras trip model, different approaches have been investigated.

Three methods have been investigated to control the transition location and the length of transition as previously described. There are two parameters x_t and x_l introduced to control the transition behavior. The parameter x_t is at the middle of the transition region while $x_s = x_t - x_l$ is the location upstream where transition starts and the location downstream $x_e = x_t + x_l$ where the flow becomes fully turbulent. The values of these parameters are:

$$x_t = 0.1196\ m, \quad x_l = 0.1\ m, \quad Re_{x_t} = 3.84\times10^6$$

These locations are also indicated in Fig. 4.

The results for the skin friction with the three proposed approaches for modeling transition have been investigated. All of the methods remain laminar a significant distance after the specified start of transition. With Method 1, where the trip function f_{t2} is modified, transition occurs downstream of the desired location with very rapid transition onset. With Method 2. where the production coefficient c_{b1} is modified, transition occurs near the desired location with a reasonable variation of the skin friction in the transition region. With Method 3, where the production term coefficient $c_{b1}(1-f_{t2})$ is modified, transition occurs downstream of the desired transition location with very rapid transition onset. From this investigation it is concluded that Method 2 provides a reasonable technique to specify the transition location with limited control over the transition region length. The results for method 2 are presented in Fig. 4. When λ varies linearly over the transition region, there is better control. The transition control Method 2 appears to be insensitive to the freestream eddy viscosity. Other approaches need to be considered and evaluated.

Flow Predictions for Reentry F Vehicle

Reentry F Description and Experimental Results

The Reentry F flight experiment[23] was performed in 1968 to provide measurements of wall heat transfer rates at reentry flow conditions that cannot be obtained in ground-based experimental facilities. The data is for the flow over a slender conical vehicle where there is only a small amount of surface ablation localized at the nosetip. The boundary layer flow is laminar, transitional, or turbulent depending on the altitude and location along the body surface. The Reentry F vehicle was a 5 degree sphere-cone with an initial nose radius of 0.1 inch and the vehicle length is 13 feet. A graphite nosetip extended for the first 7.54 inches followed by a conical beryllium frustum. The heat transfer measurements were obtained at altitudes between 120,000 and 60,000 feet. The data at a flight time of 456.0 seconds or an alti-

tude of 80,000 feet (24.383 km) is used to validate the turbulence model predictions. Although this flight experiment provides exceptional data, there are many aspects of the flow conditions, body orientation, body shape, and wall surface temperature that are not completely or precisely known.

In recent years, this experimental data set has been reevaluated with modern computational codes and is documented in Refs. 24-26. Aerothermal predictions have also been presented in these papers. It is important to observe that the freestream conditions for the three predictions are slightly different and the wall temperature in some cases is constant while in others a variation is taken into account. Most of these solutions are for axisymmetric flow with the vehicle at zero degree angle of attack, but full three-dimensional solutions have been obtained with the actual flight angle of attack of 0.14 degrees. There are many details of this flight experiment that are not well defined, but overall the heat transfer predictions are in reasonable agreement with the flight measurements. Of course, none of the modeling includes a capability to predict the transition location. Further information on the flight experiment is given in Wright and Zoby.[23]

The flow conditions at an altitude of 80,000 feet have become the location in the flight trajectory most often analyzed and are also chosen for the present investigation. The present freestream conditions are based on the U. S. Standard Atmosphere, 1976.[20] The assumed turbulent eddy viscosity is given as well as the turbulence intensity for the two-equation models. The freestream flow conditions (in SI units) that have been used in are

$$M_\infty = 19.97, \qquad \alpha = 0^\circ, \qquad \rho_\infty = 0.043523$$

$$T_\infty = 221.034, \qquad T_w = 500, \qquad p_\infty = 2761.41$$

$$V_\infty = 5951.858, \qquad a_\infty = 298.04$$

$$\mu_\infty = 1.445 \times 10^{-5}, \qquad \mu_T = 3.3227 \times 10^{-14}$$

$$Tu = 0.01\%, \qquad x_{body} = 4.0$$

Note that there is some amount of uncertainty in the specification of these properties.

The nosetip of the vehicle is graphite and initially is a sphere-cone with a nose radius $R_N = 0.00254$ *m*. Due to ablation, the nose radius increases to 0.00343 *m* at an altitude of 80,000 feet. This result is an estimated value from an ablation analysis of the nosetip.[26] For the present analysis, it is assumed that the nosetip shape remains a sphere-cone after ablation with the same cone half angle as the conical vehicle, which is $\theta_{cone} = 5^\circ$. The nosetip is illustrated below. The origin in this figure is located at the virtual tip of the conical vehicle. For the approximated sphere-cone configuration for the Reentry

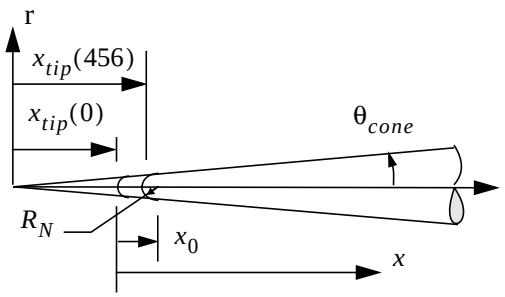

F vehicle simulation, the location of the original nosetip and ablated nosetip is specified as

$$x_0 = 0.012752\ m, \qquad x_{tip}(0) = 0.026603\ m$$

$$x_{tip}(456) = 0.035925\ m$$

In previous analyses of this vehicle, the coordinate x is defined as the axial distance without a clear definition of the origin location given in many cases. Some figures indicate that the origin is located at the ablated nose of the body. The axial location x in this paper is measured from the *nosetip of the un-ablated vehicle*. The uncertainty in the location of the axial heat flux measurements has a negligible impact on the results presented.

Due to the high velocities, the gas temperature is more than 6000 *K* in the nosetip region with dissociation of the oxygen and nitrogen occurring. Downstream of the nose the inviscid flow temperature behind the shock is 420 K, and perfect gas flow occurs. However, in the boundary layer the viscous dissipation increases the gas temperature to around 3000 *K* and dissociation of oxygen occurs. At 80,000 feet, the chemical reactions are sufficiently fast that the air is assumed to be in local thermochemical equilibrium. This is believed to be a reasonable assumption, but a finite rate solution needs to be performed in the future to validate this simplification. There is also some ablation of the nosetip which introduces chemical species from the ablation products into the boundary layer flow. As the amount of ablation is small, this influence has been neglected.

Predictions of Wall Heat Flux for Reentry F Vehicle

Simulation Code and Model Approach

The flow around the Reentry F vehicle has been determined with the SACCARA[6-9] Navier-Stokes code. This investigation is concerned with obtaining accurate numerical solutions of the wall heat flux based upon the input conditions to the code and models used in the simulation. The wall heat flux predictions are then compared with the flight measurements at an altitude of 80,000 feet. The solution is for the flow over the ablated vehicle. The small angle of attack of the vehicle (0.14°) is neglected and the flow is assumed to be axisymmetric. The solutions use a gas model of air in local thermochemical equilibrium and the flow is laminar over the

front part of the body. The flow transitions to turbulent flow at a specified location. The turbulent flow has been modeled with the Baldwin-Barth and Spalart-Allmaras one-equation eddy viscosity approaches and the low Reynolds number $k-\varepsilon$, Menter $k-\omega$, and Wilcox (1998) $k-\omega$ two-equation turbulence models. The solutions have been obtained on three meshes to judge the spatial convergence of the solution. The L2 norms of the momentum and turbulence transport equations exhibited oscillatory behavior after only a two or three order of magnitude drop, thus another method was needed to monitor convergence. The iterative convergence has been initially determined by plotting the wall heat flux at various number of time steps and assuming convergence has been obtained when there is no noticeable change in the results. Further analysis of the steady-state solution error of the wall heat flux has shown that additional time steps are required to obtain adequate steady-state solutions.

Transition Model

As previously discussed, the basic SACCARA code treats the transition process by setting the effective viscosity to the laminar value upstream of a specified transition plane, while downstream of this plane the effective viscosity is the sum of both the laminar and turbulent viscosities. This approach has been used with the Baldwin-Barth one-equation eddy viscosity model and all two-equation models. The transition plane is specified to be perpendicular to the vehicle axis and located at $x = 2.6\ m$. With the Spalart-Allmaras one-equation eddy viscosity model, a different approach has been implemented as described previously, with $x_s = 1.8844\ m$ and $x_e = 2.8844\ m$. From the results of the investigation of the flat plate flow case, it was concluded that Method 2 (coefficient c_{b1} is varied) is the best approach to control the transition process with the Spalart-Allmaras model at this time.

Iterative Convergence of the Numerical Solutions

At an altitude of 80,000 feet, steady-state solutions on three meshes have been obtained by marching the solution in time until there is no further change in the plotted solution. This method is illustrated in Fig. 5 for the coarse Mesh 0-rg (100x40) with the Spalart-Allmaras turbulence model. The laminar flow region takes the longest time to converge as there is a very fine mesh in the wall region. With Mesh 0-rg, the wall heat flux appears to have no significant changes after 4000 time steps. The iterative convergence with Mesh 1-rg (200x80) is shown in Fig. 6, while the behavior of Mesh 2-rg (400x160) is given in Fig. 7. With Mesh 1-rg, the wall heat flux appears to have no significant changes after 7000 time steps while Mesh 2-rg requires approximately 14,000 time steps. However, the results shown in these figures are misleading! A more careful analysis has been performed to estimate the iterative convergence error.

The accuracy of the wall heat flux q^n relative to the steady-state value is determined by expressing the numerical solution at time t^n as

$$q^n = q(t^n) = q_E + \varepsilon^n \tag{18}$$

The exact steady-state value of the wall heat flux is q_E and the convergence error at time t^n is ε^n. The convergence error has been observed to have an exponential decrease in time which gives the following variation as the solution approaches a steady state:

$$\varepsilon^n = \alpha e^{-\beta t^n} \tag{19}$$

Eq. (18) and Eq. (19) are rewritten as

$$\beta t^n = \ln\alpha - \ln(q^n - q_E) \tag{20}$$

Eq. (20) is evaluated at three times, $(n-1)$, n, and $(n+1)$, and the three relations are used to eliminate α and obtain

$$\beta(t^n - t^{n-1}) = \ln[(q^{n-1} - q_E)/(q^n - q_E)]$$
$$\beta(t^{n+1} - t^n) = \ln[(q^n - q_E)/(q^{n+1} - q_E)]$$

If the time increments are equal, then $(t^n - t^{n-1}) = (t^{n+1} - t^n)$ and the above becomes

$$(q^{n-1} - q_E)(q^{n+1} - q_E) = (q^n - q_E)^2$$

The exact steady-state value of the wall heat flux is solved for in the above equation which gives

$$q_E = \frac{q^n - \Lambda^n q^{n-1}}{1 - \Lambda^n}, \qquad \Lambda^n = \frac{(q^{n+1} - q^n)}{(q^n - q^{n-1})} \tag{21}$$

The iterative convergence error becomes

$$\varepsilon^n = -(q^{n+1} - q^n)/(1 - \Lambda^n)$$

and the percent convergence error relative to the exact steady-state value becomes

$$\%\ \text{Error of}\ q^n = -100\left[\frac{q^{n+1} - q^n}{q^n - \Lambda^n q^{n-1}}\right] \tag{22}$$

The foregoing results closely follow the works of Ferziger and Peric[27,28] for determining the convergence error of the numerical iterative solution of difference equations, but their results have been obtained with a different approach. In their work, the parameter Λ^n is the spectral radius (or the magnitude of the largest

eigenvalue) of the iteration matrix. If the eigenvalues are complex, the present approach is not appropriate. The complex eigenvalue case has been considered by Ferziger and Peric.

The above procedure is illustrated for the wall heat flux solution at $x = 2.14892$ m (where the flow is laminar) using the Spalart-Allmaras model. The percent error is shown in Fig. 8 for the three meshes. The percent error obtained from Eq. (22) is indicated by the symbols while the lines are the percent error obtained from the best estimate of the exact solution given by Eq. (21). The initial solution results on the finest mesh (Mesh 2-rg shown in Fig. 7) appeared converged at 10,000 iterations; however, based on the above error analysis, an additional 15,000 iterations were needed to get the error below 0.1%. The flow solution for Reentry F has also been obtained with three meshes (Mesh 0-f, Mesh 1-f and Mesh 2-f) with the same number of cells, but finer spacing near the wall than was used with Mesh rg. Results of iterative convergence similar to Fig. 5, Fig. 6, and Fig. 7 are obtained except the number of time steps is increased significantly for the solutions with finer near-wall spacing. The iterative convergence error for Mesh f is given in Fig. 9. The iterative solution errors are much smaller than the spatial solution errors, as will be demonstrated.

The iterative convergence for the two-equation turbulence models was also examined for Meshes 0-2eq (130x40 cells), 1-2eq (260x80 cells), and 2-2eq (520x160 cells). Results are presented for the low Reynolds number $k-\varepsilon$ model (Fig. 10), the Menter $k-\omega$ model (Fig. 11), and the Wilcox (1998) $k-\omega$ model (Fig. 12). There is some scatter in the symbols due to the fact that the time increments were not always equal. A larger number of iterations were required due to the stricter y^+ requirements for Mesh 2eq verses the one-equation meshes (Mesh rg and Mesh f). The two-equation results were all converged to less than 0.4% error, which is again much smaller than the grid convergence error.

Spatial Convergence of the Numerical Solutions

Spatial convergence has been judged from the steady-state solutions on the three meshes, 0, 1, and 2 (from coarsest to finest). The wall heat flux obtained with the Spalart-Allmaras turbulence model for the three meshes is given in Fig. 13 with the variable spacing given by Mesh rg. The Richardson extrapolation procedure[29] has been used to obtain a more accurate result from the relation

$$q_{RE} = q_{1,2} = q_2 + (q_2 - q_1)/3. \qquad (23)$$

The above relation assumes that the numerical scheme is second-order. The Richardson extrapolation result q_{RE} and the solution on Mesh 2-rg are nearly the same (also shown in Fig. 13). The accuracy of the solutions on the three meshes has been estimated with the exact solution approximated with q_{RE} which gives the solution error as

$$\%\ \text{Error of } q_M = 100(q_M - q_{RE})/q_{RE} \quad M = 1, 2, 3$$

If the mesh has been refined sufficiently where the solution error has second-order behavior, then the errors on the three meshes have the following relationship

$$\%\ \text{Error of } q_2 = \frac{\%\ \text{Error of } q_1}{4} = \frac{\%\ \text{Error of } q_0}{16} \qquad (24)$$

In the above equation, the first equality will always be satisfied when Eq. (23) has been used. The second equality will only be satisfied if the mesh has been sufficiently refined to be in the asymptotic range. The percent error of the wall heat flux along the vehicle is presented in Fig. 14. The laminar flow solution region is in the asymptotic range while the turbulent flow region is not in the asymptotic range. The wall heat flux prediction in the laminar flow region is more accurate than the heat flux prediction in the turbulent flow region.

For Mesh f, spatial convergence has been judged from the steady-state solutions on the three meshes 0, 1, and 2. Richardson extrapolation procedure has been used to obtain a more accurate result. The accuracy of the solutions on the three meshes has been estimated with the exact solution approximated with the Richardson extrapolated result q_{RE} and these results are given in Fig. 15. Again, the laminar flow solution region is in the asymptotic range while the turbulent flow region is not always in the asymptotic range. The wall heat flux prediction in the laminar flow region with Mesh f is less accurate than the results with Mesh rg. The heat flux predictions in the turbulent flow region with Mesh f are more accurate than the results with Mesh rg. Only the solution on Mesh 2-f is considered sufficiently accurate for comparison with the flight measurements and the Richardson extrapolated results provide even a more accurate numerical prediction.

Spatial convergence has also been examined for the three two-equation models. The spatial error of the heat flux is given in Figs. 16-18 for the low Reynolds number $k-\varepsilon$, the Menter $k-\omega$, and the Wilcox (1998) $k-\omega$ models, respectively. The spatial error in the laminar regions is generally below 2%, while in the turbulent regions it varies from approximately 2% for the $k-\varepsilon$ model to 4% for the $k-\omega$ models. The results for the $k-\omega$ models indicate that the heat flux is not fully grid independent in the turbulent region. The spike in the error for the two-equation models is due to movement of the transition location on the different size

meshes and is more apparent for the two-equation models due to the fine axial spacing around the transition point.

Wall Heat Flux

The predictions of the wall heat flux on the Reentry F vehicle at an altitude of 80,000 feet with the one-equation turbulence models are given in Fig. 19 along with the flight data. The Spalart-Allmaras prediction uses the numerical solution with Mesh 2-f and the Richardson extrapolation results for this case. The simulation overpredicts the laminar wall heat flux by roughly 10 percent while the turbulent wall heat flux is overpredicted by roughly 15 percent. At this altitude the vehicle has a 0.14 degree angle of attack and the heat transfer measurements were made on the leeward side of the conical body. A full three-dimensional solution, with the vehicle at angle of attack, would bring the prediction and flight data into closer agreement. The prediction with Mesh 2-f is believed to be a sufficiently accurate steady-state solution that it can be used to validate the turbulence model, but there are small errors in these results due to uncertainty in information used in the simulation as discussed previously.

The Baldwin-Barth turbulence model prediction (also shown in Fig. 19) uses the numerical solution with Mesh 2-rg where the wall temperature is not maintained at 500K. However, these heat transfer results are not expected to be influenced much by this inaccurate wall temperature. The simulation with the Baldwin-Barth turbulence model overpredicts the laminar wall heat flux by roughly 10 percent and is in agreement with the simulation with the Spalart-Allmaras model. Of course, in the laminar flow region the turbulence models should have no impact on the flow solution. The turbulent wall heat flux is overpredicted by roughly 100 percent with the Baldwin-Barth turbulence model. It is recommended that the Spalart-Allmaras model should be used rather than the Baldwin-Barth turbulence model for reentry flows.

Results with the Nagano and Hishida $k-\varepsilon$, the Menter $k-\omega$, and the Wilcox (1998) $k-\omega$ models are presented in Fig. 20. Fine grid results with Mesh 2eq are shown along with the results from Richardson extrapolation. The $k-\varepsilon$ results show an overprediction of the turbulent heating rates by approximately 100%. The two $k-\omega$ models show better agreement with the flight data, with the Menter model within 40% and the Wilcox (1998) model within 30% of the data. All three models display a peak in the turbulent heating just downstream of the specified transition plane, which is possibly due to crude transitional behavior of the standard method.

The present simulations have been performed with a gas model that assumes the air flow is in local thermochemical equilibrium. This study needs to be extended to include solutions obtained with a nonequilibrium thermochemical gas model for air. This type of simulation introduces the modeling of the heterogeneous chemical reactions at the vehicle surface and vibrational nonequilibrium effects.

Conclusions

Many Navier-Stokes codes require that the governing equations be written in conservation form with a source term. The Spalart-Allmaras one-equation model was originally developed in substantial derivative form and when rewritten in conservation form, a density gradient term appears in the source term. This density gradient term causes numerical problems and has a small influence on the numerical predictions. Further work has been performed to understand and to justify the neglect of this term.[11,16] The transition trip term has been included in the one-equation eddy viscosity model of Spalart-Allmaras. Several problems with this model have been discovered when applied to high-speed flows.

For the Mach 8 flat plate boundary layer flow with the standard transition method, the Baldwin-Barth and both $k-\omega$ models gave transition at the specified location. The Spalart-Allmaras and low Reynolds number $k-\varepsilon$ models required an increase in the freestream turbulence levels in order to give transition at the desired location. All models predicted the correct skin friction levels in both the laminar and turbulent flow regions.

For Mach 8 flat plate case, the transition location could not be controlled with the trip terms as given in the Spalart-Allmaras model. Several other approaches have been investigated to allow the specification of the transition location. The approach that appears most appropriate is to vary the coefficient that multiplies the turbulent production term in the governing partial differential equation for the eddy viscosity (Method 2). When this coefficient is zero, the flow remains laminar. The coefficient is increased to its normal value over a specified distance to crudely model the transition region and obtain fully turbulent flow. While this approach provides a reasonable interim solution, a separate effort should be initiated to address the proper transition procedure associated with the turbulent production term. Also, the transition process might be better modeled with the Spalart-Allmaras turbulence model with modification of the damping function f_{v1}. The damping function could be set to zero in the laminar flow region and then turned on through the transition flow region.

Predictions have been obtained for the Reentry F flight vehicle with both one- and two-equation turbulence models where the transition location is specified *a priori*. The axisymmetric turbulent predictions for wall

heat flux with the Spalart-Allmaras, Menter $k-\omega$, and Wilcox (1998) $k-\omega$ models are in reasonable agreement with the flight measurements. The mesh sensitivity has been evaluated by obtaining results on three meshes and more accurate results have been obtained with Richardson extrapolation. The simulation assumes the vehicle is at zero degree angle-of-attack while in fact, the flight vehicle is at 0.14 degree angle-of-attack. For the one-equation models, the Spalart-Allmaras model predictions for this case are much better than the results from the Baldwin-Barth model. For the two-equation models, both $k-\omega$ models give good agreement with the flight data, while the low Reynolds number $k-\varepsilon$ model greatly overpredicts the heating in the fully turbulent region.

Future Work

The Reentry F calculations need to be extended to the finite rate chemistry model. This modification should help to determine if the equilibrium air assumption is appropriate and will help determine if the turbulence model with finite chemistry is reasonable. The present Reentry F calculations have assumed a constant wall temperature and this assumption needs to be improved. As there is only limited flight information on the wall temperature and no data in the nose region, a coupled fluid/heat-conduction analysis is needed to provide the wall temperature variation along the vehicle. Further work could be done to modify the transition mechanism for the two-equation models along the lines of the Spalart-Allmaras modifications presented herein. Finally, including a realizeability limitation has been shown to improve predictions for flows with large normal stresses[30] and may also improve predictions through strong normal shocks.

Acknowledgments

This work was supported by Sandia National Laboratories and the Department of Energy's Accelerated Strategic Computing Initiative.

References

1. D. C. Wilcox, *Turbulence Modeling for CFD, 2nd Ed.*, DCW Industries, Inc. 5354 Palm Drive, La Canada, CA 91011, 1998.

2. R. Peyret (Editor), *Handbook of Computational Fluid Mechanics*, Academic Press, San Diego, CA, 1996.

3. A. J. Smits and J.-P. Dussauge, *Turbulent Shear Layers in Supersonic Flow*, American Institute of Physics, Woodbury, New York, NY, 1996.

4. P. R. Spalart and S. R. Allmaras, "A One-Equation Turbulence Model for Aerodynamic Flows," AIAA Paper 92-0439, 1992.

5. P. R. Spalart and S. R. Allmaras, "A One-Equation Turbulence Model for Aerodynamic Flows," *La Recherche Aerospatiale*, No. 1, pp. 5-21, 1994.

6. C. C. Wong, F. G. Blottner, J. L. Payne, and M. Soetrisno, "Implementation of a Parallel Algorithm for Thermo-Chemical Nonequilibrium Flow Solutions," AIAA Paper 95-0152, Jan. 1995.

7. Wong, C. C., Soetrisno, M., Blottner, F. G., Imlay, S. T., and Payne, J. L., "PINCA: A Scalable Parallel Program for Compressible Gas Dynamics with Nonequilibrium Chemistry," SAND 94-2436, Sandia National Laboratories, Albuquerque, NM, 1995.

8. B. Hassan, D. W. Kuntz, and D. L. Potter, "Coupled Fluid/Thermal Prediction of Ablating Hypersonic Vehicles," AIAA Paper No. 98-0168, Jan. 1998.

9. D. W. Kuntz, B. Hassan, and D. L. Potter, "An Iterative Approach for Coupling Fluid/Thermal Predictions of Ablating Hypersonic Vehicles," AIAA Paper 99-3460, June-July 1999.

10. B. S. Baldwin and T. J. Barth, "A One-Equation Transport Model for High Reynolds Number Wall-Bounded Flows," NASA TM-102847, Aug. 1990.

11. F. R. Menter, "Eddy Viscosity Transport Equations and Their Relation to the $k-\varepsilon$ Model," *Journal of Fluids Engineering*, Vol. 119, Dec. 1997, pp. 876-884.

12. Y. Nagano and M. Hishida, "Improved Form of the $k-\varepsilon$ Model for Wall Turbulent Shear Flows." *Journal of Fluids Engineering*, Vol. 109, pp 156-160, June 1987.

13. F. R. Menter, "Two-Equation Eddy-Viscosity Turbulence Models for Engineering Applications," *AIAA Journal*, Vol. 32, No. 8, Aug. 1994, pp. 1598-1605.

14. E. R. Van Driest. "Investigation of Laminar Boundary Layer in Compressible Fluids Using the Crocco Method," National Advisory Committee for Aeronautics, NACA TN-2597, January 1952.

15. E. R. Van Driest, "Problem of Aerodynamic Heating," *Aeronautical Engineering Review*, Vol. 15, No. 10, pp. 26-41, Oct. 1956.

16. F. R. Menter, H. Grotjans, and F. Unger, "Numerical Aspects of Turbulence Modeling for the Reynolds Averaged Navier-Stokes Equations," *Computational Fluid Dynamics Lecture Series* 1997-02, von Karman Institute for Fluid Dynamics, March 3-7, 1997.

17. B. E. Launder and B. E. Sharma, "Application of the Energy Dissipation Model of Turbulence to the Calculation of Flow Near a Spinning Disc," *Letters in Heat and Mass Transfer*, Vol. 1, No. 2, pp. 131-138.

18. G. Theodoridis, P. Prinos and A. Goulas, "Test Case T3 - Free Stream Turbulence," in *Numerical Simulation of Unsteady Flows and Transition to Turbulence*, Edited by O. Pironneau, W. Rodi, I. L. Ryhming, A. M. Savill, and T. V. Truong, Cambridge University press, 1992.

19. D. C. Wilcox, "Reassessment of the Scale Determining Equation for Advanced Turbulence Models," *AIAA Journal*, Vol. 26, No. 11, 1988, pp. 1299-1310.

20. *US Standard Atmosphere*, National Oceanic and Atmospheric Administration, NASA, and the U. S. Air Force, Washington, D. C., October 1976.

21. G. O. Roberts, "Computational Meshes for Boundary Layer Problems," Proceedings of the Second International Conference on Numerical Methods in Fluid Dynamics, *Lecture Notes in Physics*, Vol. 8, Springer-Verlag, New York, pp. 171-177.

22. J. C. Tannehill, D. A. Anderson, and R. H. Pletcher, *Computational Fluid Mechanics and Heat Transfer*, Taylor & Francis, Bristol, PA, 1997, p. 335.

23. R. L. Wright and E. V. Zoby, "Flight Boundary-Layer Transition Measurements on Slender Cone at Mach 20," AIAA Paper 77-719, June 27-29, 1977.

24. K. Sutton, E. V. Zoby and H. H. Hamilton, "Overview of CFD Methods and Comparison with Flight Aerothermal Data," *AGARD Symposium on Validation of Computational Fluid Dynamics*, Lisbon, Portugal May 2-5, 1988.

25. R. A Thompson, E. V. Zoby, K. E. Wurster, P. A. Gnoffo, "Aerothermodynamic Study of Slender Conical Vehicles," *Journal of Thermophysics and Heat Transfer*, Vol. 3, pp. 361-367, October 1989.

26. K. E. Wurster, E. V. Zoby, and R. A. Thompson, "Flow and Vehicle Parameter Influence on results of Engineering Aerothermal Methods," *AIAA Journal of Spacecraft and Rockets*, Vol. 28, Jan.-Feb. 1991, pp. 16-22.

27. J. H. Ferziger and M. Peric, *Computational Methods for Fluid Dynamics*, Springer-Verlag, Berlin, Heidelberg, and New York, 1996.

28. J. H. Ferziger and M. Peric, "Further Discussion of Numerical Errors in CFD," *International Journal for Numerical Methods in Fluids*, Vol. 23, pp. 1263-1274, 1996.

29. P. Roache, "Ch. 3: A Methodology for Accuracy Verification of Codes: the Method of Manufactured Solutions," *Verification and Validation in Computational Science and Engineering*, Hermosa Publishers, New Mexico, 1998.

30. J. G. Moore and J. Moore, "Realizeability in Two-Equation Turbulence Models," AIAA Paper 99-3779, June-July 1999.

Figures

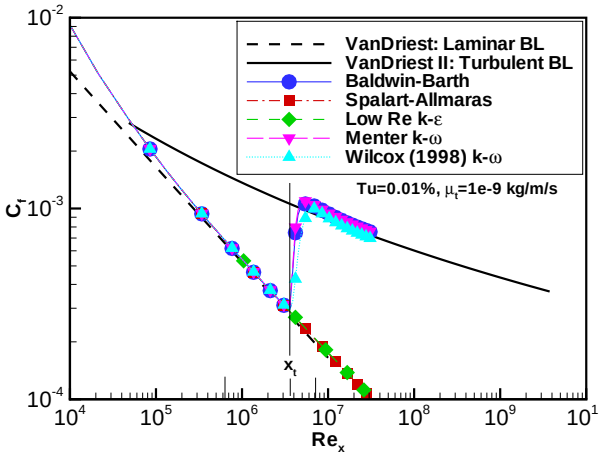

Fig. 1: Transition location with one- and two-equation turbulence models for Mach 8 flat plate flow with the standard transition model.

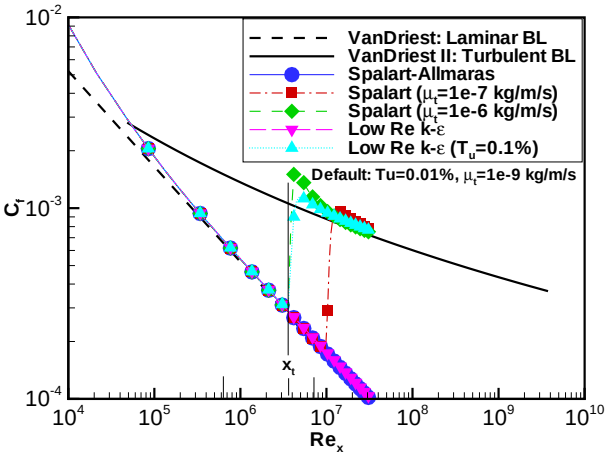

Fig. 2: Transition location for various freestream turb. levels with the Spalart-Allmaras and $k-\varepsilon$ turb. models for Mach 8 flat plate flow.

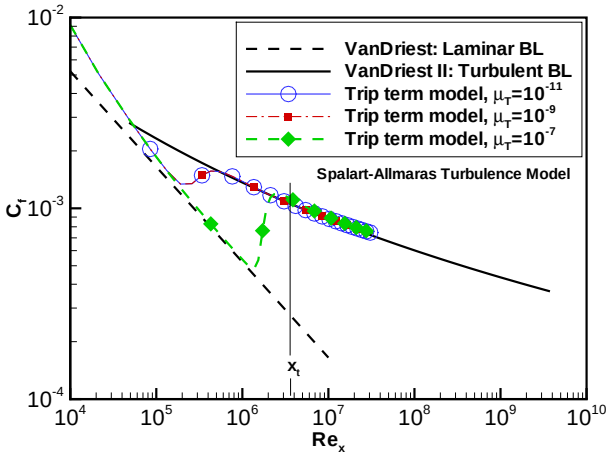

Fig. 3: Transition location for different freestream eddy viscosities with the Spalart-Allmaras turbulence model for Mach 8 flat plate flow.

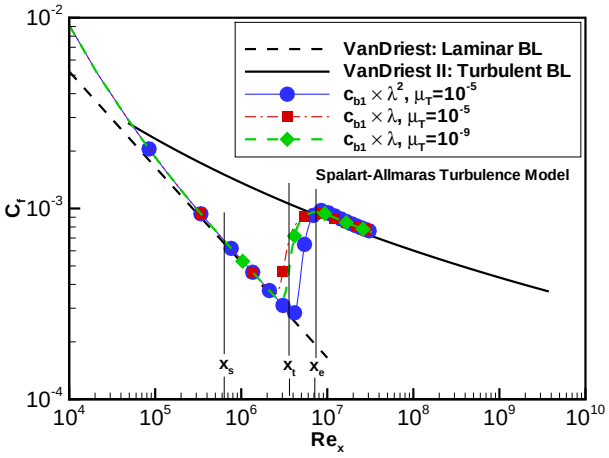

Fig. 4: Transitional flow behavior for Spalart-Allmaras (Meth. 2) with various freestream eddy viscosities for Mach 8 flat plate flow.

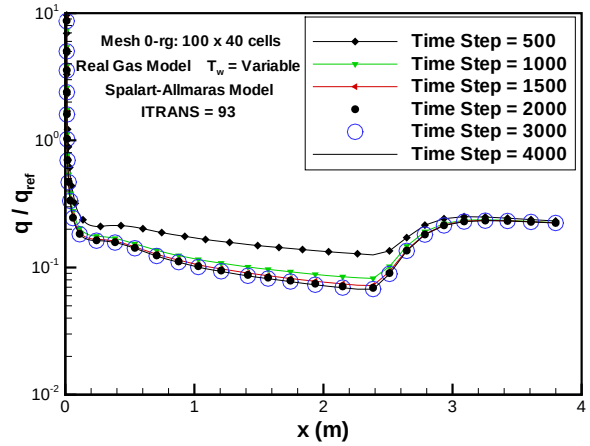

Fig. 5: Iterative convergence of heat flux on *Mesh 0-rg* with the Spalart-Allmaras turbulence model.

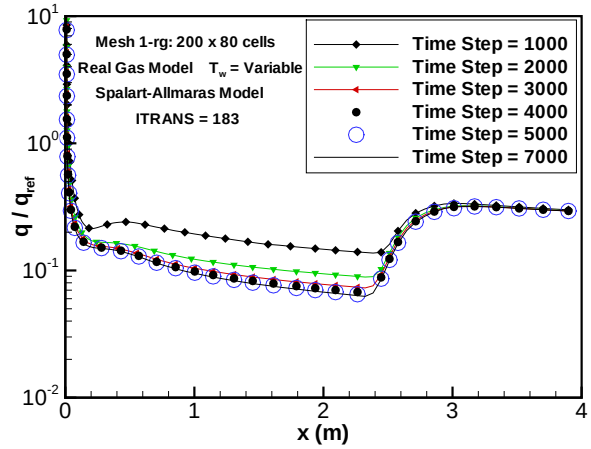

Fig. 6: Iterative convergence of heat flux on Mesh 1-rg with the Spalart-Allmaras turbulence model.

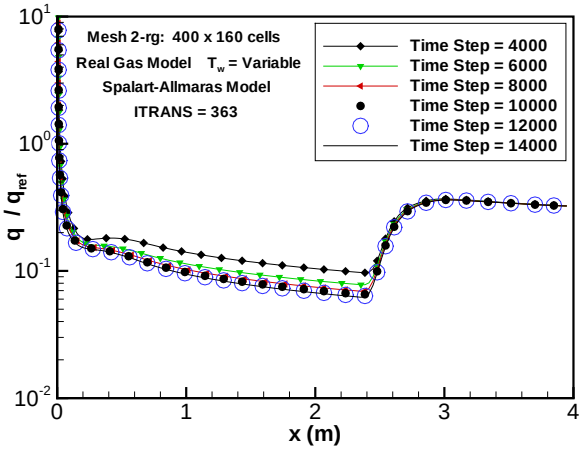

Fig. 7: Iterative convergence of heat flux on Mesh 2-rg with the Spalart-Allmaras turbulence model.

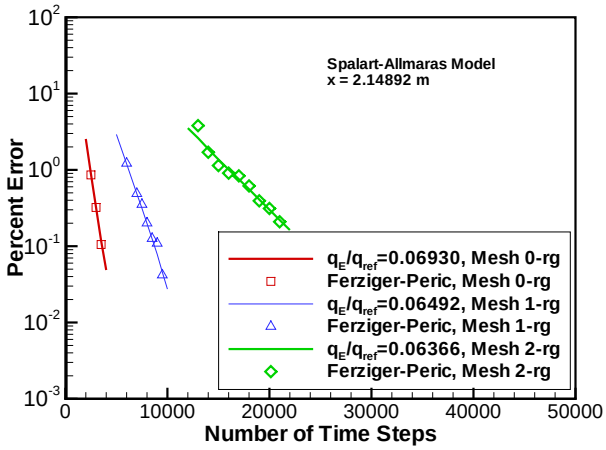

Fig. 8: Iterative convergence error of wall heat flux for the Spalart-Allmaras model at x = 2.14892 m with Mesh rg.

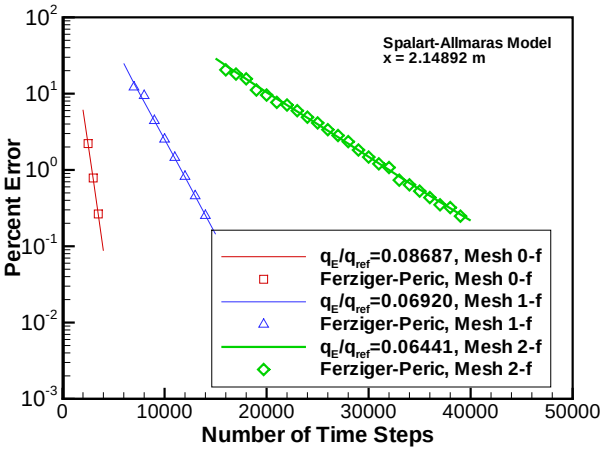

Fig. 9: Iterative convergence error of wall heat flux for the Spalart-Allmaras model at x = 2.14892 m with Mesh f.

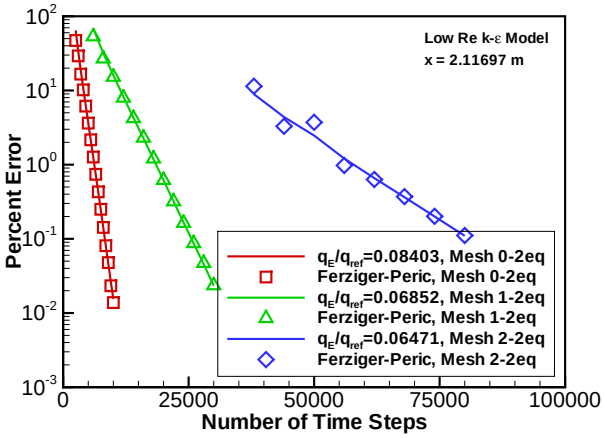

Fig. 10: Iterative convergence error of wall heat flux for the $k-\varepsilon$ model at x = 2.11697 m with Mesh 2eq.

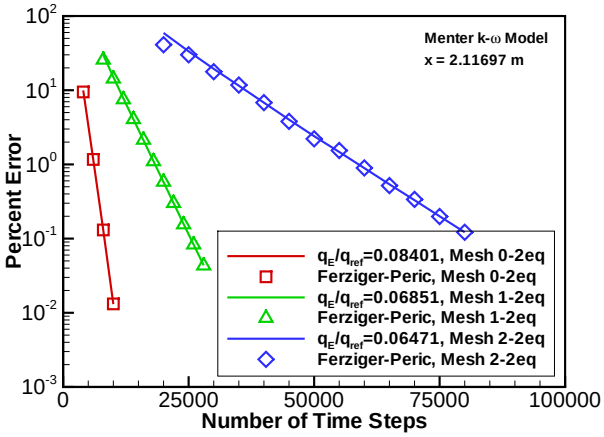

Fig. 11: Iterative convergence error of wall heat flux for the Menter $k-\omega$ model at x = 2.11697 m with Mesh 2eq.

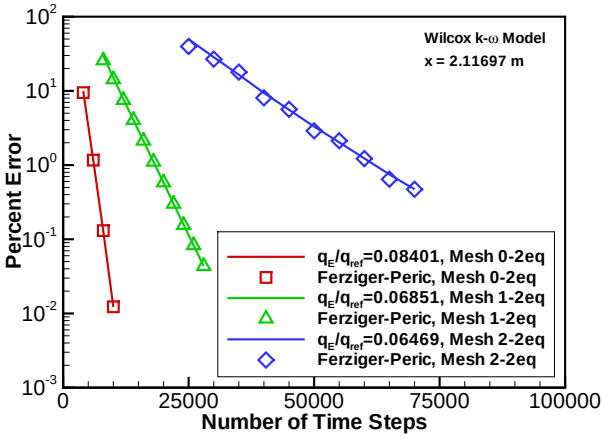

Fig. 12: Iterative convergence error of wall heat flux for the Wilcox (1998) $k-\omega$ model at x = 2.11697 m with Mesh 2eq.

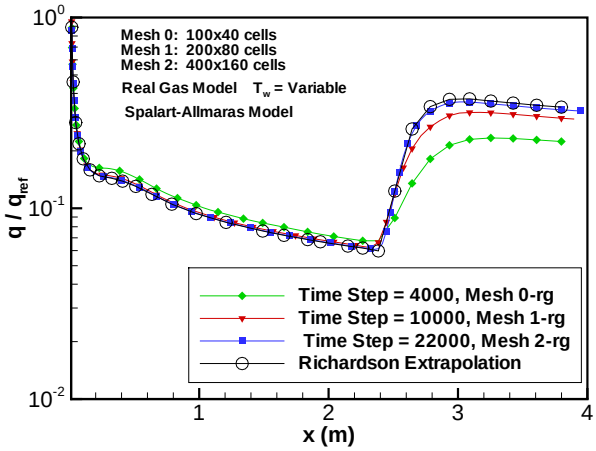

Fig. 13: Spatial convergence of heat flux as the Mesh rg is refined with the Spalart-Allmaras turbulence model.

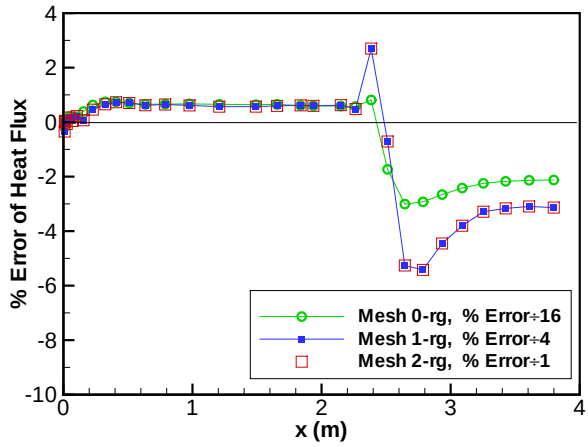

Fig. 14: Error in heat flux along the vehicle with Mesh rg refinement using the Spalart-Allmaras model.

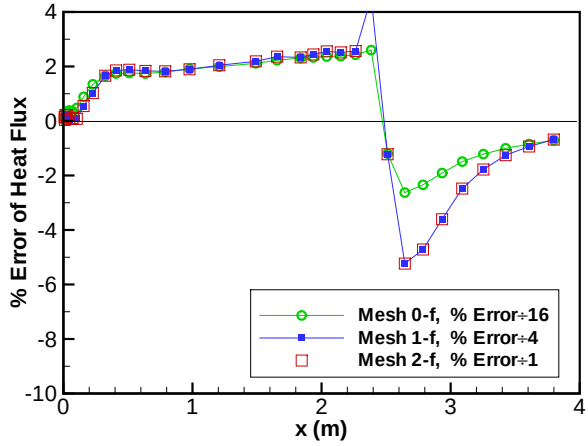

Fig. 15: Error in heat flux along the vehicle with Mesh f refinement using the Spalart-Allmaras model.

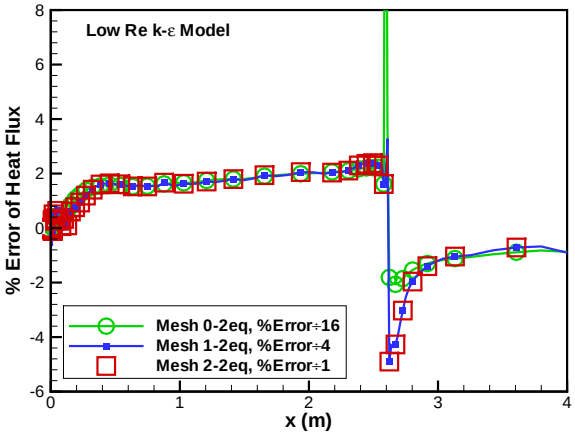

Fig. 16: Error in heat flux along the vehicle with Mesh 2eq refinement using the low Reynolds number $k-\varepsilon$ model.

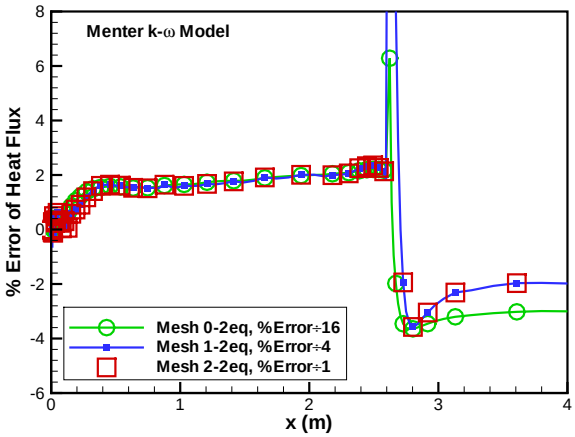

Fig. 17: Error in heat flux along the vehicle with Mesh 2eq refinement using the Menter $k-\omega$ model.

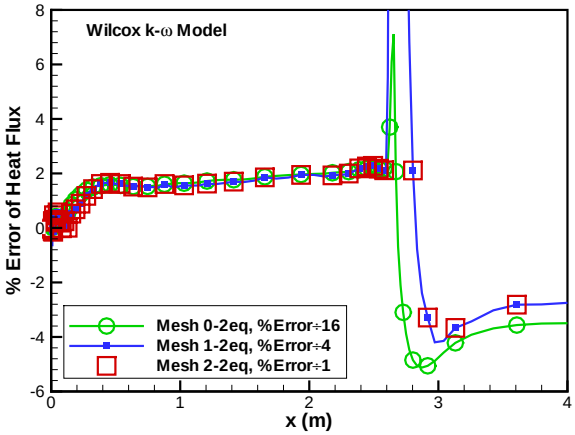

Fig. 18: Error in heat flux along the vehicle with Mesh 2eq refinement using the Wilcox (1998) $k-\omega$ model.

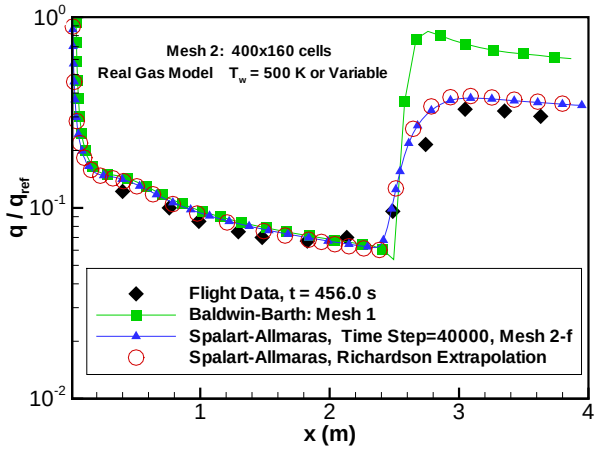

Fig. 19: Comparison of flight data for wall heat flux along Reentry F vehicle at an altitude of 80,000 feet with predictions of the one-equation turbulence models.

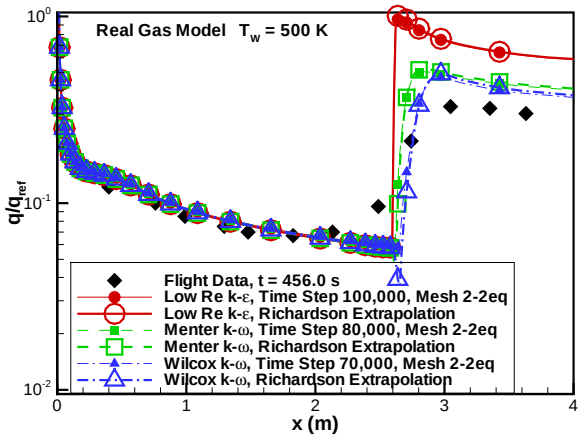

Fig. 20: Comparison of flight data for wall heat flux along Reentry F vehicle at an altitude of 80,000 feet with predictions of the two-equation turbulence models.